Take any shape but that, and my firm nerves
shall never tremble
William Shakespeare (1564–1616), Macbeth

16

Polymers and Particle Orbits in Multiply Connected Spaces

In the previous chapter, the binary interaction potential between the polymer elements was approximated by a δ-function. Quantum-mechanically, this potential is not completely impenetrable. Correspondingly, a polymer with such an interaction has a finite probability of self-intersections. This is only a rough approximation to the situation in nature where the atomic potential is of the hard-core type and self-intersections are extremely rare. In a grand-canonical ensemble, a polymer is often entangled with itself and with others. It can be disentangled only if it has open ends. Macroscopic fluctuations are required to achieve this in the form of worm-like creeping processes. Compared with local fluctuations, these take a very long time. For closed polymers, disentangling is impossible without breaking bonds at the cost of large activation energies. In order to study such entanglement phenomena in their purest form, it is useful to idealize the strongly repulsive interaction potential, as in Section 15.10, to a topological constraint of the type discussed in Chapter 6.

Entanglement phenomena play an important role also in quantum mechanics. Fluctuating particle orbits may get entangled with magnetic flux tubes or with other particle orbits. In fact, the statistical properties of Bose and Fermi particles may be viewed as entanglement phenomena, as will be shown in this chapter.

16.1 Simple Model for Entangled Polymers

Consider the simplest model system with a topological constraint producing entanglement phenomena: a fixed polymer stretched out along the z-axis and a fluctuating second polymer. Arbitrary entanglements with the straight polymer may occur. The possible entanglements of the fluctuating polymer with itself are ignored, for simplicity. Let us study the end-to-end distribution of the fluctuating second polymer. At first we neglect the third dimension, which can be trivially included at a later stage, imagining the movement to be confined entirely to the xy-plane. If the polymer along the z-axis is infinitely thin, the total end-to-end distribution of

the fluctuating polymer in the plane is certainly independent of the presence of the central polymer. In the random-chain approximation it reads for not too large R

$$P_N(\mathbf{x}_b - \mathbf{x}_a) = \sqrt{\frac{2}{2\pi La}}^2 e^{-(\mathbf{x}_b-\mathbf{x}_a)^2/2La}, \tag{16.1}$$

where $\mathbf{x}$ is a planar vector.

In the presence of the central polymer, an interesting new problem arises: How does the end-to-end distribution decompose with respect to the number of times by which the fluctuating polymer is wrapped around the central polymer? To define this number, we choose an arbitrary reference line from the origin to infinity, say the x-axis. For each path from $\mathbf{x}_a$ to $\mathbf{x}_b$, we count how often it crosses this line, including a minus sign for opposite directions of the crossings. In this way, each path receives an integer-valued label n which depends on the position of the reference line.

A property independent of the choice of the reference line exists for the pairs of paths with fixed ends. The difference path is closed. The number n of times by which a closed path encircles the origin is a topological invariant called the *winding number*. Let us find the decomposition of the probability distribution of a closed polymer $P_N(\mathbf{x}_b - \mathbf{x}_a)$ with respect to n:

$$P_N(\mathbf{x}_b - \mathbf{x}_a) = \sum_{n=-\infty}^{\infty} P_N^n(\mathbf{x}_b, \mathbf{x}_a). \tag{16.2}$$

The topological constraint destroys the translational invariance of the total distribution on the left-hand side, so that the different fixed-n distributions on the right-hand side depend separately on both $\mathbf{x}_b$ and $\mathbf{x}_a$.

In a path integral it is easy to keep track of the number of crossings n. The angular difference between initial and final points $\mathbf{x}_b$ and $\mathbf{x}_a$ is given by the integral

$$\varphi_b - \varphi_a = \int_{t_a}^{t_b} dt\, \dot{\varphi}(t) = \int_{t_a}^{t_b} dt\, \frac{x_1\dot{x}_2 - x_2\dot{x}_1}{x_1^2 + x_2^2} = \int_{\mathbf{x}_a}^{\mathbf{x}_b} \frac{\mathbf{x} \times d\mathbf{x}}{\mathbf{x}^2}. \tag{16.3}$$

Given two paths C_1 and C_2 connecting $\mathbf{x}_a$ and $\mathbf{x}_b$, this integral differs by an integer multiple of 2π. The winding number is therefore given by the contour integral over the closed difference path C:

$$n = \frac{1}{2\pi} \oint_C \frac{\mathbf{x} \times d\mathbf{x}}{\mathbf{x}^2}. \tag{16.4}$$

In order to decompose the end-to-end distribution (16.2) with respect to the winding number, we recall the angular decomposition of the imaginary-time evolution amplitude in Eqs. (8.9) and (8.17) of a free particle in two dimensions

$$P_L(\mathbf{x}_b - \mathbf{x}_a) = \sum_m \frac{1}{\sqrt{r_b r_a}} (r_b\tau_b | r_a\tau_a)_m \frac{1}{2\pi} e^{im(\varphi_b - \varphi_a)}, \tag{16.5}$$

with the radial amplitude

$$(r_b\tau_b|r_a\tau_a)_m = 2\frac{\sqrt{r_b r_a}}{La}e^{-(r_b^2+r_a^2)/La}I_m\left(2\frac{r_b r_a}{La}\right). \tag{16.6}$$

We have inserted the polymer parameters following the rules of Section 15.6, replacing $M/2\hbar(\tau_b - \tau_a)$ by $1/La$, and using the label $L = Na$ in P_L rather than N, as in Eq. (15.301).

We now recall that according to Section 6.1, an angular path integral consisting of a product of integrals

$$\prod_{n=1}^{N}\int_{-\pi}^{\pi}\frac{d\varphi_n}{2\pi}, \tag{16.7}$$

whose conjugate momenta are integer-valued, can be converted into a product of ordinary integrals

$$\prod_{n=1}^{N}\int_{-\infty}^{\infty}\frac{d\varphi_n}{2\pi}, \tag{16.8}$$

whose conjugate momenta are continuous. These become independent of the time slice n by momentum conservation, and the common momentum is eventually restricted to its proper integer values by a final sum over an integer number n occurring in the Poisson formula [see (6.9)]

$$\sum_n e^{ik(\varphi_b+2\pi n-\varphi_a)} = \sum_{m=-\infty}^{\infty}\delta(k-m)e^{im(\varphi_b-\varphi_a)}. \tag{16.9}$$

Obviously, the number n on the left-hand side is precisely the winding number by which we want to sort the end-to-end distribution. The desired restricted probability $P_L^n(\mathbf{x}_b, \mathbf{x}_a)$ for a given winding number n is therefore obtained by converting the sum over m in Eq. (16.5) into an integral over μ and another sum over n as in Eq. (1.205), and by omitting the sum over n. The result is:

$$P_L^n(\mathbf{x}_b, \mathbf{x}_a) = \frac{2}{La}\int_{-\infty}^{\infty}d\mu e^{-(r_b^2+r_a^2)/La}I_{|\mu|}\left(2\frac{r_b r_a}{La}\right)\frac{1}{2\pi}e^{i\mu(\varphi_b-\varphi_a+2\pi n)}. \tag{16.10}$$

From this we find the desired probability of a closed polymer running through a point $\mathbf{x}$ with various winding numbers n around the central polymer:

$$P_L^n(\mathbf{x}, \mathbf{x}) = \frac{2}{La}\int_{-\infty}^{\infty}d\mu e^{-2r^2/La}I_{|\mu|}\left(2\frac{r^2}{La}\right)\frac{1}{2\pi}e^{i2\pi\mu n}. \tag{16.11}$$

Let us also calculate the partition function of a closed polymer with a given winding number n. To make the partition function finite, we change the system by

adding a harmonic oscillator potential centered at the origin.[1] If ω is measured in units 1/length, the above probability becomes

$$P_L^n(\mathbf{x},\mathbf{x}) = \frac{2}{a}\frac{\omega}{\sinh\omega L}\int_{-\infty}^{\infty} d\mu e^{-2(r^2/a)\omega\coth\omega L} I_{|\mu|}\left(\frac{2}{a}\frac{r^2\omega}{\sinh\omega L}\right)\frac{1}{2\pi}e^{i2\pi\mu n}. \quad (16.12)$$

This can be integrated over the entire space using the formula (2.475). The result is

$$P_L^n \equiv \int d^2x P_L^n(\mathbf{x},\mathbf{x}) = \frac{1}{2\sinh\omega L}\int_{-\infty}^{\infty} d\mu e^{-|\mu|\omega L}e^{2\pi i\mu n}. \quad (16.13)$$

To check this formula, we sum both sides over all n. Then the integral over μ is reduced, via Poisson's formula, to a sum over integers $\mu = m = 0, \pm1, \pm2, \ldots$, and we find

$$\begin{aligned} P_L &\equiv \int d^2x P_L(\mathbf{x},\mathbf{x}) = \sum_{n=-\infty}^{\infty} P_L^n \\ &= \frac{1}{2\sinh\omega L}\left(\frac{2}{1-e^{-\omega L}} - 1\right) = \frac{1}{\left[2\sinh(\omega L/2)\right]^2}. \end{aligned} \quad (16.14)$$

As we should have expected, this is the partition function of the two-dimensional harmonic oscillator.

To find the contribution of the various winding numbers, we perform the integral over μ and obtain

$$P_L^n = \frac{\omega L}{\sinh\omega L}\,\frac{1}{4\pi^2n^2+\omega^2L^2}. \quad (16.15)$$

The right-hand factor is recognized as a term arising in the expansion

$$\begin{aligned} \frac{1}{2\omega L}\coth(\omega L/2) &= \sum_{n=-\infty}^{\infty}\frac{1}{4\pi^2n^2+(\omega L)^2} \\ &= \frac{1}{L^2}\sum_{n=-\infty}^{\infty}\frac{1}{\omega_n^2+\omega^2}. \end{aligned} \quad (16.16)$$

The quantities $\omega_n \equiv 2\pi n/L$ are the polymer analogs of the Matsubara frequencies. Thus we may write

$$P_L^n = P_L\cdot\alpha_n, \quad (16.17)$$

where α_n is the relative probability of finding the winding number n (with the normalization $\Sigma_n\alpha_n = 1$),

$$\begin{aligned} \alpha_n &= \frac{1}{\omega_n^2+\omega^2}\left[\sum_{n=-\infty}^{\infty}\frac{1}{\omega_n^2+\omega^2}\right]^{-1} \\ &= \frac{1}{L^2}\frac{1}{\omega_n^2+\omega^2}\left[\frac{1}{2\omega L}\coth\frac{\omega L}{2}\right]^{-1}. \end{aligned} \quad (16.18)$$

[1] Alternatively, we may add a magnetic field with the Landau frequency $\omega = -eB/Mc$, as done in (16.33). Then the amplitude contains $\omega/2$ instead of ω, and an extra factor $e^{m\omega L/2}$.

16.2 Entangled Fluctuating Particle Orbit: Aharonov-Bohm Effect

The entanglement of a fluctuating polymer around a straight central polymer has an interesting quantum-mechanical counterpart known as the *Aharonov-Bohm effect*. Consider a free nonrelativistic charged particle moving through a space containing an infinitely thin tube of finite magnetic flux along the z-direction:

$$B_3 = \frac{g}{2\pi}\,\epsilon_{3jk}\partial_j\partial_k\varphi = g\;\delta^{(2)}(\mathbf{x}_\perp), \tag{16.19}$$

where $\mathbf{x}_\perp$ is the transverse vector $\mathbf{x}_\perp \equiv (x_1, x_2)$. Let us study the associated path integral. The magnetic interaction is given by [recall Eq. (2.635)]

$$\mathcal{A}_{\rm mag} = \frac{e}{c}\int_{t_a}^{t_b} dt\,\dot{\mathbf{x}}\cdot\mathbf{A}, \tag{16.20}$$

where e is the charge and $\mathbf{A}$ the vector potential. The flux tube (16.19) is obtained from the components in the xy-plane.

$$A_i = \frac{g}{2\pi}\partial_i\varphi, \quad (i = 1, 2), \tag{16.21}$$

where φ is the azimuthal angle around the tube:

$$\varphi(\mathbf{x}) \equiv \arctan(x_2/x_1). \tag{16.22}$$

Note that the derivatives in front of φ in (16.19) commute everywhere, except at the origin where Stokes' theorem yields

$$\int d^2x\,(\partial_1\partial_2 - \partial_2\partial_1)\varphi = \oint d\varphi = 2\pi. \tag{16.23}$$

The total magnetic flux through the tube is defined by the integral

$$\Phi = \int d^2x\,B_3. \tag{16.24}$$

Inserting (16.19) we see that the total flux is equal to g:

$$\Phi = g. \tag{16.25}$$

With the vector potentoal (16.21), the interaction (16.20) takes the form

$$\mathcal{A}_{\rm mag} = -\hbar\mu_0\int_{t_a}^{t_b} dt\;\dot{\varphi}, \tag{16.26}$$

where μ_0 is the dimensionless number

$$\mu_0 \equiv -\frac{eg}{2\pi\hbar c}. \tag{16.27}$$

The minus sign is a matter of convention.

Since the particle orbits are present at all times, their worldlines in spacetime can be considered as being closed at infinity, and the integral

$$n = \frac{1}{2\pi}\int_{t_a}^{t_b} dt\,\dot{\varphi} \tag{16.28}$$

is the topological invariant (16.4) with integer values of the winding number n. The magnetic interaction (16.26) is therefore a purely topological one, its value being

$$\mathcal{A}_{\rm mag} = -\hbar\mu_0\, 2\pi n. \tag{16.29}$$

After adding this to the action of a free particle in the radial decomposition (8.9) of the quantum-mechanical path integral,we rewrite the sum over the azimuthal quantum numbers m via Poisson's summation formula as in (16.10), and obtain

$$\begin{aligned}(\mathbf{x}_b\tau_b|\mathbf{x}_a\tau_a) = \int_{-\infty}^{\infty} d\mu \frac{1}{\sqrt{r_b r_a}}(r_b\tau_b|r_a\tau_a)_\mu \\ \times \sum_{n=-\infty}^{\infty}\frac{1}{2\pi}e^{i(\mu-\mu_0)(\varphi_b+2\pi n-\varphi_a)}.\end{aligned} \tag{16.30}$$

Since the winding number n is often not easy to measure experimentally, let us extract observable consequences which are independent of n. The sum over all n forces μ to be equal to μ_0 modulo an arbitrary integer number $m = 0, \pm1, \pm2, \dots$. The result is

$$(\mathbf{x}_b\tau_b|\mathbf{x}_a\tau_a) = \sum_{m=-\infty}^{\infty}\frac{1}{\sqrt{r_b r_a}}(r_b\tau_b|r_a\tau_a)_{m+\mu_0}\frac{1}{2\pi}e^{im(\varphi_b-\varphi_a)}, \tag{16.31}$$

with the radial amplitude

$$(r_b\tau_b|r_a\tau_a)_{m+\mu_0} = \sqrt{r_b r_a}\frac{M}{\hbar}\frac{1}{(\tau_b-\tau_a)}\exp\left\{-\frac{M}{2\hbar}\frac{r_b^2+r_a^2}{\tau_b-\tau_a}\right\} I_{|m+\mu_0|}\left(\frac{M}{\hbar}\frac{r_b r_a}{\tau_b-\tau_a}\right). \tag{16.32}$$

For the sake of generality, we allow for the presence of a homogeneous magnetic field B whose Landau frequency is $\omega = -eB/Mc$. In analogy with the parameter μ_0 in (16.27), it is defined with a minus sign. Using the radial amplitude (9.105), we see that (16.32) is simply generalized to

$$\begin{aligned}(r_b\tau_b|r_a\tau_a)_{m+\mu_0} = \sqrt{r_b r_a}\frac{M\omega}{2\hbar\eta}\frac{\eta}{\sinh\eta}\exp\left[-\frac{M}{2\hbar}\frac{\omega}{2}\coth\eta(r_b^2+r_a^2)\right] \\ \times I_{|m+\mu_0|}\left(\frac{M\omega r_b r_a}{2\hbar\sinh\eta}\right)e^{(m+\mu_0)\eta},\end{aligned} \tag{16.33}$$

where $\eta \equiv \omega(\tau_b-\tau_a)/2$.

At this point we can make an interesting observation: If μ_0 is an integer number, i.e., if

$$\frac{eg}{2\pi\hbar c} = \text{integer}, \tag{16.34}$$

the quantum-mechanical particle distribution function $(\mathbf{x}\,t_b|\mathbf{x}\,t_a)$ in (16.31) becomes *independent* of the magnetic flux tube along the z-axis. The condition implies that the magnetic flux is an integer multiple of the fundamental flux quantum

$$\Phi_0 \equiv g_0 \equiv \frac{2\pi\hbar c}{e} = \frac{hc}{e}. \tag{16.35}$$

We recognize this infinitely thin tube as a *Dirac string*. Such undetectable strings were used in Sections 8.12, Appendix 10A.3, and Section 14.6 to import the magnetic flux of a magnetic monopole from infinity to a certain point where the magnetic field lines emerge radially. In Appendix 10A.3 we have made the string invisible mathematically imposing monopole gauge invariance. The present discussion shows explicitly that the flux quantization makes Dirac strings indeed undetectable by any charged particle. This observation inspired Dirac his speculation on the existence of magnetic monopoles.

In low-temperature physics, a quantization of magnetic flux is observable in type-II superconductors. Superconductors are perfect diamagnets which expel magnetic fields. Those of type II have the property that above a certain critical external field called H_{c_1}, the expulsion is not perfect but they admit quantized magnetic tubes of flux Φ_0 (*Shubnikov phase*). For increasing fields, there are more and more such flux tubes. They are squeezed together and can form a periodically arranged bundle. When cut across in the xy-plane, the bundle looks like a hexagonal planar flux lattice [4]. If the central magnetic flux tube in (16.19) carries an amount of flux that is not an integer multiple of Φ_0, the amplitude of particles passing the tube displays an interesting interference pattern. This was initially a surprise since the space is free of magnetic fields. To calculate this pattern we consider the fixed-energy amplitude of a free particle in two dimensions (9.12), decomposed into partial waves via the addition theorem (9.14) for Bessel functions as in (9.15):

$$(\mathbf{x}_b|\mathbf{x}_a)_E = -\frac{2iM}{\hbar}\sum_{m=-\infty}^{\infty} I_m(\kappa r_<)K_m(\kappa r_>)\frac{1}{2\pi}e^{im(\varphi_b-\varphi_a)}. \tag{16.36}$$

Comparing this with (16.30) and repeating the arguments leading to (16.31), (16.32), we can immediately write down the fixed-energy amplitude in the presence of a flux Φ_0:

$$(\mathbf{x}_b|\mathbf{x}_a)_E = -\frac{2iM}{\hbar}\sum_{m=-\infty}^{\infty} I_{|m+\mu_0|}(\kappa r_<)K_{|m+\mu_0|}(\kappa r_>)\frac{1}{2\pi}e^{im(\varphi_b-\varphi_a)}. \tag{16.37}$$

The wave functions are now easily extracted. In the complex E-plane, the right-hand side has a discontinuity across the positive real axis. By going through the same steps as in (9.15)–(9.22), we derive for the discontinuity

$$\int_{-\infty}^{\infty}\frac{dE}{2\pi\hbar}\mathrm{disc}(\mathbf{x}_b|\mathbf{x}_a)_E = \sum_{m=-\infty}^{\infty}\int_0^{\infty} dk k J_{|m+\mu_0|}(kr_b)J_{|m+\mu_0|}(kr_a)\frac{1}{2\pi}e^{im(\varphi_b-\varphi_b)}. \tag{16.38}$$

The integration measure $\int (dE/2\pi\hbar)(2\pi M/\hbar)$ has been replaced by $\int_0^\infty dkk$ according to Eq. (9.23).

In the absence of the flux tube, the amplitude (16.38) reduces to that of a free particle, which has the decomposition

$$\begin{aligned}\int_{-\infty}^{\infty} \frac{dE}{2\pi\hbar} \mathrm{disc}(\mathbf{x}_b|\mathbf{x}_a)_E &= \int \frac{d^2k}{(2\pi)^2} e^{i\mathbf{k}(\mathbf{x}_b-\mathbf{x}_a)} = \frac{1}{2\pi}\int_0^\infty dkkJ_0(k|\mathbf{x}_b-\mathbf{x}_a|) \\ &= \sum_{m=-\infty}^{\infty} \int_0^\infty dkkJ_m(kr_b)J_m(kr_a)\frac{1}{2\pi}e^{im(\varphi_b-\varphi_a)}. \qquad (16.39)\end{aligned}$$

If a flux tube is present, a beam of incoming charged particles is deflected even though the space around the z-axis contains no magnetic field. Let us calculate the scattering amplitude and the ensuing cross section from the fixed-energy amplitude (16.37). Recall the results of the quantum-mechanical scattering theory due to Lippmann and Schwinger. In this theory one studies the effect of an interaction upon an incoming free-particle state $\varphi_{\mathbf{k}}$ of wave vector $\mathbf{k}$. The result is the scattering state $\psi_{\mathbf{k}}$ obtained from the *Lippmann-Schwinger* integral equation

$$\begin{aligned}\psi_{\mathbf{k}} &= \varphi_{\mathbf{k}} + \frac{1}{E-\hat{H}_0+i\eta}\hat{V}\psi_{\mathbf{k}} \\ &= \varphi_{\mathbf{k}} - \frac{i}{\hbar}\hat{R}(E)\ \hat{V}\varphi_{\mathbf{k}}, \qquad (16.40)\end{aligned}$$

where E is the energy of the incoming particle, $\hat{V}$ the potential, and $\hat{R}(E)$ the resolvent operator (1.319). The scattering states $\psi_{\mathbf{k}}$ are solutions of the Schrödinger equation

$$\hat{H}\psi_{\mathbf{k}} = (\hat{H}_0+\hat{V})\psi_{\mathbf{k}} = E\psi_{\mathbf{k}}. \qquad (16.41)$$

In $\mathbf{x}$-space, the Lippmann-Schwinger equation reads

$$\psi_{\mathbf{k}}(\mathbf{x}) = \varphi_{\mathbf{k}}(\mathbf{x}) - \frac{i}{\hbar}\int d^Dx'\,(\mathbf{x}|\mathbf{x}')_E V(\mathbf{x}')\varphi_{\mathbf{k}}(\mathbf{x}'). \qquad (16.42)$$

The first term describes the impinging particles, the second the scattered ones. For the scattering amplitude, only the large-$\mathbf{x}$ behavior of the second term matters. One usually normalizes $\varphi_{\mathbf{k}}(\mathbf{x})$ to $e^{i\mathbf{kx}}$ and factorizes the second term asymptotically into a product of an outgoing spherical wave times a scattering amplitude. In three dimensions, the asymptotic behavior far away from the scattering center is

$$\psi_{\mathbf{k}}(\mathbf{x}) \xrightarrow{|\mathbf{x}|\to\infty} e^{i\mathbf{k}x} + \frac{e^{i|\mathbf{k}||\mathbf{x}|}}{|\mathbf{x}|}f(\theta,\varphi) + \dots\ , \qquad (16.43)$$

where θ and φ are the scattering angles of the outgoing beam and f is the scattering amplitude. Its square gives directly the differential cross section

$$\frac{d\sigma}{d\Omega} = |f(\theta,\varphi)|^2. \qquad (16.44)$$

In two dimensions, the corresponding splitting is

$$\psi_{\mathbf{k}}(\mathbf{x}) \xrightarrow{|\mathbf{x}|\to\infty} e^{i\mathbf{k}x} + \frac{e^{i|\mathbf{k}||\mathbf{x}|}}{\sqrt{|\mathbf{x}|}} f(\varphi) + \dots \ . \tag{16.45}$$

The scattering amplitude $f(\varphi)$ which depends only on the azimuthal angle $\varphi = \arctan(x_2/x_1)$ yields the differential cross section

$$\frac{d\sigma}{d\varphi} = |f(\varphi)|^2. \tag{16.46}$$

To calculate $f(\varphi)$, we observe that the most general solution $\Psi(\mathbf{x})$ of the Schrödinger equation (16.41) is obtained by forming the convolution integral of the discontinuity of the resolvent with an arbitrary wave function $\phi(\mathbf{x})$:

$$\psi(\mathbf{x}) = \int d^D x' \ \mathrm{disc}(\mathbf{x}|\mathbf{x}')_E \ \phi(\mathbf{x}'). \tag{16.47}$$

Using (16.38), this becomes some linear combination of wave functions $J_{|m+\mu_0|}(kr)$

$$\psi(\mathbf{x}) = \sum_{m=-\infty}^{\infty} a_m J_{|m+\mu_0|}(kr) e^{im\varphi}, \tag{16.48}$$

which certainly satisfies the Schrödinger equation (16.41). The coefficients a_m have to be chosen to satisfy the scattering boundary condition at spatial infinity. Suppose that the incident particles carry a wave vector $\mathbf{k} = (-k, 0)$. In the incoming region $x \to \infty$, they are described by a wave function

$$\lim_{x\to\infty} \psi(\mathbf{x}) = e^{-ikx} e^{-i\mu_0\varphi}. \tag{16.49}$$

The extra phase factor is necessary for the correct wave vector since in the presence of the gauge field

$$eA_i = -\hbar c \mu_0 \partial_i \varphi, \tag{16.50}$$

the physical momentum $\mathbf{p} = \hbar\mathbf{k}$ is not given by the usual derivative operator $-i\hbar\boldsymbol{\nabla}$ but by the gauge-invariant momentum operator

$$\hat{\mathbf{P}} = -i\hbar\boldsymbol{\nabla} - \frac{e}{c}\mathbf{A} = -i\hbar(\boldsymbol{\nabla} + i\mu_0\boldsymbol{\nabla}\varphi). \tag{16.51}$$

The corresponding incident gauge-invariant particle current is

$$\mathbf{j}(\mathbf{x}) = -i\frac{\hbar}{2M}\psi^\dagger \overset{\leftrightarrow}{\boldsymbol{\nabla}} \psi(\mathbf{x}) - \frac{e}{Mc}\mathbf{A}(\mathbf{x})\psi^\dagger\psi(\mathbf{x}). \tag{16.52}$$

We demonstrate below that the correct choice for the coefficients a_m is

$$a_m = (-i)^{|m+\mu_0|}, \tag{16.53}$$

leading to the scattering amplitude

$$f(\varphi) = \frac{1}{\sqrt{2\pi}} e^{-i\pi/4} \sin \pi\mu_0 \frac{e^{-i\varphi/2}}{\cos(\varphi/2)}, \tag{16.54}$$

i.e., to the cross section

$$\frac{d\sigma}{d\varphi} = \frac{1}{2\pi} \sin^2 \pi\mu_0 \frac{1}{\cos^2(\varphi/2)}. \tag{16.55}$$

It has a strong peak near the forward direction $\varphi \approx \pi$. For $\mu_0 =$ integer, there is no scattering at all and the flux tube becomes an invisible Dirac string.

To derive (16.53) and (16.54) we may assume that $\mu_0 \in (0, 1)$. Otherwise, we could simply shift the sum over m in (16.37) by an integer Δm, and this would merely produce an overall factor $e^{i\Delta m(\varphi_b - \varphi_a)}$ in $\mathrm{disc}(\mathbf{x}_b|\mathbf{x}_a)_E$. This would wind up as a factor $e^{i\Delta m\,\varphi}$ in $\psi(\mathbf{x})$. For $\mu_0 \in (0, 1)$, we split the wave function (16.48) into three parts:

$$\psi_{\mathbf{k}} = \psi^{(1)} + \psi^{(2)} + \psi^{(3)}. \tag{16.56}$$

The first collects the terms with positive m,

$$\psi^{(1)} = \sum_{m=1}^{\infty} (-i)^{m+\mu_0} J_{m+\mu_0} e^{im\varphi}, \tag{16.57}$$

the second those with negative m,

$$\begin{aligned} \psi^{(2)} &= \sum_{m=-\infty}^{-1} (-i)^{m+\mu_0} J_{|m+\mu_0|} e^{im\varphi} \\ &= \sum_{m=1}^{\infty} (-i)^{m-\mu_0} J_{m-\mu_0} e^{-im\varphi}, \end{aligned} \tag{16.58}$$

and the third contains only the term $m = 0$,

$$\psi^{(3)} = (-i)^{|\mu_0|} J_{|\mu_0|}. \tag{16.59}$$

Obviously, $\psi^{(2)}$ may be obtained from $\psi^{(1)}$ via the identity

$$\psi^{(2)}(r, \varphi, \mu_0) = \psi^{(1)}(r, -\varphi, -\mu_0). \tag{16.60}$$

Thus, the wave function (16.56) requires only a calculation of $\psi^{(1)}$.

As a first step we observe that the sum (16.57) has an integral representation

$$\psi^{(1)} = \frac{1}{2}(-i)^{\mu_0} e^{-i\rho\cos\varphi}\, I(\rho), \tag{16.61}$$

with $I(\rho)$ being the integral

$$I(\rho) \equiv \int_0^{\rho} d\rho' e^{i\rho'\cos\varphi} \left(J_{1+\mu_0} - i J_{\mu_0} e^{i\varphi} \right). \tag{16.62}$$

We have set $kr \equiv \rho$ such that $\mathbf{kx} \equiv \rho\cos\varphi$. To prove the integral representation, we differentiate (16.61) and find the differential equation

$$\partial_\rho \psi^{(1)} = -i\cos\varphi\ \psi^{(1)} + \frac{1}{2}(-i)^{\mu_0}\left(J_{1+\mu_0} - iJ_{\mu_0}e^{i\varphi}\right), \tag{16.63}$$

with all functions depending only on $kr \equiv \rho$. Precisely the same equation is obeyed by the sum (16.57):

$$\begin{aligned}
\partial_\rho \psi^{(1)} &= \sum_{m=1}^{\infty}(-i)^{m+\mu_0}\partial_\rho J_{m+\mu_0}e^{im\varphi} \\
&= \sum_{m=1}^{\infty}(-i)^{m+\mu_0}\frac{1}{2}\left(J_{m+\mu_0-1} - J_{m+\mu_0+1}\right)e^{im\varphi} \qquad (16.64)\\
&= -\frac{i}{2}\sum_{m=1}^{\infty}(-i)^{m+\mu_0}J_{m+\mu_0}e^{im\varphi}\left(e^{i\varphi}+e^{-i\varphi}\right) + \frac{1}{2}(-i)^{\mu_0}\left(J_{1+\mu_0} - iJ_{\mu_0}e^{ie}\right).
\end{aligned}$$

Thus, the two expressions (16.57) and (16.61) for $\psi^{(1)}$ can differ at most by an integration constant. However, the constant must be zero since both expressions vanish at $\rho = 0$. This proves the integral representation (16.61).

In order to derive the scattering amplitude for the magnetic flux tube, we have to find the asymptotic of the wave function. This is done by splitting $\psi^{(1)}_\infty$ into two terms, a contribution $\psi^{(1)}_\infty$ in which the integral I is carried all the way to infinity, to be denoted by I_∞, and a remainder $\Delta\psi^{(1)}$ which vanishes for $r \to \infty$. The integral I_∞ can be calculated analytically using the formula

$$\int_0^\infty d\rho e^{i\beta\rho}J_\alpha(k\rho) = \frac{1}{(k^2-\beta^2)^{1/2}}e^{i\alpha\arcsin(\beta/k)}, \quad 0<\beta<k,\ \alpha>-2. \tag{16.65}$$

This gives

$$\begin{aligned}
I_\infty &\equiv \int_0^\infty d\rho' e^{i\rho'\cos\varphi}\left(J_{1+\mu_0} - iJ_{\mu_0}e^{i\varphi}\right) = \frac{1}{|\sin\varphi|}\left[e^{i\mu_0(\pi/2-|\varphi|)} - ie^{i\varphi}e^{i(1+\mu_0)(\pi/2-|\varphi|)}\right] \\
&= \frac{i}{|\sin\varphi|}e^{i\mu_0(\pi/2-|\varphi|)}\left(e^{-i|\varphi|} - e^{i\varphi}\right) = \begin{cases} 0, & \varphi<0, \\ e^{-i\mu_0\varphi}2i^{\mu_0}, & \varphi>0, \end{cases} \qquad (16.66)
\end{aligned}$$

with $\varphi \in (-\pi, \pi)$. Hence we have

$$\psi^{(1)}_\infty = \begin{cases} 0, & \varphi<0, \\ e^{-ikx}e^{-i\mu_0\varphi}, & \varphi>0. \end{cases} \tag{16.67}$$

Using (16.60), we find

$$\psi^{(2)}_\infty = \begin{cases} e^{-ikx}e^{-i\mu_0\varphi}, & \varphi<0, \\ 0, & \varphi>0. \end{cases} \tag{16.68}$$

The sum $\psi^{(1)}_\infty + \psi^{(2)}_\infty$ represents the incoming wave (16.49). The scattered wave must therefore reside in the remainder

$$\psi_{\rm sc} = \Delta\psi^{(1)} + \Delta\psi^{(2)} + \psi^{(3)}. \tag{16.69}$$

For the scattering amplitude, only the leading $1/\sqrt{r}$-behavior of the three terms is relevant. To find it for $\Delta\psi^{(1)}$, we take (16.61) and write the remainder of the integral (16.62) as

$$\Delta I(\rho) \equiv I(\rho) - I_\infty = \int_\rho^\infty d\rho' e^{i\rho'\cos\varphi} \left(J_{1+\mu_0} - ie^{i\varphi} J_{\mu_0} \right). \tag{16.70}$$

At large ρ, the asymptotic expansion

$$J_\alpha(\rho) \sim \sqrt{2/\pi\rho}\,\cos(\rho - \alpha/2 - \pi/4) \tag{16.71}$$

renders

$$\Delta I(\rho) = \sqrt{\frac{2}{\pi}}[A(\rho) + B(\rho)], \tag{16.72}$$

with the integrals

$$\begin{aligned} A(\rho) &= \int_\rho^\infty \frac{d\rho'}{\sqrt{\rho'}} e^{i\rho'\cos\varphi} \cos\left[\rho' - (1+\mu_0)/2 - \pi/4\right], \\ B(\rho) &= -ie^{i\varphi} \int_{\rho'}^\infty \frac{d\rho'}{\sqrt{\rho'}} e^{i\rho'\cos\varphi} \cos\left[\rho' - \mu_0/2 - \pi/4\right]. \end{aligned} \tag{16.73}$$

Separating the cosine into exponentials and changing the variable ρ' in the two terms to $\rho' = t^2/(1 \pm \cos\varphi)$, we find

$$A(\rho) = \left[\frac{(-i)^{1/2+\mu_0}}{\sqrt{1+\cos\theta}} \int_{\sqrt{\rho(1+\cos\varphi)}}^\infty dt e^{it^2} + \frac{i^{3/2+\mu_0}}{\sqrt{1-\cos\theta}} \int_{\sqrt{\rho(1-\cos\varphi)}}^\infty dt e^{-it^2} \right], \tag{16.74}$$

and a corresponding expression for $B(\rho)$. The asymptotic expansion of the error function

$$\int_x^\infty dt e^{\pm it^2} = \pm\frac{i}{2}\frac{\exp(\pm ix^2)}{x} + \ldots \tag{16.75}$$

leads to

$$\begin{aligned} A(\rho) &= \frac{1}{2}\left[(-i)^{\frac{1}{2}+\mu_0} \frac{e^{i\rho}}{\sqrt{\rho(1+\cos\varphi)^2}} + i^{\frac{1}{2}+\mu_0} \frac{e^{-i\rho}}{\sqrt{\rho(1-\cos\varphi)^2}} \right] e^{i\rho\cos\varphi}, \\ B(\rho) &= (-i)\frac{e^{i\varphi}}{2} \\ &\quad \times \left[(-i)^{-\frac{1}{2}+\mu_0} \frac{e^{i\rho}}{\sqrt{\rho(1+\cos\varphi)^2}} + i^{-\frac{1}{2}+\mu_0} \frac{e^{-i\rho}}{\sqrt{\rho(1-\cos\varphi)^2}} \right] e^{i\rho\cos\varphi}. \end{aligned} \tag{16.76}$$

Adding the two terms together in (16.72) and inserting everything into (16.61) gives the asymptotic behavior

$$\Delta\psi^{(1)} = \frac{\sqrt{-i}}{2\sqrt{2\pi\rho}} \left[(-1)^{\mu_0} e^{i\rho} \frac{1+e^{i\varphi}}{1+\cos\varphi} + ie^{-i\rho} \frac{1-e^{i\varphi}}{1-\cos\varphi} \right]. \tag{16.77}$$

Together with $\Delta\psi^{(2)}$ found via (16.60), we obtain

$$\Delta\psi^{(1)} + \Delta\psi^{(2)} = \frac{\sqrt{-i}}{\sqrt{2\pi\rho}} \left[e^{i\rho} \frac{\cos(\pi\mu_0 - \varphi/2)}{\cos(\varphi/2)} + ie^{-i\rho} \right] + e^{-i(\rho\cos\varphi + \mu_0\varphi)}. \tag{16.78}$$

Adding further $\psi^{(3)}$ from (16.59) with the asymptotic limit given by (16.71), the total wave function is seen to behave like

$$\psi(\mathbf{x}) \to e^{-i(\rho\cos\varphi+\mu_0\varphi)} + \psi_{\rm sc}(\mathbf{x}), \tag{16.79}$$

with the scattered wave

$$\psi_{\rm sc} = \frac{1}{\sqrt{2\pi i\rho}} e^{i\rho} \frac{\sin\pi\mu_0}{\cos(\varphi/2)} e^{-i\varphi/2}. \tag{16.80}$$

This corresponds precisely to the scattering amplitude (16.54) with the cross section (16.55).

Let us mention that for half-integer values of μ_0, the solution of the Schrödinger equation has the simple integral representation

$$\psi(\mathbf{x}) = \sqrt{\frac{i}{2}} e^{-i(\varphi/2+\rho\cos\varphi)} \int_0^{\sqrt{\rho(1+\cos\varphi)}} dt e^{it^2}. \tag{16.81}$$

It vanishes on the line $\varphi = \pi$, i.e., directly behind the flux tube and is manifestly single-valued.

16.3 Aharonov-Bohm Effect and Fractional Statistics

It was noted in Section 7.5 and it is worth mentioning once more in this context that the amplitude for the relative motion of two fermion orbits can be obtained from the amplitude of the Aharonov-Bohm effect.

For this, we take the amplitude with $\mu_0 = 1$ and sum it over the final states with φ_b, $\varphi_b + \pi$, to account for particle identity. The result is

$$\begin{aligned}(\mathbf{x}_b|\mathbf{x}_a)_E + (-\mathbf{x}_b|\mathbf{x}_a)_E &= -\frac{2iM}{\hbar} \sum_m I_{|m+1|}(\kappa r_<) K_{|m+1|}(\kappa r_>) \\ &\qquad \times \frac{1}{2\pi} \left[e^{im(\varphi_b-\varphi_a)} + (-)^m e^{im(\varphi_b-\varphi_a)} \right] \\ &= -\frac{4iM}{\hbar} e^{-i(\varphi_b-\varphi_a)} \sum_{m=\rm odd} I_{|m|}(\kappa r_<) K_{|m|}(\kappa r_>) \frac{1}{2\pi} e^{im(\varphi_b-\varphi_a)}. \end{aligned} \tag{16.82}$$

The sum over the two identical final states selects only the odd wave functions, as in (7.267)–(7.268). When calculating observable quantities such as particle densities or partition functions which involve only the trace of the amplitude, the phase factor $e^{-i(\varphi_b-\varphi_a)}$ has no observable consequences and can be omitted.

For $\mu_0 \neq 1$, the resulting amplitudes may be interpreted as describing particles in two dimensions obeying an unusual fractional statistics. This interpretation has recently come to enjoy great popularity,[2] since it has led to an understanding of the experimental data of the fractional quantum Hall effect. The data can be explained by the following assumption: The excitations of a gas of electrons with Coulomb interactions in a quasi-two-dimensional material traversed by a strong magnetic field can be viewed, to lowest approximation, as a gas of quasi-particles which has *no* Coulomb interactions, but a new effective pair interaction. Each pair behaves as if one partner were accompanied by a thin magnetic flux tube of a certain value of μ_0. While the quasi-particles of the ground state carry an integer-valued μ_0 and act statistically like ordinary electrons, the elementary excitations carry a fractional value of μ_0 and display fractional statistics (more in Section 16.11).

To study the fundamental thermodynamic properties of an ensemble of such particles, we calculate the partition function of a particle running around a thin flux tube along the z-axis. For finiteness, we assume the presence of an additional homogeneous magnetic field in the z-direction. Ignoring the third dimension, we take the amplitude (16.33), integrate it over all space, and find

$$\begin{aligned} Z &= \int d^2x (\mathbf{x}_b \tau_b | \mathbf{x}_a \tau_a) \\ &= \frac{1}{2} e^{\mu_0 \eta} \sum_{m=-\infty}^{\infty} e^{m\eta} \int_0^\infty d\xi e^{-\xi \cosh \eta} I_{|m+\mu_0|}(\xi), \end{aligned} \tag{16.83}$$

where

$$\xi \equiv M\omega r^2 / 2\hbar \sinh \eta \tag{16.84}$$

[recall that $\omega = -eB/Mc$ and $\eta = \omega(\tau_b - \tau_a)/2$]. To calculate the partition function, the difference between the Euclidean times τ_b, τ_a is set equal to $\tau_b - \tau_a = \hbar / k_\beta T = \hbar\beta$, so that $\eta = \omega\hbar\beta/2$.

To deal with two identical particles, we also need the integral in which $\mathbf{x}_b$ is exchanged by $-\mathbf{x}_b$:

$$Z_{\text{ex}} = \int d^2x (-\mathbf{x}_b \tau_b | \mathbf{x}_a \tau_a) = \frac{1}{2} e^{\mu_0 \eta} \sum_{m=-\infty}^{\infty} (-)^m e^{m\eta} \int_0^\infty d\xi e^{-\xi \cosh \eta} I_{|m+\mu_0|}(\xi). \tag{16.85}$$

In order to facilitate writing joint equations for both expansions, let us denote Z and Z_{ex} by Z_1 and $Z_{1_{\text{ex}}}$, respectively. The integrals are performed with the help of formula (2.474), yielding the sums

$$Z_{1,1_{\text{ex}}} = \frac{1}{2} \sum_{m=-\infty}^{\infty} (\pm)^m e^{\eta(m+\mu_0)} \frac{1}{\sinh \eta} e^{-\eta|m+\mu_0|}. \tag{16.86}$$

These sums are obviously periodic under $\mu_0 \to \mu_0 + 2$. Because of translational invariance, the partition function $Z \equiv Z_1$ diverges with the total area $V = \int d^2x$ as

[2] See Notes and References at the end of Chapter 7.

an overall factor. To enforce convergence, we multiply the volume elements d^2x with an exponential regulating factor $e^{-\epsilon\xi}$. Then the area integrals can be extended over all space. In terms of the variable ξ of (16.84), the measure in the above rotationally symmetric integrals can be written as

$$d^2x = l_{\rm e}^2(T)\frac{\sinh\eta}{\eta}d\xi, \tag{16.87}$$

with the thermal length $l_{\rm e}(T) \equiv \sqrt{2\pi\hbar^2/k_BTM}$ introduced in Eq. (2.354). The role of the total area $V = \int d^2x$ is now played by the finite quantity

$$V \equiv \int d^2x e^{-\epsilon\xi} = \frac{l_{\rm e}^2(T)}{\epsilon}\frac{\sinh\eta}{\eta}. \tag{16.88}$$

Inserting the factor $e^{-\epsilon\xi}$ into the integrals in Eqs. (16.83) and (16.85), and defining a variable η' slightly different from η by

$$\cosh\eta' \equiv \epsilon + \cosh\eta, \tag{16.89}$$

which has the expansion

$$\begin{aligned} e^{\eta'} &= \cosh\eta' + \sqrt{\cosh^2\eta' - 1} \\ &= e^{\eta}\left(1 + \frac{\epsilon}{\sinh\eta} - \frac{1}{2}e^{-\eta}\frac{\epsilon^2}{\sinh^3\eta} + \ldots\right), \quad \eta > 0, \end{aligned} \tag{16.90}$$

the regulated sums (16.86) for Z_1 and $Z_{1_{\rm ex}}$ look almost the same as before:

$$Z_{1,1_{\rm ex}} = \frac{1}{2}\sum_{m=-\infty}^{\infty}(\pm)^m e^{\eta(m+\mu_0)}\frac{1}{\sinh\eta'}e^{-\eta'|m+\mu_0|}. \tag{16.91}$$

Separating positive and negative values of $m + \mu_0$, the two sums can be done for $\mu_0 \in (0, 1)$ and for $\mu_0 \in (-1, 0)$. In the combined interval $\mu_0 \in (-1, 1)$, we find

$$Z_{1,1_{\rm ex}} = \frac{1}{2}e^{\eta\mu_0}\frac{1}{\sinh\eta'}\left\{\frac{e^{-\eta'\mu_0}}{1\mp a} + \frac{e^{\eta'\mu_0}}{1\mp b} - e^{\eta'|\mu_0|}\right\}, \tag{16.92}$$

where

$$a \equiv e^{\eta-\eta'}, \quad b \equiv e^{-\eta-\eta'}.$$

Two identical particles have the partition function

$$Z = \frac{1}{2}(Z_1 + Z_{1_{\rm ex}}) = \frac{1}{2}e^{\eta\mu_0}\frac{1}{\sinh\eta'}\left\{\frac{e^{-\eta'\mu_0}}{1-a^2} + \frac{e^{\eta'\mu_0}}{1-b^2} - e^{\eta'|\mu_0|}\right\}. \tag{16.93}$$

It is symmetric under the simultaneous exchange $\mu_0 \to -\mu_0,\ \eta \to -\eta$. Outside the interval $\mu_0 \in (-1, 1)$, it is defined by periodic extension.

In the absence of the thin flux tube we may take $Z_{1,1_{\rm ex}}$ directly from the amplitude (2.668). For $\mathbf{x}_b = \mathbf{x}_a$ and $\mathbf{x}_b = -\mathbf{x}_a$, this yields with the present variables

$$(\mathbf{x}_a\tau_b|\mathbf{x}_a\tau_a) = l_{\rm e}^{-2}(T)\frac{\eta}{\sinh\eta}, \quad (-\mathbf{x}_a\tau_b|\mathbf{x}_a\tau_a) = l_{\rm e}^{-2}(T)\frac{\eta}{\sinh\eta}e^{-2\cosh\eta\ \xi}. \quad (16.94)$$

Their regulated spatial integrals are

$$\begin{aligned} Z_{1,0} &= \frac{1}{2}\int_0^\infty d\xi e^{-\epsilon\xi} = \frac{1}{2\epsilon}, \\ Z_{1_{\rm ex},0} &= \frac{1}{2}\int_0^\infty d\xi e^{-(\epsilon+2\cosh\eta)\xi} = \frac{1}{2(\epsilon+2\cosh\eta)}. \end{aligned} \quad (16.95)$$

The subtracted partition functions $\Delta Z_{1,1_{\rm ex}} \equiv Z_{1,1_{\rm ex}} - \frac{1}{2}Z_{1,0}$ have a finite $\epsilon \to 0$ -limit, and $\Delta Z = Z - \frac{1}{2}Z_{1,0}$ becomes for $\mu_0 \in (0,2)$

$$\Delta Z = -\frac{1}{8\sinh\eta}\left[\coth\eta + 2(\mu_0 - 1) - 2e^{2(\mu_0+1)\eta}\frac{1}{\sinh 2\eta} + 4e^{2\eta\mu_0}\right]. \quad (16.96)$$

These results can be used to calculate the second coefficient appearing in a *virial expansion* of the equation of state. For a dilute gas of particles with the above magnetic interactions it reads

$$\frac{pV}{Nk_BT} = 1 + \sum_{r=2}^{\infty} B_r n^{r-1}. \quad (16.97)$$

Here n is the number density of the particles N/V. In many-body theory it is shown that the coefficient B_2 depends on the two-body partition function Z_2 as follows:

$$B_2 = V\left(\frac{1}{2} - \frac{Z_2}{Z_1^2}\right), \quad (16.98)$$

where Z_1 is the two-dimensional single particle partition function of mass M. In the presence of the homogeneous magnetic field, Z_1 is given by $Z_{1,0}$ of Eq. (16.95). Without the regulating factor, the spatial integral over the imaginary-time amplitude in (16.94) gives directly

$$Z_1 = V\frac{\eta}{l_{\rm e}^2(T)\sinh\eta}. \quad (16.99)$$

Separating the center of mass from the relative motion, we see that $Z_2 = 2Z_1Z_{\rm rel}$ and obtain

$$B_2 = \frac{V}{Z_1}(Z_1/2 - 2Z_{\rm rel}) = \frac{l_{\rm e}^2(T)\sinh\eta}{2\eta}(Z_1 - 4Z_{\rm rel}). \quad (16.100)$$

The difference on the right-hand side is convergent for $V \to \infty$. It can be evaluated using *any* regulator for the area integration, in particular the exponential regulator of Eq. (16.88).

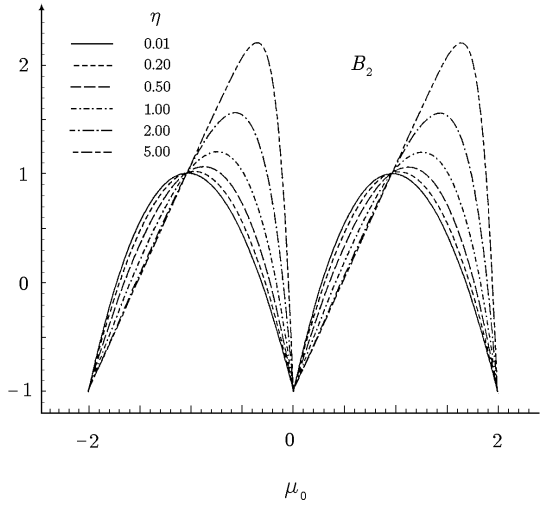

Figure 16.1 Second virial coefficient B_2 as function of flux μ_0 for various external magnetic field strengths parametrized by $\eta = -(eB/2Mc)\hbar\beta$. For a better comparison, each curve has been normalized to unity at $\mu_0 = 0$.

The partition function for the relative motion of two identical particles is obtained from Z by replacing M by the reduced mass, i.e., $M \to M/2$. This renders a factor $1/2$ via $l_{\rm e}^{-2}(T)$. Hence $Z_1/2 - 2Z_{\rm rel}$ becomes equal to $-\Delta Z$ and (16.100) yields [5]

$$B_2 = \frac{l_{\rm e}^2(T)}{4\eta}\left[\coth\eta + 2(\mu_0 - 1) - 2e^{2(\mu_0+1)\eta}\frac{1}{\sinh(2\eta)} + 4e^{2\eta\mu_0}\right]. \tag{16.101}$$

The behavior of B_2 as a function of μ_0 is shown in Fig. 16.1. In the absence of a magnetic field, it reduces to

$$B_2 = \frac{l_{\rm e}^2(T)}{4}\left[1 - 2(1 - |\mu_0|^2)^2\right], \quad \mu_0 \in (-1, 1). \tag{16.102}$$

As μ_0 grows from zero to infinity, B_2 oscillates with a period 2 between $B_2 = -l_{\rm e}^2(T)/4$ for even values of μ_0, and $B_2 = l_{\rm e}^2(T)/4$ for odd values. These are the well-known second *virial coefficients* of free bosons and fermions. They can, of course, be obtained in a simpler and more direct way from the symmetric and antisymmetric combinations of (16.95), $Z_0 = (1/2)(Z_{1,0} \pm Z_{1_{\rm ex},0})$. Subtracting $Z_{1,0}$ leaves $\pm Z_{1_{\rm ex},0}/2$ which reduces for $\eta = 0$ to $\pm 1/8$. Accounting for the factor 2 in the reduced mass, this yields $B_2 = \mp l_{\rm e}^2(T)/4$.

The expression (16.102) can be interpreted as the *virial coefficient* of particles which are neither bosons nor fermions, but obey the laws of fractional statistics. These particles are the *anyons* introduced in Section 7.5. Unfortunately, there are at present no experimental data for the virial coefficients to which the theoretical expressions (16.102) [or (16.101)] could be compared.

At this point we should mention older, meanwhile discarded speculations that the phenomenon of high-temperature superconductivity might be explained by fractional statistics of some elementary excitations. Indeed, the change in statistics can

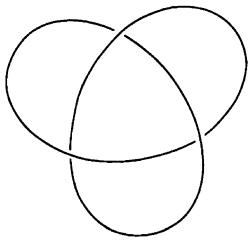

Figure 16.2 Lefthanded trefoil knot in polymer.

be derived from the electromagnetic interaction between the electrons in a quasi-two-dimensional layer of material moving in a strong magnetic field. Also, it is possible to construct a model of anyonic two-dimensional superconductivity in which topological effects lead to a Meissner screening of magnetic fields (see Section 16.13). A closer investigation, however, shows that the currents in the model show dissipation after all.

It must be emphasized that the equality between electromagnetic and statistical interaction used in the above calculations is restricted to two-particle systems and cannot be extended to arbitrarily many particles as in Section 7.5. Although it is possible to distribute the magnetic flux in a many-particle system equally between the constituents producing the desired behavior under particle exchange, an equal distribution of the charges would create an unwanted additional Coulomb potential, and the purely topological character of the interaction would be destroyed. The problem does not arise for charged particles such as electrons. Nevertheless, there is a definite need for a better and universally applicable theoretical description of anyons. This will be presented in Section 16.7.

16.4 Self-Entanglement of Polymer

An interesting consequence of the excluded-volume properties of polymers is the possibility of a self-entanglement of a closed polymer. Since its line elements are forbidden to cross each other, the fluctuations are unable to explore all possible configurations. An initially circular polymer, for example, can never turn into a *trefoil knot* of the form shown in Fig. 16.2 without breaking a molecular bond.
In the chemical formation process of a large number of polymers, many

entangled configurations arise. It is an interesting problem to find the distribution of the various independent topology classes. Until recently, the lack of theoretical methods has made analytic work almost impossible, restricting it to classification questions. Only Monte Carlo methods have yielded quantitative insights. Since 1989, however, interesting new quantum field-theoretic methods have been developed promising significant progress in the near future. Here we survey these methods and indicate how to derive analytic results. First, we introduce the relevant topological concepts.

A closed polymer will in general form a knot. A circular polymer represents a trivial knot. Two knots are called *equivalent* if they can be deformed into each

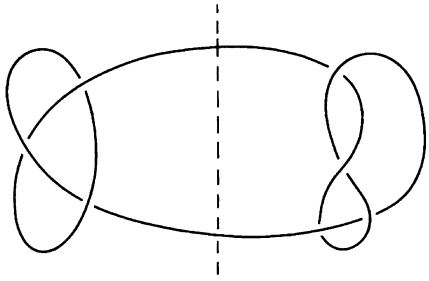

Figure 16.3 Nonprime (compound) knot. The dashed line separates two pieces. After closing the open ends, the pieces form two prime knots.

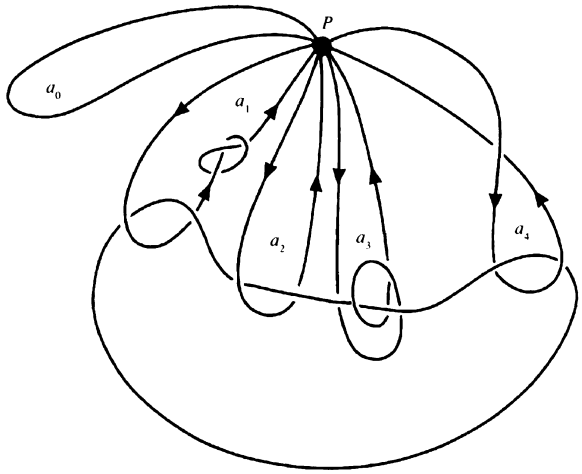

Figure 16.4 Illustration of multiplication law $a_1 a_2 \approx a_3$ in knot group. The loops a_1 and a_2 are equivalent, $a_1 \approx a_2$, while $a_4 \approx a_1^{-1}$.

other without breaking any line. Such deformations are called *isotopic*. A first step towards the classification consists in separating the equivalence classes into irreducible and reducible ones, defining *prime* or *simple* knots and *nonprime* or *compound* knots, respectively. A *compound* knot is characterized by the existence of a plane which is intersected twice (after some isotopic deformation) (see Fig. 16.3). By closing the open ends on each side of the plane one obtains two new knots. These may or may not be reduced further in the same way until one arrives at simple knots. One important step towards distinguishing different equivalence classes of simple and compound knots is the *knot group* defined as follows. In the multiply connected space created by a certain knot, choose an arbitrary point P (see Fig. 16.4). Then consider all possible closed loops starting from P and ending again at P. Two such loops are said to be *equivalent* if they can be deformed into each other without crossing the lines of the knot under consideration. The loops are, however, allowed to have arbitrary self-intersections. The classes of equivalent knots form the knot group. Group multiplication is defined by running through any two loops of two equivalence classes successively. The class whose loops can be contracted into the

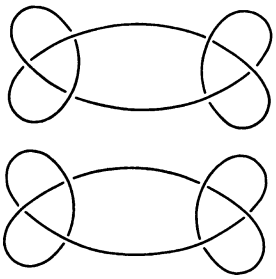

Figure 16.5 Inequivalent (compound) knots possessing isomorphic knot groups. The upper is the *granny knot*, the lower the *square knot*. They are stereoisomers characterized by the same Alexander polynomial $(t^2 - t + 1)^2$ but different HOMFLY polynomials [see (16.126)].

point P is defined as the unit element e. Changing the orientation of the loops in a class corresponds to inverting the associated group element.

In this way, the classification of knots can be related to the classification of all possible knot groups. Consider the trivial knot, the circle. Obviously, the closed loops through P fall into classes labeled by an integer number n. The associated knot group is the group of integers. Conversely, no nontrivial knot is associated with this group.

Although this trivial example might at first suggest a one-to-one correspondence between the simple knots and their knot groups, there is none. Many examples are known where inequivalent knots have isomorphic knot groups. In particular, all mirror-reflected knots which usually are inequivalent to the original ones (such as the right- and left-handed trefoil), have the same knot group. Thus, the knot groups necessarily yield an *incomplete* classification of knots. An example is shown in Fig. 16.5.

Fortunately, the degeneracies are quite rare. Only a small fraction of inequivalent knots cannot be distinguished by their knot groups.

The easiest way of picturing a knot in 3 dimensions is by drawing its projection onto the paper plane. The lines in the projection show a number of *crossings*, and the drawing must distinguish the top from the bottom line. The knot is then deformed isotopically until the projection has the minimal number of crossings. In the projection, all isotopic deformations can be decomposed into a succession of three elementary types, the so-called *Reidemeister moves* shown in Fig. 16.6.

A picture of all simple knots up to $n = 8$ is shown in Fig. 16.7. The numbers of inequivalent simple and compound knots with a given number n of minimal crossings are listed in Table 16.1.

The projected pictures can be used to construct an important algebraic quantity characterizing the knot group, called the *Alexander polynomial* discovered in 1928. It reduces the classification of knot groups to that of polynomials. This type of work is typical of the field of algebraic topology.

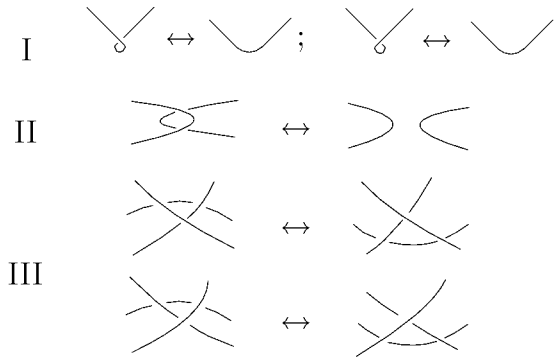

Figure 16.6 *Reidemeister moves* in projection image of knot which do not change its class of isotopy. They define the movements of *ambient isotopy*. For ribbons, only the second and third movements are allowed, defining the *regular isotopy*. The first movement is forbidden since it changes its writhe [for the definition see Eq. (16.110)].

Table 16.1 Numbers of simple and compound knots with n minimal crossings in a projected plane.

n	simple knots	compound knots
0	1	0
1	0	0
2	0	0
3	1	0
4	1	0
5	2	0
6	3	1
7	7	1
8	21	3
9	49	5
10	166	10
11	548	37
12	–	154
13	–	484
14	–	1115

We explain the construction for the trefoil knot. Attaching a directional arrow to the polymer and selecting an arbitrary starting point, we follow the arrow until we run into a first underpass. This point is denoted by 1. Now we continue to the next underpass denoted by 2, etc., up to n (see Fig. 16.8). The polymer sections between two successive underpasses i and $i+1$ are named x_{i+1}. At each underpass from x_i to x_{i+1}, we record (see Table 16.2) whether the overpassing section x_k runs from right to left (type r) or from left to right (type l). We now set up a matrix A_{ij}. Each underpass with label i defines a row $A_{ij},\ j = 1, 2, 3, \ldots$ according to the

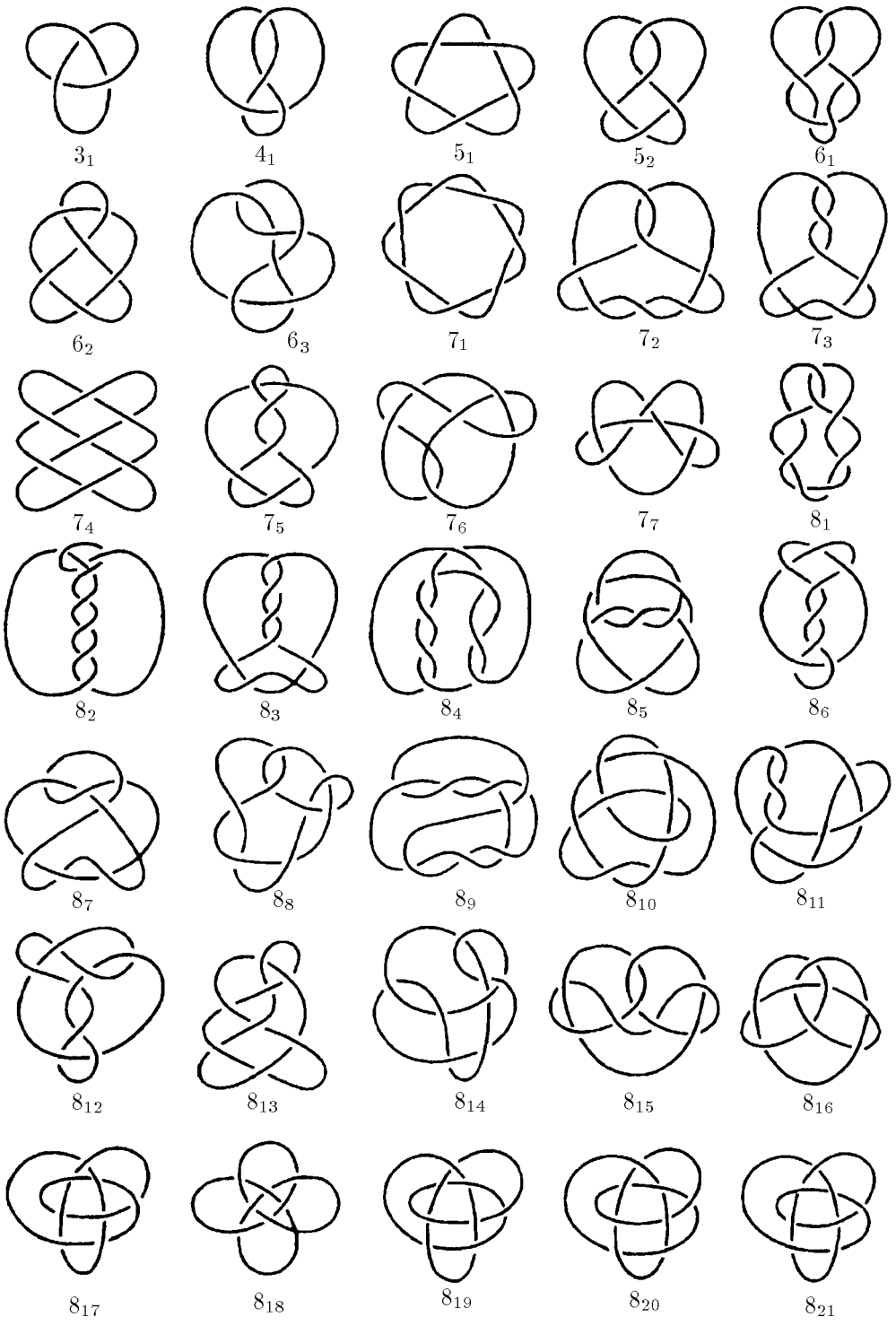

Figure 16.7 Simple knots with up to 8 minimal crossings. The number of crossings under each picture carries a subscript enumerating the equivalence classes.

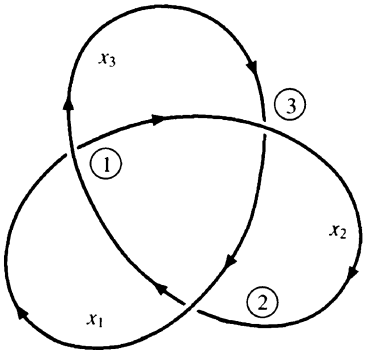

Figure 16.8 Labeling of underpasses for construction of Alexander polynomial t^2-t+1 of the left-handed trefoil.

Table 16.2 Tables of underpasses (under) and directions (dir) r or l ofoverpassing lines (over), for trefoil knot 3_1 and knot 4_1 of Fig. 16.7.

3_1 :

under	over	dir
x_1	x_3	r
x_2	x_1	r
x_3	x_2	r

4_1 :

under	over	dir
x_1	x_4	r
x_2	x_1	l
x_3	x_2	r
x_4	x_3	l

following rules: Let x_k be the overpassing section. If x_k coincides with x_i or x_{i+1} the underpass is called *trivial*. In this, case the ith row of the matrix A_{ij} has the elements

$$A_{ii}=-1, \quad A_{i,i+1}=1. \tag{16.103}$$

All other row elements A_{ij} vanish. If the underpass is nontrivial, the nonvanishing row elements are

$$A_{ii}=1,\ A_{ii+1}=-t,\ A_{ik}=t-1, \quad \text{type r (right to left)}, \tag{16.104}$$

$$A_{ii}=-t,\ A_{ii+1}=1,\ A_{ik}=t-1, \quad \text{type l (left to right)}. \tag{16.105}$$

In this way, we find the matrix of the trefoil knot:

$$A_{ij}=\begin{pmatrix} 1 & -t & t-1 \\ t-1 & 1 & -t \\ -t & t-1 & 1 \end{pmatrix}. \tag{16.106}$$

As another example, the knot 4_1 in Fig. 16.7 has the matrix

$$A_{ij}=\begin{pmatrix} 1 & -t & 0 & t-1 \\ t-1 & -t & 1 & 0 \\ 0 & t-1 & 1 & -t \\ 1 & 0 & t-1 & -t \end{pmatrix}. \tag{16.107}$$

Table 16.3 Alexander, Jones, and HOMFLY polynomials for smallest simple knots up to 8 crossings. The numbers specify the coefficients; for instance, the knot 7_1 has the Alexander polynomial $A(t) = 1 - t + t^2 - t^3 + t^4 - t^5 + t^6$ and the knot 8_8 has the Jones polynomial $J(t) = t^{-3}(1 - t + 2t^2 - t^3 + t^4)$. For the HOMFLY polynomial $H(t, \alpha)$, see the explanation on p. 1125.

	$A(t)$	$J(t)$	$H(t,\alpha)$	
3_1	1−11	(0)1	([0]2−1)([0]1)	
4_1	1−31	(−2)−1	(1[−1]1)([−1])	
5_1	1−11−11	(0)1101	([0]03−2)([0]041)([0]01)	
5_2	2−32	(0)101	([0]11−1)([0]11)	
6_1	2−52	(−2)−10−1	(1[0]−11)([−1]−1)	
6_2	1−33−31	(−1)−11−1	([2]−21)(1[−3]1)([0]1)	
6_3	1−35−31	(−3)1−11	(−1[3]−1)(−1[3]−1)(1)	s
7_1	1−11−11−11	(0)1111101	([0]004−3)([0]0010−4)([0]006−1)([0]001)	
7_2	3−53	(0)10101	([0]10−11)([0]111)	
7_3	2−33−32	(0)110201	(−22−10[0])(−1330[0])(1100[0])	
7_4	4−74	(0)10201	(−1020[0])(121[0])	
7_5	2−45−42	(0)1102−11	([0]020−1)([0]032−1)([0]011)	
7_6	1−57−51	(−1)−12−11	([1]−12−1)([1]−22)([0]−1)	
7_7	1−59−52	(−3)1−21−1	(1−2[2])(−2[2]−1)([1])	
8_1	3−73	(−2)−10−10−1	(1−10[0]1)(−1−1[−1])	
8_2	1−33−33−31	(1)1−11−1	(1−33[0])(3−74[0])(1−51[0])(−10[0])	
8_3	4−94	(−4)−10−20−1	(10[−1]01)(−1[−2]−1)	s
8_4	2−55−52	(−3)−10−21−1	(2[−2]01)(1[−3]−21)([−1]−1)	
8_5	1−34−55−31	(1)1−21−1	(2−54[0])(3−84[0])(1−51[0])(−10[0])	
8_6	2−67−62	(−1)−11−21−1	(1−1−1[2])(1−2−2[1])(−1−1[0])	
8_7	1−35−55−31	(−2)1−12−11	([−1]4−2)([−3]8−3)([−1]5−1)([0]1)	
8_8	2−69−62	(−3)1−12−11	(−1[2]1−1)(−1[2]2−1)([1]1)	
8_9	1−35−75−31	(−4)−11−21−1	(2[−3]2)(3[−8]3)(1[−5]1)([−1])	s
8_{10}	1−36−76−31	(−2)1−13−11	([−2]6−3)([−3]9−3)([−1]5−1)([0]1)	
8_{11}	2−79−72	(−1)−12−21−1	(1−21[1])(1−2−1[1])(−1−1[0])	
8_{12}	1−7(13)−71	(−4)−11−31−1	(1−1[1]−11)(−2[1]−2)([1])	s
8_{13}	2−7(11)−72	(−3)1−22−11	([0]2−1)(−1[1]2−1)([1]1)	
8_{14}	2−8(11)−82	(−1)−12−22−1	([1])(1−1−1[1])(1−1[0])	
8_{15}	3−8(11)−83	(0)1103−22−1	(1−4310[0])(−3520[0])(210[0])	
8_{16}	1−48−98−41	(−2)1−23−21	([0]2−1)([−2]5−2)([−1]4−1)([0]1)	
8_{17}	1−48−(11)8−41	(−4)−12−32−1	(1[−1]1)(2[−5]2)(1[−4]1)([−1])	s
8_{18}	1−5(10)−(13)(10)−51	(−4)−13−33−1	(−1[3]−1)(1[−1]1)(1[−3]1)([−1])	s
8_{19}	1−1010−11	(0)11111	(1−5500[0])(−5(10)00[0])(−1600[0])(100[0])	
8_{20}	1−23−21	(−1)101	([−1]4−2)([−1]4−1)([0]1)	
8_{21}	1−45−41	(0)1−11−1	(1−33[0])(1−32[0])(−10[0])	

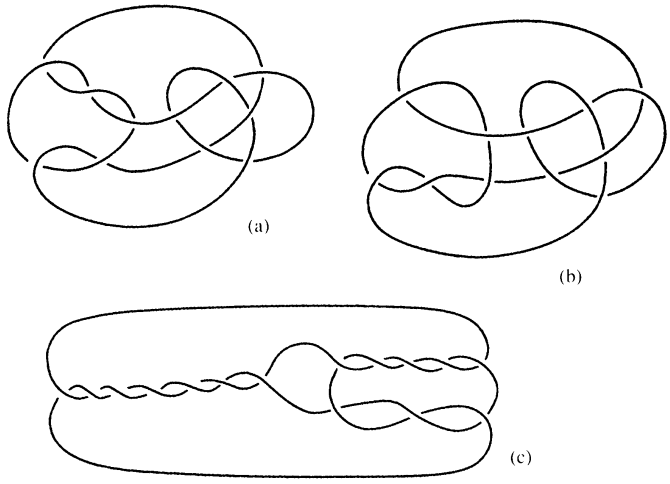

Figure 16.9 Exceptional knots found by Kinoshita and Terasaka (a), Conway (b), and Seifert (c), all with same Alexander polynomial as trivial knot [$|A(t)| \equiv 1$].

Having set up the $n \times n$-matrix A_{ij}, we choose an arbitrary subdeterminant (minor) of order $n-1$. It is a polynomial in t with integer coefficients. This polynomial is divided by a suitable power of t to make it start out with a constant. The result is the Alexander polynomial $A(t)$. It is independent of the choice of the subdeterminant.

For the left-handed trefoil, the matrix (16.106) yields

$$A(t) = t^2 - t + 1. \tag{16.108}$$

For the knot 4_1, we find from (16.107)

$$A(t) = t^2 - 3t + 1. \tag{16.109}$$

The Alexander polynomials of the simple knots in Fig. 16.7 are shown in Table 16.3. Note that the replacement $t \to 1/t$ leaves the Alexander polynomial invariant (after renormalizing it back by some power of t to start out with a constant).

The Alexander polynomial of a composite knot factorizes into those of the simple knots it is composed of. If two knots are mirror images of each other, they have the same knot group and the same Alexander polynomials. Due to the factorization property, two composite knots whose simple parts differ by mirror reflection (*stereoisomers*; see Fig. 16.5) have the same polynomial. Thus the Alexander polynomial cannot render a complete classification of inequivalent knots. This is true even after removing degeneracies of the above type. In Fig. 16.9, we give the simplest examples of knots with an Alexander polynomial $A(t) \equiv \pm 1$ of the trivial knot. Up to 11 crossings, these are the only examples. Since the total number of simple knots up to $n = 11$ is 795, the exceptions are indeed very few.

Recent years have witnessed the development of simpler construction procedures and more efficient polynomials for the classification of knots and links of several

knots, the Jones and the *HOMFLY polynomials*[3] and their generalizations. The former depend on one, the latter on two variables, one of which occurs also with inverse powers, i.e., in this variable the polynomials are of the Laurent type. Other polynomials found in the literature, such as *Conway*, *X*-, or *Kauffman's bracket polynomials*, are special cases of the HOMFLY polynomials. In addition, there exist a different type of *Kauffman polynomials* and of *BLM/Ho polynomials* $F(a, z)$ and $Q(x)$, respectively, which are capable of distinguishing some knots with accidentally degenerate HOMFLY polynomials. They will not be discussed here. For their definition see Appendix 16B.

The X-polynomial $X(a)$ is trivially related to the Jones polynomial $J(t)$, to which it reduces after a variable change $a = t^{1/4}$. The X-polynomial is closely related to the Kauffman polynomial $K(a)$ by

$$X(a) = (-a)^{-3w} K(a). \tag{16.110}$$

The number w is the *cotorsion*, also called *twist number*, *Tait number*, or *writhe* [6]. It is defined by giving the loop or link an orientation and attributing to each crossing a number 1 or -1 according to the following rule. At each crossing follows the overpass along the direction of orientation. If the underpass runs from right to left, the crossing carries the number 1, otherwise -1. The sum of these numbers is the cotorsion w. In the trefoil knot in Fig. 16.2 each crossing carries a -1 so that $w = -3$.

The Kauffman polynomial is found by a very simple construction procedure. A set of n trivial loops is defined to have the Laurent polynomial

$$K_n(a) = -(a^2 + a^{-2})^{n-1}. \tag{16.111}$$

Every knot or link can be reduced to such loops by changing the crossings recursively into two new configurations according to the graphical rule shown in Fig. 16.10.

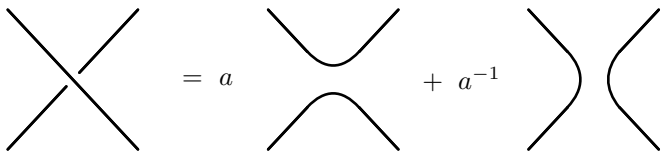

Figure 16.10 Graphical rule for removing crossing in generating Kauffman polynomial.

The first configuration is associated with a factor a, the second with a factor a^{-1}. The configuration receiving the factor a is most easily identified by approaching the crossing on the underpassing curve and taking a right turn. The two new

[3]The word "HOMFLY" collects the initials of the authors (Hoste, Ocneanu, Millet, Freyd, Lickorish, Yetter). The papers are quoted in Notes and References.

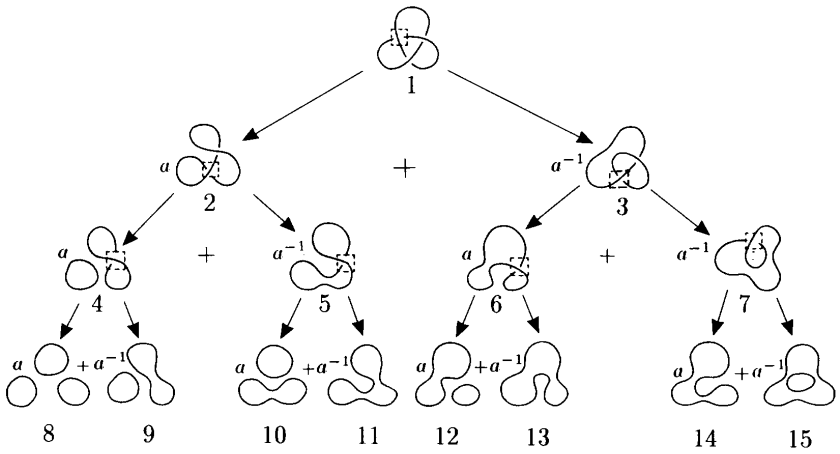

Figure 16.11 Kauffman decomposition of trefoil knot. The configuration 3 is the Hopf link. The calculation of the associated polynomials is shown in Table 16.4.

Table 16.4 Kauffman polynomials in decomposition of trefoil knot.

link	bracket polynomial	rule
15	$-a^2 - a^{-2}$	Eq. 16.111
14	1	Eq. 16.111
13	1	Eq. 16.111
12	$-a^2 - a^{-2}$	Eq. 16.111
11	1	Eq. 16.111
10	$-a^2 - a^{-2}$	Eq. 16.111
9	$-a^2 - a^{-2}$	Eq. 16.111
8	$-a^4 - 2 - a^{-4}$	Eq. 16.111
7	$-a^{-3}$	$a\langle 14\rangle + a^{-1}\langle 15\rangle$, Fig. 16.10
6	$-a^3$	$a\langle 12\rangle + a^{-1}\langle 13\rangle$, Fig. 16.10
5	$-a^3$	$a\langle 10\rangle + a^{-1}\langle 11\rangle$, Fig. 16.10
4	$a^5 + a$	$a\langle 8\rangle + a^{-1}\langle 9\rangle$, Fig. 16.10
3	$-a^4 - a^{-4}$	$a\langle 6\rangle + a^{-1}\langle 7\rangle$, Fig. 16.10
2	a^6	$a\langle 4\rangle + a^{-1}\langle 5\rangle$, Fig. 16.10
1	$a^7 - a^3 - a^{-5}$	$a\langle 2\rangle + a^{-1}\langle 3\rangle$, Fig. 16.10

configurations are processed further in the same way and so on until one arrives only at trivial loops. By applying these rules to a trefoil knot, we obtain a knot and a link known as the *Hopf link*. These are decomposed further as shown in Fig. 16.11. The Kauffman polynomials of each part are listed in Table 16.4. The polynomial of the trefoil knot is

$$K(a) = a^7 - a^3 - a^{-5}. \tag{16.112}$$

Since $w = -3$, we obtain with the factor $(-a)^{-3w} = -a^9$ the X-polynomial

$$X(a) = -a^{16} + a^{12} + a^4. \tag{16.113}$$

This corresponds to a Jones polynomial $J(t) = t + t^3 - t^4$.

For the Jones polynomials, there exists a simple direct construction. According to J.H. Conway, any knot can be related to lower knots or links by performing the *skein operations* shown in Fig. 16.12 on any crossing in the projection plane. Either

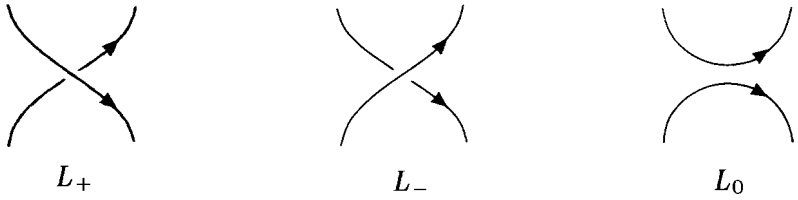

Figure 16.12 Skein operations relating higher knots to lower ones.

a crossing L_+ is transformed into L_- and L_+, or L_+ is transformed into L_- and L_0. For knots related in this way one defines the Jones polynomial $J(t)$ recursively by the *skein relation*

$$\frac{1}{t} J_{L_+}(t) - t J_{L_-}(t) = \left(\sqrt{t} - \frac{1}{\sqrt{t}}\right) J_{L_0}(t). \tag{16.114}$$

The circular loop is defined to have the trivial polynomial $J(t) \equiv 1$. By applying the skein operations to two disjoint unknotted loops in Fig. 16.13, one finds the Jones polynomial

$$J_2(t) = -(\sqrt{t} + 1/\sqrt{t}). \tag{16.115}$$

Upon carrying this procedure to n such loops, we find

$$J_n(t) = [-(\sqrt{t} + 1/\sqrt{t})]^{n-1}, \tag{16.116}$$

in agreement with (16.111). For the lowest knots, the Jones polynomials are listed in Table 16.3. Up to nine crossings, the Jones polynomials distinguish mirror-symmetric knots.

Conway discovered the first skein relation in 1970 when trying to develop a computer program for calculating Alexander polynomials. He found the Alexander polynomials to obey modulo the normalization convention, the skein relation

$$A_{L_+}(t) - A_{L_-}(t) = (\sqrt{t} - 1/\sqrt{t}) A_{L_0}(t), \tag{16.117}$$

which eventually reduces the polynomials of all knots to the trivial one $A_1(t) = 1$. The skein relation simplifies the procedure so much that Conway was able to work out by hand all polynomials known at that time. Because of the simplicity of

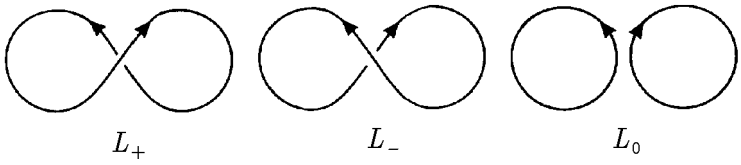

Figure 16.13 Skein operations for calculating Jones polynomial of two disjoint unknotted loops.

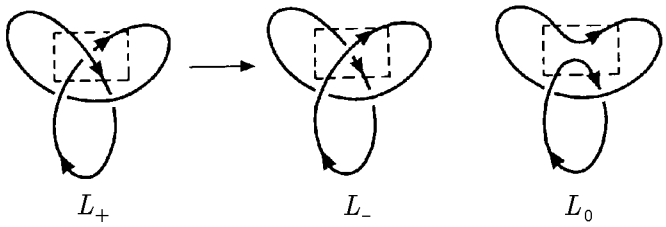

Figure 16.14 Skein operation for calculating Jones polynomial of trefoil knot.

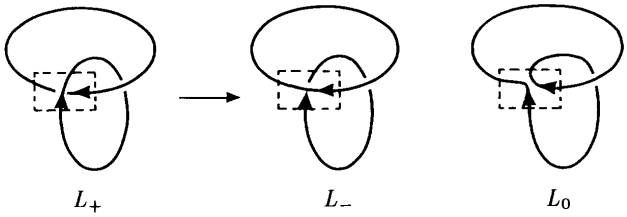

Figure 16.15 Skein operation for calculating Jones polynomial of Hopf link.

this procedure, the Alexander polynomials are now often referred to as *Alexander-Conway polynomials*.

Let us now calculate the Jones polynomial for the trefoil knot 3_1 of Fig. 16.7. First we apply the skein operation shown in Fig. 16.14. The loop L_- is unknotted and has a unit polynomial. Thus we obtain the polynomial relation

$$J_{\text{trefoil}}(t)J_{L_+}(t) = t^2 \cdot 1 + t(\sqrt{t} - 1/\sqrt{t})J_{L_0}(t). \tag{16.118}$$

The configuration L_0 is known as a *Hopf link*. It needs one more reduction[4] via the operation shown in Fig. 16.15, resulting in the relation

$$\frac{1}{t}J_{L_+^0}(t) = tJ_2(t) + (\sqrt{t} - 1/\sqrt{t})J_1(t). \tag{16.119}$$

[4]The Kauffman bracket polynomial of the Hopf link is $K_{L_0}(a) = -a^4 - a^{-4}$. Together with the cotorsion $w = -2$, this amounts to an X-polynomial $X(a) = -a^{10} - a^2$ and the Jones polynomial $J_{L_0}(t) = -\sqrt{t}(1 + t^2)$ as in (16.120).

Using (16.111), we find

$$J_{L_0}(t) = -\sqrt{t}(1+t^2). \tag{16.120}$$

Inserting this into (16.118) leads to the Jones polynomial of the trefoil knot

$$J_{\text{trefoil}} = t + t^3 - t^4. \tag{16.121}$$

It differs from the result found above for the left-handed trefoil by the substitution $t \to t^{-1}$.

The HOMFLY polynomials $H_L(t,\alpha)$ are obtained from a slight generalizations of the skein relation (16.114) of the Jones polynomials: The factor $(\sqrt{t} - 1/\sqrt{t})$ on the right-hand side is replaced by an arbitrary parameter α, leading to the skein relation

$$\frac{1}{t} H_{L_+}(t,\alpha) - t H_{L_-}(t,\alpha) = \alpha H_{L_0}(t,\alpha). \tag{16.122}$$

The trivial knot is defined to have the trivial polynomial $H_1(t,\alpha) = 1$. For two independent loops, the relation yields

$$H_2(t,\alpha) = (t^{-1} - t)\alpha^{-1}. \tag{16.123}$$

The HOMFLY polynomials $H(t,\alpha)$ transform under a mirror reflection of the knot into $H(-t^{-1},\alpha)$. Note that $H_2(t,\alpha)$ is mirror-symmetric [$H_1(t,\alpha)$ is trivially so].[5] In general, the HOMFLY polynomials give reliable information on a possible mirror symmetry. There are, however, a few exceptions, i.e., mirror-related pairs of knots possessing the same HOMFLY polynomial.[6]

Examples for HOMFLY polynomials are

$$\begin{aligned}
H_{\text{trefoil(rh)}}(t,\alpha) &= -t^4 + 2t^2 + t^2\alpha^2, \\
H_{\text{trefoil(lh)}}(t,\alpha) &= -t^{-4} + 2t^{-2} + t^{-2}\alpha^2, \\
H_{\text{Hopf(rh)}}(t,\alpha) &= (t - t^3)\alpha^{-1} + t\alpha, \\
H_{\text{knot } 4_1}(t,\alpha) &= t^{-2} - 1 + t^2 - \alpha^2.
\end{aligned} \tag{16.124}$$

Setting $\alpha = t^{1/2} - t^{-1/2}$ produces the Jones polynomials, while $t \to 1, \alpha \to t^{1/2} - t^{-1/2}$ leads, with appropriate powers of t as normalization factors, back to the Alexander-Conway polynomials.

In Table 16.3, the HOMFLY polynomials are listed for knots up to 8 crossings. For mirror-unsymmetric knots, only one partner is recorded. The reflected polynomial is obtained by the substitution $t \to -t^{-1}$. The meaning of the entries is best explained with an example: The knot 7_1 has an entry $([0]004 - 3)([0]00(10) - 4)([0]006 - 1)([0]001)$, which stands for the polynomial

[5] For the Kauffman polynomials $F(a,x)$ defined in Appendix 16B, mirror reflection implies $F(a,x) \to F(a^{-1},x)$.

[6] The first degeneracy of this type occurs for a link of 3 loops with 8 crossings.

$H(t,\alpha) = (4t^6 - 3t^8) + (10t^6 - 4t^8)\alpha^2 + (6t^6 - t^8)\alpha^4 + t^6\alpha^6$. A bracket marks the position and coefficient of the zeroth power in t^2; the numbers to the right and the left of it specify the coefficients of the adjacent higher and lower powers of t^2, respectively. Numbers with more than one digit are put in parentheses. The polynomial of the reflected knot is obtained by reflecting the numbers in parentheses on the associated bracket. The knots marked by an s are mirror-symmetric.

The Alexander-Conway polynomials are special cases of the HOMFLY polynomials. A comparison with the skein relation (16.117) shows that they are obtained from them by setting $t = 1$ and replacing α by $t^{1/2} - t^{-1/2}$:

$$A_L(t) = H_L(1, t^{1/2} - t^{-1/2}). \tag{16.125}$$

The reducible granny and square knots in Fig. 16.5 are distinguished by the Jones and the HOMFLY polynomials; the latter are

$$\begin{aligned} H_{\text{granny}}(t,\alpha) &= (2t^2 - t^4 + t^2\alpha^2)^2, \\ H_{\text{square}}(t,\alpha) &= (2t^2 - t^4 + t^2\alpha^2)(2t^{-2} - t^{-4} + t^2\alpha^2); \end{aligned} \tag{16.126}$$

the former are obtained by inserting $\alpha = t^{1/2} - t^{-1/2}$.

Up to now, there exists no complete algebraic classification scheme. For example, the Jones polynomials of the knots with 10 and 13 crossings shown in Fig. 16.16 are

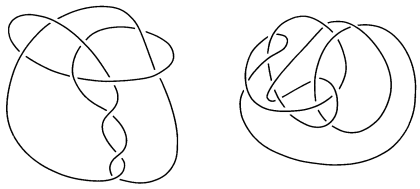

Figure 16.16 Knots with 10 and 13 crossings, not distinguished by Jones polynomials.

the same.[7] For further details, see the mathematical literature quoted at the end of the chapter.

Even with the incomplete classification of knots, it has until now been impossible to calculate the probability distribution of the various equivalence classes of knots. Modern computers allow us to enumerate the different topological configurations for not too long polymers and to simulate their distributions by Monte Carlo methods. In Fig. 16.17 we show the result of a simulation by Michels and Wiegel, where they measure the fraction f_N of unknotted polymers of N links. They fit their curve by a power law

$$f_N = C\mu^N N^\alpha, \tag{16.127}$$

[7] The HOMFLY polynomials have their first degeneracy for prime knots with 9 crossings. It was checked that up to 13 crossings (amounting to 12 965 knots) no polynomial of a nontrivial knot is accidentally degenerate with the trivial polynomial of a circle.

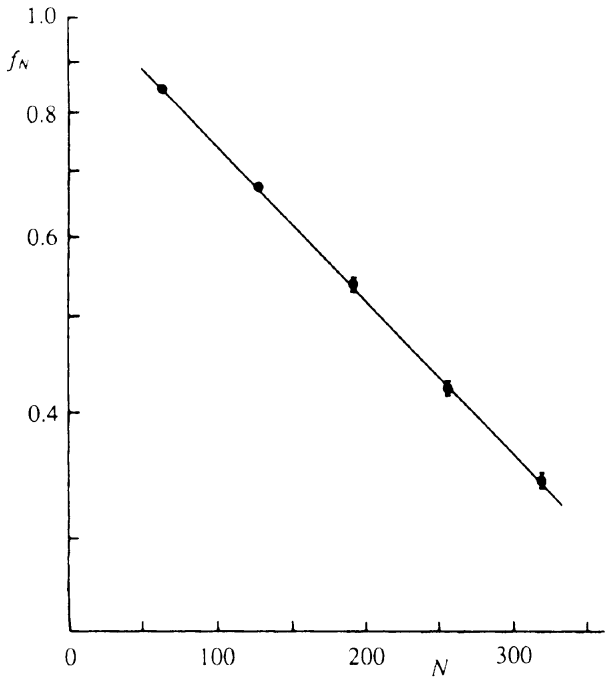

Figure 16.17 Fraction f_N of unknotted closed polymers in ensemble of fixed length $L = Na$.

with the parameters $C \approx 1.026,\ \mu \approx 0.99640,\ \alpha \approx 0.0088$. Thus f_N falls off exponentially in N like μ^N with $\mu < 1$. The exponent α is extremely small. A more recent simulation by S. Windwer takes account of the fact that the line elements are self-avoiding. It yields the parameters[8]

$$C \approx 1.2325, \quad \mu \approx 0.9949, \quad \alpha \approx 0. \tag{16.128}$$

For a polymer enclosed in a sphere of radius R, the distribution has the finite-size dependence

$$f_N(R) = e^{-A(N^\beta l/R)^\gamma}, \tag{16.129}$$

where l is the length of a link. The "critical exponents" are $\beta \approx 0.76$ and $\gamma \approx 3$.

16.5 The Gauss Invariant of Two Curves

For any analytic calculation of topological properties one needs a functional of the polymer shape which is capable of distinguishing the different knot classes. Initially,

[8] A first theoretical determination of these parameters has recently been given by mapping the problem onto a four-state Potts model. A presentation of this method which does not involve path integrals would go beyond the scope of this book. See the papers by A. Kholodenko quoted at the end of the chapter.

a hopeful candidate was the one-loop version of the contour integral introduced almost two centuries ago by Gauss for a pair of closed curves C and C':

$$G(C,C') = \frac{1}{4\pi}\oint_C \oint_{C'} [d\mathbf{x}\times d\mathbf{x}']\cdot\frac{\mathbf{x}-\mathbf{x}'}{|\mathbf{x}-\mathbf{x}'|^3}. \tag{16.130}$$

Gauss proved this to be a topological invariant. In fact, we may rewrite (16.134) with the help of the δ-function (10A.8) as

$$\oint_C d\mathbf{x}\oint_{C'}\frac{d\mathbf{x}'\times(\mathbf{x}-\mathbf{x}')}{|\mathbf{x}-\mathbf{x}'|^3} = -\int d^3x\,\boldsymbol{\delta}(\mathbf{x};C)\cdot\left[\int d^3x'\,\boldsymbol{\delta}(\mathbf{x}';C')\times\frac{\mathbf{R}'}{R'^3}\right] \tag{16.131}$$

The second integral is recognized as the gradient of the multivalued field $\Omega(\mathbf{x};C')$ defined by Eqs. (10A.18), which is the solid angle under which the contour C' is seen from the point $\mathbf{x}$, so that

$$G(C,C') = -\frac{1}{4\pi}\int d^3x\,\boldsymbol{\delta}(\mathbf{x};C)\cdot\boldsymbol{\nabla}\Omega(\mathbf{x};C'). \tag{16.132}$$

Inserting here Eq. (10A.27), where S' is any surface enclosed by the contour L', and using the fact that

$$\int d^3x\,\boldsymbol{\delta}(\mathbf{x};C)\cdot\boldsymbol{\nabla}\Omega(\mathbf{x};S') = -\int d^3x\,\boldsymbol{\nabla}\cdot\boldsymbol{\delta}(\mathbf{x};C)\Omega(\mathbf{x};S') = 0, \tag{16.133}$$

due to (10A.9) and the fact that $\Omega(\mathbf{x};S)=0$ is single-valued, we obtain

$$G(C,C') = -\int d^3x\,\boldsymbol{\delta}(\mathbf{x};C)\cdot\boldsymbol{\delta}(\mathbf{x};S'). \tag{16.134}$$

This is a purely topological integral. By rewriting it as

$$G(C,C') = -\oint_C dx_i\,\delta_i(\mathbf{x};S'), \tag{16.135}$$

we see that $G(C,C')$ gives the linking number of C and C'. It is defined as the number of times by which one of the curves, say C', perforates the surface S spanned by the other.

Alternative expressions for the Gauss integral (16.134) are

$$G(C,C') = -\frac{1}{4\pi}\oint_{C'} d\Omega'(\mathbf{x}';C) = -\frac{1}{4\pi}\oint_C d\Omega(\mathbf{x},C'), \tag{16.136}$$

where where $\Omega'(\mathbf{x}';S)$ is the solid angle under which the curve C is seen from the point $\mathbf{x}'$.

The values of the Gauss integral for various pairs of linked curves up to 8 crossings are given in the third column of Table 16.5. All the intertwined pairs of curves labeled by $2_1, 7_1, 7_2, 8_7$, for instance, have a Gauss integral $G(C,C') = \pm 1$.

Let us end this section by another interpretation of the Gauss integral. According to Section 10A.1, the solid angle Ω is equal to the magnetic potential of a current 4π running through the curve C'. Its gradient is the magnetic field

$$B_i = \partial_i \Omega. \tag{16.137}$$

Hence we can write

$$G(C, C') = -\oint_C dx_i B_i = -\oint_{C'} dx'_i B'_i. \tag{16.138}$$

According to this expression, $G(C, C')$ gives the total work required to move a unit magnetic charge around the closed orbit C in the presence of the magnetic field due to a unit electric current along C'.

Unfortunately, there exists no such topologically invariant integral for a single closed polymer. If we identify the curves C and C', the Gauss integral ceases to be a topological invariant. It can, however, be used to classify self-entangled *ribbons*. These possess two separate edges identified with C and C'. Such ribbons play an important role in biophysics. The molecules of DNA, the carriers of genetic information on the structure of living organisms, can be considered as ribbons. They consist of two chains of molecules connected by weak hydrogen bridges. These can break up thermally or by means of enzymes decomposing the ribbon into two single chains.

16.6 Bound States of Polymers and Ribbons

Two or more polymers may line up parallel to each other and form a bound state. The most famous example is the molecule of DNA. It is a bound state of two long chains of molecules which may contain a few thousand up to several billion links. The distance d between the two chains is about 20Å. In equilibrium, the two chains are twisted up in the form of a double helix, rising by about 20Å (i.e., about 10 monomers) per turn (see Fig. 16.18). The DNA molecule may be idealized as an infinitesimally thin ribbon. The ribbon is always *two-sided* since the edges of the ribbon are made up of different phosphate groups whose chemical structure makes the binding unique. One-sided structures formed by a Möbius strip are excluded.

Circular DNA molecules have interesting topological properties. In the double helix, one edge passes through the other an integer number of times. This is the *linking number* L_k of the double helix. Being a topological invariant, it does not change if the two closed edges become unbound and distorted into an arbitrary shape.

If the total number of windings N_w in the DNA helix is different from the linking number L_k, a circular helix is always under mechanical stress. It can relax by forming a supercoil (see Fig. 16.19). The number of excess turns

$$\tau = L_\mathrm{k} - N_w, \tag{16.139}$$

provides a measure for the *supercoiling density* which is defined by the ratio

$$\sigma \equiv \frac{\tau}{N_w}. \tag{16.140}$$

In natural DNA, the supercoiling density is usually $-\sigma \sim 0.03 - -0.1$. The negative sign implies that the natural twist of the double helix is slightly *decreased* by the supercoiling. The negative sign seems to be essential in the main biological process, the *replication*. It may be varied by an enzyme, called DNA gyrase. A cell has a large arsenal of enzymes which can break one of the chains in the helix and unwind the linking number $L_{\rm k}$ by one or more units, changing the topology. Such enzymes run under the name of *topoisomerases* of type I. There is also one of a type II which breaks *both* chains and can tie or untie knots in the double helix of DNA as a whole.

The biophysical importance of the supercoil derives from the fact that the stress carried by such a configuration can be relaxed by breaking a number of bonds between the two chains. In fact, a number $\theta = -\sigma$ of broken bonds leads to a complete relaxation. During a cell division, all bonds are broken. Note that this process would be energetically unfavorable if the supercoiling density were positive.

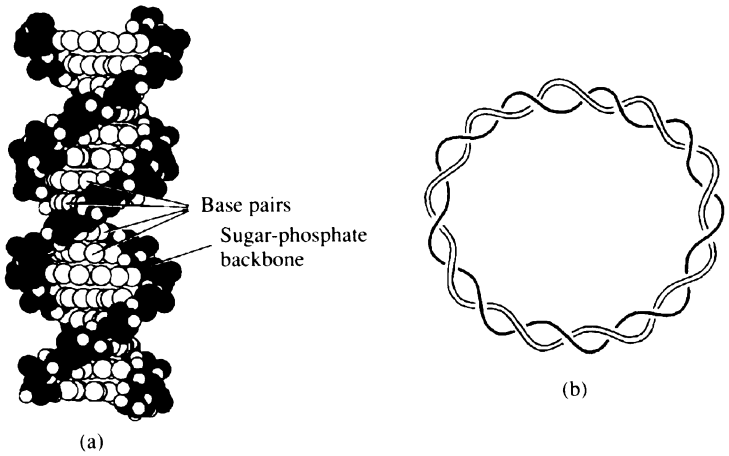

Figure 16.18 Small section and idealized view of circular DNA molecule. The link number $L_{\rm k}$ (defined as number of times one chain passes through arbitrary surface spanned by the other) is $L_{\rm k} \approx 9$.

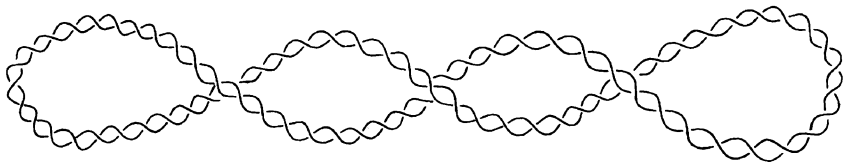

Figure 16.19 A supercoiled DNA molecule. This is the natural shape when carefully extracted from a cell. The supercoiling is negative.

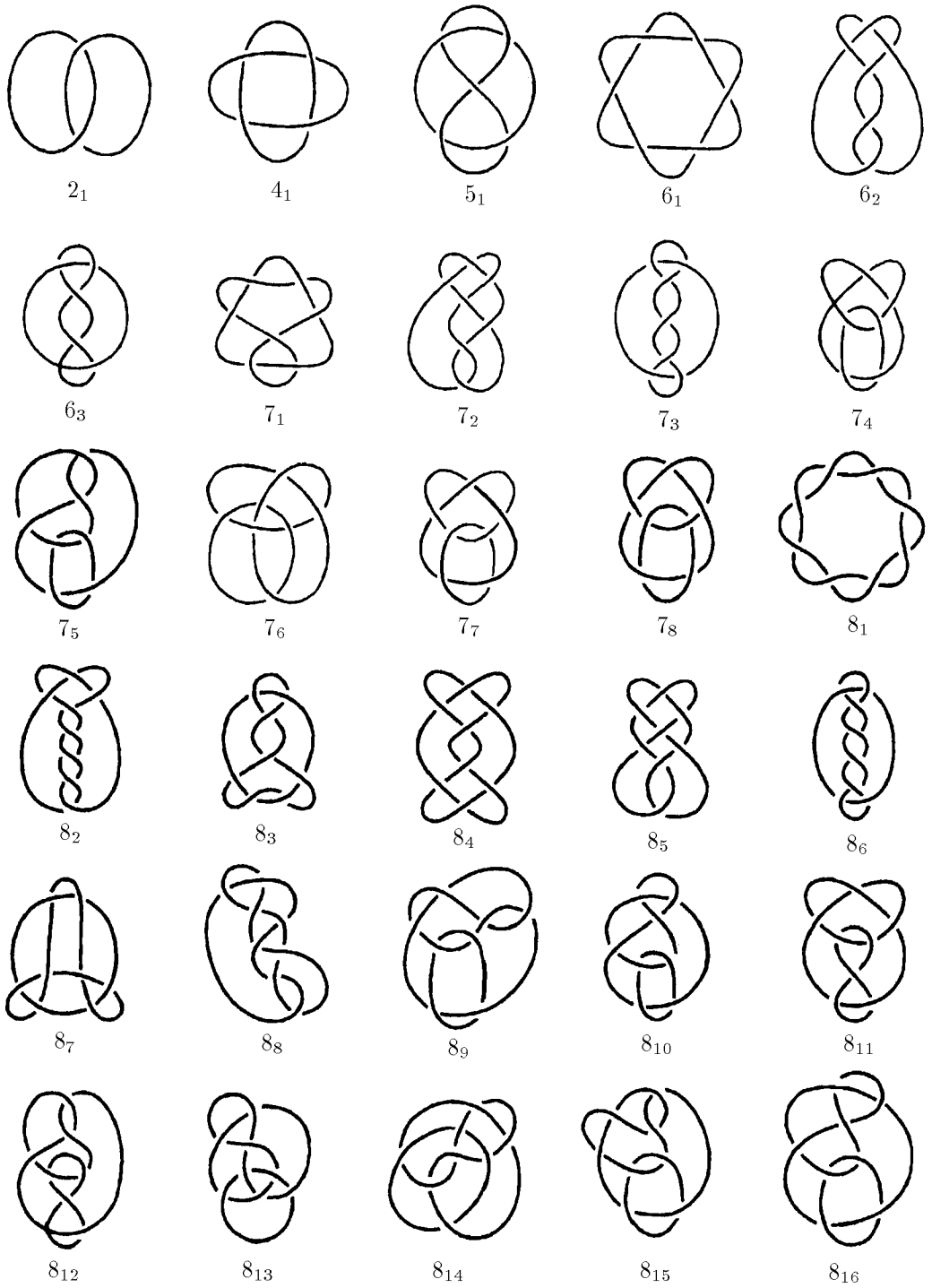

Figure 16.20 Simple links of two polymers up to 8 crossings.

Just as for knots, no complete topological invariants are known for such types of links of two (or more) closed polymers. Historically, generalized Alexander polynomials were used to achieve an approximate classification of links. They are polynomials of two variables. To construct them, we take one of the two polymers and label all underpasses in the same way as for knots. The same thing is done for the other polymer. For each underpass, a row of the Alexander matrix A_{ij} is written down with two variables s and t. The Alexander polynomial $A(s,t)$ is again given by any $(n-1)\times(n-1)$-subdeterminant of the $n\times n$-matrix A_{ij}. The links up to 8 crossings are shown in Fig. 16.20. The Alexander polynomials associated with these are listed in Table 16.5. Note that the replacements $s\to 1/s, t\to 1/t$, or both, leave the Alexander polynomial invariant (due to the prescription of renormalizing the lowest coefficients to an integer). For unlinked polymers one has $A(s,t)=0$.

There is no need to go through the details of the procedure since the more recent and powerful Jones and HOMFLY polynomials can be constructed for arbitrary links without additional prescriptions. The latter are tabulated in the fourth column of Table 16.5. In many cases, a change in the orientation of the second loop gives rise to an inequivalent link. Then the table shows two entries underneath each other. For the knot 7_2, the upper entry $\{-1\}(1*-1)(1*0-11)(*-1-1)$ indicates the polynomial $H(t,\alpha)=\alpha^{-1}(t^{-1}-t)+\alpha(t^{-1}-t^2+t^3)+\alpha^3(-t-t^3)$. The curly bracket shows the lowest power of α and the star marks the position of the zeroth power of t. The coefficients of $t, t^3, \ldots$ stand to the right of it, those of $\ldots, t^{-3}, t^{-1}$ to the left of it.

For the special case of a circular ribbon such as a DNA molecule, the Gauss integral over the two edges, being a topological invariant, renders also a classification of the ribbon as a whole. As shown in Eq. (16.135), the Gauss integral yields precisely the linking number $L_{\rm k}$.

It is useful to calculate $G(C,C')$ for a ribbon in the limit of a very small edge-to-edge distance d. This will also clarify why the Gauss integral $G(C,C')$ in which both C and C' run over the same single loop is not a topological invariant. We start with the Gauss integral for the two edges C, C' of the ribbon

$$G(C,C')=\frac{1}{4\pi}\oint_C\oint_{C'}[d\mathbf{x}\times d\mathbf{x}']\cdot\frac{\mathbf{x}-\mathbf{x}'}{|\mathbf{x}-\mathbf{x}'|^3} \tag{16.141}$$

and shift the two neighboring integration contours C, C' both towards the ribbon axis called $\bar{C}$. Let ϵ measure the distance between the two edges, and let $\mathbf{n}(\tau)$ be the unit vector orthogonal to the axis pointing from C to C'. Then we write

$$G(C,C')=\frac{1}{4\pi}\oint_{\bar{C}}d\tau\oint_{\bar{C}}d\tau'\,[\dot{\mathbf{x}}(\tau)\times(\dot{\mathbf{x}}(\tau')+\epsilon\dot{\mathbf{n}}(\tau'))]\cdot\frac{\mathbf{x}(\tau)-\mathbf{x}(\tau')-\epsilon\mathbf{n}(\tau')}{|\mathbf{x}(\tau)-\mathbf{x}(\tau')-\epsilon\mathbf{n}(\tau')|^3}. \tag{16.142}$$

In the limit $\epsilon\to 0$, $G(C,C')$ does not just become equal to $G(\bar{C},\bar{C})$ [which then would be the same as $G(C,C)$ or $G(C',C')$]. A careful limiting procedure performed below shows that there is a remainder $T_{\rm w}$,

$$L_{\rm k}=G(\bar{C},\bar{C})+T_{\rm w}. \tag{16.143}$$

Table 16.5 Alexander polynomials $A(s,t)$ and the coefficients of HOMFLY polynomials $H(t,\alpha)$ for simple links of two closed curves up to 8 minimal crossings, labeled as in Fig. 16.20. The value $|A(1,1)|$ is equal to the absolute value of the Gauss integral $|G(C,C')|$ for the two curves. The entries in the last column are explained in the text.

	$A(s,t)$	$\lvert A\rvert$	$H(t,\alpha)$
2_1	1	1	$\{-1\}(*1-1)(*1)$
4_1	$s+t$	2	$\{-1\}(*01-1)(*11)$ $\{-1\}(*01-1)(*03-1)(*01)$
5_1	$(s-1)(t-1)$	0	$\{-1\}(1*-1)(-12*-1)(1*)$
6_1	s^2+t^2+st	3	$\{-1\}(*001-1)(*006-3)(*005-1)(*001)$ $\{-1\}(*001-1)(*111)$
6_2	$st(s+t)-st+s+t$	3	$\{-1\}(*001-1)(*022-1)(*011)$
6_3	$2st-(s+t)+2$	2	$\{-1\}(*01-1)(*021-1)(*011)$ $\{-1\}(1-10*)(-21*-1)(1*)$
7_1	$s^2t^2-st(s+t)+st-(s+t)+1$	1	$\{-1\}(1-1*)(-24-3*)(10*)$ $\{-1\}(*1-1)(-11*2-1)(1*1)$
7_2	$st(s+t)-t^2-s^2-3st+s+t$	1	$\{-1\}(*1-1)(1*0-11)(*-1-1)$ $\{-1\}(*1-1)(-2*5-2)(-1*4-1)(*1)$
7_3	$2(s-t)(t-1)$	0	$\{-1\}(1*-1)(1*-1-1)(*-1-1)$
7_4	$(s-1)(t-1)(s^2+1)$	0	$\{-1\}(-13-2*)(-25-3*)(-14-1*)(10*)$
7_5	$2s^3t-t^2-s+2$	2	$\{-1\}(*002-3)(*014-3)(*012)$ $\{-1\}(-1*3-2)(-2*6-2)(-1*4-1)(*1)$
7_6	$(s+1)^2(s-1)(t-1)$	0	$\{-1\}(1*-1)(1-2*1)(1-3*1)(-1*)$
7_7	s^3+t	2	$\{-1\}(-1*3-2)(-1*4-1)(*1)$ $\{-1\}(*002-31)(*006-4)(*005-1)(*001)$
7_8	$(s-t)(t-1)$	0	$\{-1\}(-13-2*)(-13-2*)(10*)$
8_1	$(s+t)(s^2+t^2)$	4	$\{-1\}(*0001-1)(*00010-6)(*00015-5)(*0007-1)(*0001)$ $\{-1\}(*0001-1)(*1111)$
8_2	$st(s+t-1)(st+1)+s+t$	4	$\{-1\}(*0001-1)(*0034-3)(*0044-1)(*0011)$ $\{-1\}(*0001-1)(*0212-1)(*0111)$
8_3	$2s^2t^2-st(s+t)+3st-(s+t)+2$	3	$\{-1\}(*001-1)((*0041-2)(*0043-1)(*0011)$ $\{-1\}(1-100*)(-200*-1)(11*)$
8_4	$s^2t^2(s+t)-2s^2t^2+2st(s+t)-2st+s+t$	4	$\{-1\}(*0001-1)(*0131-1)(*0121)$ $\{-1\}(*0001-1)(*0042-2)(*0043-1)(*0011)$
8_5	$s^2t^2-2st(s+t)+3st-2(s+t)+1$	3	$\{-1\}(*001-1)(*0130-1)(*0121)$ $\{-1\}(1-100*)(1-42-2*)(-23-1*)(10*)$
8_6	$2st-3(s+t)+2$	2	$\{-1\}(*01-1)(*0201-1)(*0111)$ $\{-1\}(1-10*)(-20*1-1)(1*1)$
8_7	$s^2t^2-2st(s+t)+s^2+3st+t^2-2(s+t)+1$	1	$\{-1\}(1-1*)(1-4*3-1)(-2*3-1)(*1)$ $\{-1\}(*1-1)(*2-33-1)(*1-32)(*0-1)$
8_8	$s^2t^2-2st(s+t)+s^2+st+t^2-2(s+t)+1$	3	$\{-1\}(*1-1)(-1*4-31)(-1*3-2)(*1)$ $\{-1\}(*1-22-1)(1*1-33)(*-1-2)$
8_9	$s^3+2s^2t-4s^2-4st+s+2t$	2	$\{-1\}(*1-22-1)(1*1-33)(*-1-2)$ $\{-1\}(*1-22-1)(*2-34-1)(*1-32)(*0-1)$
8_{10}	$(s^2-1)(t-1)$	0	$\{-1\}(1-2*2-1)(1-4*4-1)(1-3*2)(-1*)$
8_{11}	$s^3t-2s^2(s+t)+2s(s+t)-2(s+t)+1$	2	$\{-1\}(*002-31)(*005-2-1)(*0042-1)(*0011)$ $\{-1\}(2-3*1)(1-5*3-1)(-2*3-1)(*1)$
8_{12}	$(s^2-1)(t-1)$	0	$\{-1\}(-13-2*)(-14-4*1)(2-3*1)(-1*)$
8_{13}	$(s^2+1)(s-1)(t-1)$	0	$\{-1\}(1*-1)(*1-21)(-1*2-2)(*1)$
8_{14}	$s^3t-4s^2t+4s^2+4st-4s+1$	2	$\{-1\}(*002-31)(*005-2-1)(*0131)$ $\{-1\}(-1*3-2)(1-3*5-1)(-2*3-1)(*1)$
8_{15}	$(s-1)(t-1)$	0	$\{-1\}(1-2*2-1)(-2*3-1)(*1)$
8_{16}	$s^3-2s(s+1)+1$	2	$\{-1\}(*1-22-1)(*2-22)(*0-1)$ $\{-1\}(*1-22-1)(*3-43)(*1-41)(*0-1)$

The remainder is called the *twist* of the ribbon, defined by

$$T_{\rm w} \equiv \frac{1}{2\pi} \oint_{\bar{C}} d\tau \dot{\mathbf{x}}(\tau) \cdot [\mathbf{n}(\tau) \times \dot{\mathbf{n}}(\tau)]/|\dot{\mathbf{x}}(\tau)|. \tag{16.144}$$

Incidentally, this integral makes sense also for a single curve if $\mathbf{n}(\tau)$ is taken to be the principal normal vector of the curve. Then $T_{\rm w}$ gives what is called the *total integrated torsion* of the single curve. The first term in (16.143), the Gauss integral for a single closed curve $\bar{C}$, is called in this context the *writhing number* of the curve

$$W_{\rm r} \equiv G(\bar{C}, \bar{C}) = \frac{1}{4\pi} \oint_{\bar{C}} d\tau \oint_{\bar{C}} d\tau' \, [\dot{\mathbf{x}}(\tau) \times \dot{\mathbf{x}}(\tau')] \cdot \frac{\mathbf{x}(\tau) - \mathbf{x}(\tau')}{|\mathbf{x}(\tau) - \mathbf{x}(\tau')|^3}. \tag{16.145}$$

Thus one writes the relation (16.143) commonly in the form

$$L_{\rm k} = W_{\rm r} + T_{\rm w}. \tag{16.146}$$

Only the sum $W_{\rm r} + T_{\rm w}$ is a topological invariant, with $T_{\rm w}$ containing the information on the ribbon structure of the closed loop $\bar{C}$. This formula was found by Calagareau in 1959 and generalized by White in 1969.

From what we have seen above in Eq. (16.136), the writhing number may also be written as an integral

$$W_{\rm r} = -\frac{1}{4\pi} \oint_{\bar{C}} d\Omega(\mathbf{x}), \tag{16.147}$$

where $\Omega(\mathbf{x})$ is the solid angle under which the axis of the ribbon is seen from another point on the axis. When rewritten in the form (16.138), it has the magnetic interpretation stated there.

This interpretation is relevant for understanding the spacetime properties of the dionium atom which in turn may be viewed as a world ribbon whose two edges describe an electric and a magnetic charge. We have pointed out in Section 14.6 that for a half-integer charge parameter q, a dionium atom consisting of two bosons is a fermion. For this reason, a path integral over a fluctuating ribbon can be used to describe the quantum mechanics of a fermion in three spacetime dimensions [7].

Let us derive the relation (16.146). We split the integral (16.142) over τ into two parts: a small neighborhood of the point τ' , i.e.,

$$\tau \in (\tau' - \delta, \tau' + \delta) \tag{16.148}$$

and the remainder, for which the integrand is regular. In the regular part, we can set the distance ϵ between the curves C and C' equal to zero, and obtain the Gauss integral $G(\bar{C}, \bar{C})$, i.e., the writhing number $W_{\rm r}$. In the singular part, we approximate $x(\tau)$ within the small neighborhood (16.148) by the straight line

$$\begin{aligned} \mathbf{x}(\tau) &\approx \mathbf{x}(\tau') + \dot{\mathbf{x}}(\tau')(\tau - \tau'), \\ \dot{\mathbf{x}}(\tau) &\approx \dot{\mathbf{x}}(\tau'). \end{aligned} \tag{16.149}$$

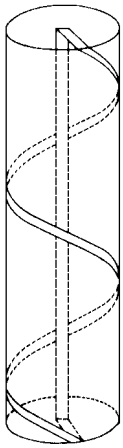

Figure 16.21 Illustration of Calagareau-White relation (16.146). The number of windings around the cylinder is $L_{\rm k} = 2$, while $T_{\rm w} = L_{\rm k} - p/\sqrt{p^2 + R^2}$, where p is the pitch of the helix and R the radius of the cylinder.

Then the τ-integral can be performed. For $\epsilon \ll \delta \ll 1$, we find

$$\begin{aligned} T_{\rm w} &= -\frac{1}{4\pi} \oint_{C'} d\tau' \, [\mathbf{n}(\tau') \times \dot{\mathbf{x}}(\tau')] \cdot \dot{\mathbf{n}}(\tau') \epsilon^2 \int_{\tau'-\delta}^{\tau'+\delta} d\tau \frac{1}{\sqrt{|\dot{\mathbf{x}}(\tau')|^2 (\tau - \tau')^2 + \epsilon^2}} \\ &= \frac{1}{2\pi} \oint_{C'} d\tau' \, [\dot{\mathbf{x}}(\tau') \times \mathbf{n}(\tau')] \cdot \dot{\mathbf{n}}(\tau') / |\dot{\mathbf{x}}(\tau')|. \end{aligned} \tag{16.150}$$

It is worth emphasizing that in contrast to the Gauss integral for two curves C, C', the value of the Gauss integral for $\bar{C}$ is *not* an integer but a continuous number. It depends on the shape of the ribbon, changing continuously when the ribbon is deformed isotopically. If one section of the ribbon passes through the other, however, it changes by 2 units. The defining equation shows that $W_{\rm r}$ vanishes if the ribbon axis has a center or a plane of symmetry. To give an example for a circular closed ribbon with an integer number $L_{\rm k}$ and an *arbitrary writhing number* $W_{\rm r}$ we follow Brook-Fuller and Crick. A cylinder with a closed ribbon is wound flat around the surface of a cylinder, returning along the cylinder axis (see Fig. 16.21). While the two edges of the ribbon perforate each other an integer number of times such that $L_{\rm k} = 2$, the ribbon axis has a noninteger Gauss integral $W_{\rm r}$ depending on the ratio between pitch and radius, $W_{\rm r} = 2 - p/\sqrt{p^2 + R^2}$.

16.7 Chern-Simons Theory of Entanglements

The Gauss integral has a form very similar to the Biot-Savart law of magnetostatics found in 1820. That law supplies an action-at-a-distance formula for the interaction energy of two currents I, I' running along the curves C and C':

$$E = -\frac{II'}{c^2}\oint_C \oint_{C'} d\mathbf{x}\cdot d\mathbf{x}'\,\frac{1}{|\mathbf{x}-\mathbf{x}'|}, \tag{16.151}$$

where c is the light velocity. It was a decisive conceptual advance of Maxwell's theory to explain formula (16.151) by means of a *local* field energy arising from a vector potential $\mathbf{A}(\mathbf{x})$. In view of the importance of the Gauss integral for the topological classification of entanglements, it is useful to derive a local field theory producing the Gauss integral as a topological action-at-a-distance. Imagine the two contours C and C' carrying stationary currents of some pseudo-charge which we normalize at first to unity. These currents are coupled to a vector potential $\mathbf{A}(\mathbf{x})$, which is now unrelated to magnetism and which will be called *statisto-magnetic vector potential*:

$$\mathcal{A}_{\rm e,curr} = -i\oint_C d\mathbf{x}\mathbf{A}(\mathbf{x}) - i\oint_{C'} d\mathbf{x}\mathbf{A}(\mathbf{x}). \tag{16.152}$$

The action is of the Euclidean type as indicated by the subscript e (recall the relation with the ordinary action $\mathcal{A} = i\mathcal{A}_{\rm e}$). We now construct a field action for $\mathbf{A}(\mathbf{x})$ so that the field equations render an interaction between the two currents which is precisely of the form of the Gauss integral. This field action reads

$$\mathcal{A}_{\rm e,CS} = \frac{i}{2}\int d^3x\,\mathbf{A}\cdot(\boldsymbol{\nabla}\times\mathbf{A}) \tag{16.153}$$

and is called the *Chern-Simons action*. It shares with the ordinary Euclidean magnetic field action the quadratic dependence on the vector potential $\mathbf{A}(\mathbf{x})$, as well as the invariance under local gauge transformations

$$\mathbf{A}(\mathbf{x}) \to \mathbf{A}(\mathbf{x}) + \boldsymbol{\nabla}\Lambda(\mathbf{x}), \tag{16.154}$$

which is obvious when transforming the second vector potential in (16.153). The gauge transformation of the first vector potential produces no change after a partial integration. Also the coupling in (16.152) to the contours C and C' is gauge-invariant after a partial integration, since the contours are closed, satisfying

$$\boldsymbol{\nabla}\cdot\oint d\mathbf{x} = 0. \tag{16.155}$$

In contrast to the magnetic field energy, however, the action (16.153) is purely imaginary. The factor i is important for the applications in which the Chern-Simons action will give rise to phase factors of the form $e^{i2\theta G(C,C')}$.

By extremizing the combined action, we obtain the field equation

$$\boldsymbol{\nabla} \times \mathbf{A}(\mathbf{x}) = \left(\oint_C + \oint_{C'} \right) d\mathbf{x}. \tag{16.156}$$

Its solution is

$$A_i(\mathbf{x}) = \left(\oint_C + \oint_{C'} \right) G_{ij}(\mathbf{x}, \mathbf{x}') dx'_j, \tag{16.157}$$

where $G_{ij}(\mathbf{x}, \mathbf{x}')$ is a suitable Green function solving the inhomogeneous field equation (16.157) with a δ-function source instead of the current. Due to the gauge invariance of the left-hand side, however, there is no unique solution. Given a solution $G_{ij}(\mathbf{x}, \mathbf{x}')$, any gauge-transformed Green function

$$G_{ij}(\mathbf{x}, \mathbf{x}') \to G_{ij}(\mathbf{x}, \mathbf{x}') + \nabla_i \Lambda_j(\mathbf{x}, \mathbf{x}') + \nabla_j \Lambda_i(\mathbf{x}, \mathbf{x}')$$

will give the same curl $\boldsymbol{\nabla} \times \mathbf{A}$. Only the transverse part of the vector potential (16.157) is physical, and the Green function has to satisfy

$$\epsilon_{ijk} \nabla_j G_{kl}(\mathbf{x}, \mathbf{x}') = \delta^{(3)}_{ij}(\mathbf{x} - \mathbf{x}')^T, \tag{16.158}$$

where

$$\delta^{(3)}_{ij}(\mathbf{x} - \mathbf{x}')^T = \left(\delta_{ij} - \frac{\nabla_i \nabla_j}{\boldsymbol{\nabla}^2} \right) \delta^{(3)}(\mathbf{x} - \mathbf{x}') \tag{16.159}$$

is the transverse δ-function. The vector potential is then obtained from (16.157) in the transverse gauge with

$$\boldsymbol{\nabla} \cdot \mathbf{A}(\mathbf{x}) = 0. \tag{16.160}$$

The solution of the differential equation (16.158) is easily found in the two-dimensional transverse subspace. The Fourier transform of Eq. (16.158) reads

$$i\epsilon_{ijk} p_j G_{kl}(\mathbf{p}) = \delta_{il} - \frac{p_j p_l}{\mathbf{p}^2}, \tag{16.161}$$

and this is obviously solved by

$$G_{ij}(\mathbf{p}) = i\epsilon_{ikj} p_k \frac{1}{\mathbf{p}^2}. \tag{16.162}$$

The transverse gauge (16.160) may be enforced in an action formalism by adding to the action (16.153) a *gauge-fixing term*

$$\mathcal{A}_{\mathrm{GF}} = \frac{1}{2\alpha} (\boldsymbol{\nabla} \cdot \mathbf{A})^2, \tag{16.163}$$

with an intermediate gauge parameter α which is taken to zero at the end. The field equation (16.158) is then changed to

$$\left(\epsilon_{ijk} \nabla_j + \frac{i}{\alpha} \nabla_i \nabla_k \right) G_{kl}(\mathbf{x}, \mathbf{x}') = \delta_{ik} \delta^{(3)}(\mathbf{x} - \mathbf{x}'), \tag{16.164}$$

which reads in momentum space

$$\left(i\epsilon_{ijk}p_j - \frac{i}{\alpha}p_i p_k\right) G_{kl}(\mathbf{p}) = \delta_{ik}. \tag{16.165}$$

This has the unique solution

$$G_{ik}(\mathbf{p}) = \left(i\epsilon_{ijk}p_j + i\alpha\,\frac{p_i p_k}{\mathbf{p}^2}\right)\frac{1}{\mathbf{p}^2}, \tag{16.166}$$

whose $\alpha \to 0$ -limit is (16.162).

Going back to configuration space, the Green function becomes

$$G_{ij}(\mathbf{x},\mathbf{x}') = \int \frac{d^3p}{(2\pi)^3} e^{i\mathbf{p}(\mathbf{x}-\mathbf{x}')}\frac{i\epsilon_{ikj}p_k}{\mathbf{p}^2} = \frac{1}{4\pi}\epsilon_{ikj}\nabla_k \frac{1}{|\mathbf{x}-\mathbf{x}'|} = \frac{1}{4\pi}\epsilon_{ijk}\frac{(x-x')_k}{|\mathbf{x}-\mathbf{x}'|^3}. \tag{16.167}$$

Inserting this into $\mathcal{A}_{\rm e,curr} + \mathcal{A}_{\rm e,CS}$ yields the interaction between the currents[9]

$$\mathcal{A}_{\rm e,int} = -i \oint_C \oint_{C'} dx_i dx'_j G_{ij}(\mathbf{x},\mathbf{x}'). \tag{16.168}$$

Up to the prefactor $-i$, this is precisely the Gauss integral $G(C,C')$ of the two curves C, C'. In addition there are the self-interactions of the two curves

$$\mathcal{A}_{\rm e,int} = -\frac{i}{2}\left(\oint_C \oint_C + \oint_{C'} \oint_{C'}\right) dx_i dx'_j G_{ij}(\mathbf{x},\mathbf{x}'), \tag{16.169}$$

which are equal to $-(i/2)[G(C,C)+G(C',C')]$. Due to their nontopological nature discussed earlier, these have no quantized values and must be avoided.

Such unquantized self-interactions can be avoided by considering systems whose orbits are subject to appropriate restrictions. They may, for instance, contain only lines which are not entangled with themselves and run in a preferred direction from $-\infty$ to ∞. Ensembles of nonrelativistic particles in two space dimensions have precisely this type of worldlines in three-dimensional spacetime. They are therefore an ideal field for the Chern-Simons theory, as we shall see below in more detail.

Another way of avoiding unquantized self-interactions is based on a suitable limiting procedure. If the lines C and C' coincide, the Gaussian integral $G(C,C')$ over $C = C'$ may be spread over a large number N of parallel running lines C_i $(i = 1,\ldots,N)$, each of which carries a topological charge $1/N$. The sum $(1/N^2)\sum_{ij} G(C_i,C_j)$ contains N-times the same self-interaction and $N(N-1)$-times the same integer-valued linking number $L_{\rm k}$ of pairs of lines. In the limit $N \to \infty$, only the number $L_{\rm k}$ survives. The result coincides with the Gauss integral for the two frame lines C_1 and C_N of the ribbon. The number L_K may therefore be called the *frame linking number*. This number depends obviously on the choice of the framing. There is a preferred choice for which $L_{\rm k}$ vanishes. This eliminates the self-interaction trivially.

[9] Compare this with the derivation of Eq. (3.247).

Although the limiting procedure makes the self-interaction topological, the arbitrariness of the framing destroys all information on the knot classes. This information can be salvaged by means of a generalization of the above topological action leading to a nonabelian version of the Chern-Simons theory. That theory has the same arbitrariness in the choice of the framing. However, by choosing the framing to be the same as in the abelian case and calculating only ratios of observable quantities, it is possible to eliminate the framing freedom. This will enable us to distinguish the different knot classes after all.

16.8 Entangled Pair of Polymers

For a pair of polymers, the above problems with self-entanglement can be avoided by a slight modification of the Chern-Simons theory. This will allow us to study the entanglement of the pair. In particular, we shall be able to calculate the *second topological moment* of the entanglement, which is defined as the expectation value $\langle m^2 \rangle$ of the square of the linking number m [8]. The self-entanglements will of the individual polymers will be ignored.

The result will apply approximately to a polymer in an ensemble of many others, since these may be considered roughly as a single very long effective polymer.

Consider two polymers running along the contours C_1 and C_2 which statistically can be linked with each other any number of times $m = 0, 1, 2, \dots$. The situation is illustrated in Fig. 16.22 for $m = 2$. The linking number (16.134) for these two polymers can be calculated with the help of

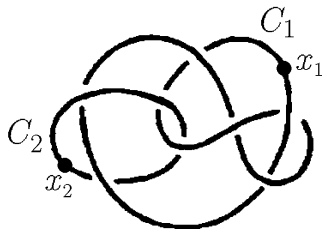

Figure 16.22 Closed polymers along the contours C_1, C_2 respectively.

a slight modification of the Chern-Simons action (16.153) and the couplings (16.152). We simply introduce two vector potentials and the Euclidean action

$$\mathcal{A}_{\rm e} = \mathcal{A}_{\rm e,CS12} + \mathcal{A}_{\rm e,curr}, \tag{16.170}$$

where

$$\mathcal{A}_{\rm e,CS12} = i \int d^3x\, \mathbf{A}_1 \cdot (\boldsymbol{\nabla} \times \mathbf{A}_2) \tag{16.171}$$

and

$$\mathcal{A}_{\rm e,curr} = -i \oint_{C_1} d\mathbf{x} \mathbf{A}_1(\mathbf{x}) - i \oint_{C_2} d\mathbf{x} \mathbf{A}_2(\mathbf{x}). \tag{16.172}$$

If we choose the gauge fields to be transverse, as in (16.160), we obtain with the same technique as before the correlation functions of the gauge fields

$$D^{\mu\nu}_{ab}(\mathbf{x}, \mathbf{x}') \equiv \langle A^\mu_a(\mathbf{x}) A^\nu_b(\mathbf{x}') \rangle, \quad a, b = 1, 2 \tag{16.173}$$

are

$$D_{11}^{ij}(\mathbf{x},\mathbf{x}') = 0, \qquad D_{22}^{ij}(\mathbf{x},\mathbf{x}') = 0, \tag{16.174}$$

$$\begin{aligned} D_{12}^{ij}(\mathbf{x},\mathbf{x}') &= D_{21}^{ij}(\mathbf{x},\mathbf{x}') = \int \frac{d^3p}{(2\pi)^3} e^{i\mathbf{p}(\mathbf{x}-\mathbf{x}')} \frac{i\epsilon_{ikj}k^k}{\mathbf{p}^2} = \frac{1}{4\pi}\epsilon_{ikj}\nabla_k \frac{1}{|\mathbf{x}-\mathbf{x}'|} \\ &= \frac{1}{4\pi}\epsilon_{ij\kappa}\frac{(x-x')^k}{|\mathbf{x}-\mathbf{x}'|^3}. \end{aligned} \tag{16.175}$$

The transverse gauge is enforced by adding to the action (16.171) a gauge-fixing term

$$\mathcal{A}_{\rm GF} = \frac{1}{2\alpha}[(\boldsymbol{\nabla}\cdot\mathbf{A}_1)^2 + (\boldsymbol{\nabla}\cdot\mathbf{A}_2)^2], \tag{16.176}$$

and taking the limit $\alpha \to 0$ at the end. Extremizing the extended action produces the Gaussian linking number $-iG(C_1,C_2)$ of Eq. (16.134). The calculation is completely analogous to that leading to Eq. (16.168).

The partition function of the two polymers and the gauge fields is given by the path integral

$$Z = \int_{C_1} \mathcal{D}\mathbf{x}_1 \int_{C_2} \mathcal{D}\mathbf{x}_2 \int \mathcal{D}\mathbf{A}_1 \mathcal{D}\mathbf{A}_2 e^{-\mathcal{A}_{\rm e}-\mathcal{A}_{\rm GF}}. \tag{16.177}$$

Performing the functional integral over the gauge fields, we obtain from the extremum

$$Z = \text{const} \times \int_{C_1} \mathcal{D}\mathbf{x}_1 \int_{C_2} \mathcal{D}\mathbf{x}_2 \, e^{iG(C_1,C_2)}, \tag{16.178}$$

where the constant is the trivial fluctuation factor of the vector potentials. The Gaussian integral $G(C_1,C_2)$ has the values $m = 0, \pm 1, \pm 2, \ldots$ of the linking numbers.

In order to analyze the distribution of linking number in the two-polymer system we must be able to fix a certain linking number. This is possible by replacing the phase factor e^{im} in the path integral (16.178) by $e^{im\lambda}$, and calculating $Z(\kappa)$. An integral $\int d\kappa e^{-i\overline{m}\lambda} Z(\lambda)$ will then select any specific linking number $\overline{m}$. But a phase factor $e^{im\lambda}$ is simply produced in the partition function (16.178) by attaching to one of the current couplings in the interaction (16.172), say to that of C_2, a factor λ, thus changing (16.172) to

$$\mathcal{A}_{\rm e,curr,\lambda} = -i \oint_{C_1} d\mathbf{x}\, \mathbf{A}_1(\mathbf{x}) - i\lambda \oint_{C_2} d\mathbf{x}\, \mathbf{A}_2(\mathbf{x}). \tag{16.179}$$

The λ-dependent partition function is then

$$\begin{aligned} Z(\lambda) &= \int_{C_1} \mathcal{D}\mathbf{x}_1 \int_{C_2} \mathcal{D}\mathbf{x}_2 \int \mathcal{D}\mathbf{A}_1 \mathcal{D}\mathbf{A}_2 e^{-\mathcal{A}_{\rm e,CS12}-\mathcal{A}_{\rm e,curr,\lambda}-\mathcal{A}_{\rm GF}} \\ &= \text{const} \times \int_{C_1} \mathcal{D}\mathbf{x}_1 \int_{C_2} \mathcal{D}\mathbf{x}_2 \, e^{im\lambda}. \end{aligned} \tag{16.180}$$

Ultimately, we want to find the probability distribution of the linking numbers m as a function of the lengths of C_1 and C_2. The solution of this two-polymer problem may be considered as an approximation to a more interesting physical problem in which a particular polymer is linked to any number N of polymers, which are effectively replaced by a single long "effective" polymer [9]. Unfortunately, the full distribution of m is very hard to calculate. Only a calculation of the second topological moment is possible with limited effort. This quantity is given by the expectation value $\langle m^2 \rangle$ of the square of the linking number m.

Let $P_{L_1,L_2}(\mathbf{x}_1,\mathbf{x}_2;m)$ be the configurational probability to find the polymer C_1 of length L_1 with fixed coinciding endpoints at $\mathbf{x}_1$ and the polymer C_2 of length L_2 with fixed coinciding

endpoints at $\mathbf{x}_2$, entangled with a Gaussian linking number m. The second moment $\langle m^2 \rangle$ is given by the ratio of integrals

$$\langle m^2 \rangle = \frac{\int d^3x_1 d^3x_2 \int_{-\infty}^{+\infty} dm\ m^2 P_{L_1,L_2}(\mathbf{x}_1, \mathbf{x}_2; m)}{\int d^3x_1 d^3x_2 \int_{-\infty}^{+\infty} dm\, P_{L_1,L_2}(\mathbf{x}_1, \mathbf{x}_2; m)}, \tag{16.181}$$

performed for either of the two probabilities. The integrations in $d^3\mathbf{x}_1 d^3x_2$ covers all positions of the endpoints. The denominator plays the role of a partition function of the system:

$$Z \equiv \int d^3x_1 d^3x_2 \int_{-\infty}^{+\infty} dm\, P_{L_1,L_2}(\mathbf{x}_1, \mathbf{x}_2; m). \tag{16.182}$$

Due to translational invariance of the system, the probabilities depend only on the differences between the endpoint coordinates:

$$P_{L_1,L_2}(\mathbf{x}_1, \mathbf{x}_2; m) = P_{L_1,L_2}(\mathbf{x}_1 - \mathbf{x}_2; m). \tag{16.183}$$

Thus, after the shift of variables, the spatial double integrals in (16.181) can be rewritten as

$$\int d^3x_1 d^3x_2 P_{L_1,L_2}(\mathbf{x}_1, \mathbf{x}_2; m) = V \int d^3x\, P_{L_1,L_2}(\mathbf{x}; m), \tag{16.184}$$

where V denotes the total volume of the system.

16.8.1 Polymer Field Theory for Probabilities

The calculation of the path integral over all line configurations is conveniently done within the polymer field theory developed in Section 15.12. It permits us to rewrite the partition function (16.180) as a functional integral over two $\psi_1^{\alpha_1}(\mathbf{x}_1)$ and $\psi_2^{\alpha_2}(\mathbf{x}_2)$ with n_1 and n_2 replica ($\alpha_1 = 1, \ldots, n_1,\ \alpha_2 = 1, \ldots, n_2$). At the end we shall take $n_1, n_2 \to 0$ to ensure that these fields describe only one polymer each, es explained in Section 15.12. For these fields we define an auxiliary probability $P_{\vec{z}}(\vec{\mathbf{x}}_1, \vec{\mathbf{x}}_2; \lambda)$ to find the polymer C_1 with open ends at $\mathbf{x}_1, \mathbf{x}_1'$ and the polymer C_2 with open ends at $\mathbf{x}_2, \mathbf{x}_2'$. The double vectors $\vec{\mathbf{x}}_1 \equiv (\mathbf{x}_1, \mathbf{x}_1')$ and $\vec{\mathbf{x}}_2 \equiv (\mathbf{x}_2, \mathbf{x}_2')$ collect initial and final endpoints of the two polymers C_1 and C_2. The auxiliary probability $P_{\vec{z}}(\vec{\mathbf{x}}_1, \vec{\mathbf{x}}_2; \lambda)$ is given by a functional integral

$$P_{\vec{z}}(\vec{\mathbf{x}}_1, \vec{\mathbf{x}}_2; \lambda) = \lim_{n_1, n_2 \to 0} \int \mathcal{D}(\text{fields})\, \psi_1^{\alpha_i}(\mathbf{x}_1) \psi_1^{*\alpha_1}(\mathbf{x}_1') \psi_2^{\alpha_2}(\mathbf{x}_2) \psi_2^{*\alpha_2}(\mathbf{x}_2') e^{-\mathcal{A}}, \tag{16.185}$$

where $\mathcal{D}(\text{fields})$ indicates the measure of functional integration, and $\mathcal{A}$ the total action (16.180) governing the fluctuations. The expectation value is calculated for any fixed pair (α_1, α_2) of replica labels, i.e., replica labels are not subject to Einstein's summation convention of repeated indices. The action $\mathcal{A}$ consists of kinetic terms for the fields, a quartic interaction of the fields to account for the fact that two monomers of the polymers cannot occupy the same point, the so-called *excluded-volume effect*, and a Chern-Simons field to describe the linking number m. Neglecting at first the excluded-volume effect and focusing attention on the linking problem only, the action reads

$$\mathcal{A} = \mathcal{A}_{\text{CS12}} + \mathcal{A}_{\text{e,curr}} + \mathcal{A}_{\text{pol}} + \mathcal{A}_{\text{GF}}, \tag{16.186}$$

with a polymer field action

$$\mathcal{A}_{\text{pol}} = \sum_{i=1}^{2} \int d^3\mathbf{x} \left[|\bar{\mathbf{D}}^i \psi_i|^2 + m_i^2 |\Psi_i|^2 \right]. \tag{16.187}$$

They are coupled to the polymer fields by the covariant derivatives

$$\mathbf{D}^i = \boldsymbol{\nabla} + i\gamma_i \mathbf{A}^i, \tag{16.188}$$

with the coupling constants $\gamma_{1,2}$ given by

$$\gamma_1 = 1, \qquad \gamma_2 = \lambda. \tag{16.189}$$

The square masses of the polymer fields are given by

$$m_i^2 = 2Mz_i. \tag{16.190}$$

where $M = 3/a$, with a being the length of the polymer links [recall (15.79)], and z_i the chemical potentials of the polymers, measured in units of the temperature. The chemical potentials are conjugate variables to the length parameters L_1 and L_2, respectively. The symbols Ψ_i collect the replica of the two polymer fields

$$\Psi_i = \left(\psi_i^1, \ldots, \psi_i^{n_i}\right), \tag{16.191}$$

and their absolute squares contain the sums over the replica

$$|\mathbf{D}^i \bar{\Psi}_i|^2 = \sum_{\alpha_i=1}^{n_i} |\mathbf{D}^i \psi_i^{\alpha_i}|^2, \qquad |\Psi_i|^2 = \sum_{\alpha_i=1}^{n_i} |\psi_i^{\alpha_i}|^2. \tag{16.192}$$

Having specified the fields, we can now write down the measure of functional integration in Eq. (16.185):

$$\mathcal{D}(\text{fields}) = \int \mathcal{D}A_1^i \mathcal{D}A_2^j \mathcal{D}\Psi_1 \mathcal{D}\Psi_1^* \mathcal{D}\Psi_2 \mathcal{D}\Psi_2^*. \tag{16.193}$$

By Eq. (16.180), the parameter λ is conjugate to the linking number m. We can therefore calculate the probability $P_{L_1,L_2}(\vec{\mathbf{x}}_1, \vec{\mathbf{x}}_2; m)$ in which the two polymers are open with different endpoints from the auxiliary one $P_{\vec{z}}(\vec{\mathbf{x}}_1, \vec{\mathbf{x}}_2; \lambda)$ by the following Laplace integral over $\vec{z} = (z_1, z_1)$:

$$P_{L_1,L_2}(\vec{\mathbf{x}}_1, \vec{\mathbf{x}}_2; m) = \lim_{\substack{\mathbf{x}_1' \to \mathbf{x}_1 \\ \mathbf{x}_2' \to \mathbf{x}_2}} \int_{c-i\infty}^{c+i\infty} \frac{Mdz_1}{2\pi i} \frac{Mdz_2}{2\pi i} e^{z_1 L_1 + z_2 L_2} \int_{-\infty}^{\infty} dk e^{-im\lambda} P_{\vec{z}}\left(\vec{\mathbf{x}}_1, \vec{\mathbf{x}}_2; \lambda\right). \tag{16.194}$$

16.8.2 Calculation of Partition Function

Let us use the polymer field theory to calculate the partition function (16.182). By Eq. (16.194), it is given by the integral over the auxiliary probabilities

$$Z = \int d^3x_1 d^3x_2 \lim_{\substack{\mathbf{x}_1' \to \mathbf{x}_1 \\ \mathbf{x}_2' \to \mathbf{x}_2}} \int_{c-i\infty}^{c+\infty} \frac{Mdz_1}{2\pi i} \frac{Mdz_2}{2\pi i} e^{z_1 L_1 + z_2 L_2} \int_{-\infty}^{\infty} dm \int_{-\infty}^{+\infty} d\lambda e^{-im\lambda} P_{\vec{z}}\left(\vec{\mathbf{x}}_1, \vec{\mathbf{x}}_2; \lambda\right). \tag{16.195}$$

The integration over m is trivial and gives $2\pi\delta(\lambda)$, enforcing $\lambda = 0$, so that

$$Z = \int d^3x_1 d^3x_2 \lim_{\substack{\mathbf{x}_1' \to \mathbf{x}_1 \\ \mathbf{x}_2' \to \mathbf{x}_2}} \int_{c-i\infty}^{c+i\infty} \frac{Mdz_1 Mdz_2}{2\pi i} e^{z_1 L_1 + z_2 L_2} P_{\vec{z}}\left(\vec{\mathbf{x}}_1, \vec{\mathbf{x}}_2; 0\right). \tag{16.196}$$

To calculate $P_{\vec{z}}\left(\vec{\mathbf{x}}_1, \vec{\mathbf{x}}_2; 0\right)$, we observe that the action $\mathcal{A}$ in Eq. (16.186) depends on λ only via the polymer part (16.187), and is quadratic in λ. Let us expand $\mathcal{A}$ as

$$\mathcal{A} = \mathcal{A}_0 + \lambda \mathcal{A}_1 + \lambda^2 \mathcal{A}_2, \tag{16.197}$$

with the λ-independent part

$$\mathcal{A}_0 \equiv \mathcal{A}_{\rm CS12} + \mathcal{A}_{\rm GF} + \int d^3x \left[|\mathbf{D}_1\Psi_1|^2 + |\boldsymbol{\nabla}\Psi_2|^2 + \sum_{i=1}^{2} |\Psi_i|^2 \right], \tag{16.198}$$

a linear coefficient

$$\mathcal{A}_1 \equiv \int d^3x \; \mathbf{j}_2(\mathbf{x}) \cdot \mathbf{A}_2(\mathbf{x}) \tag{16.199}$$

containing a pseudo-current of the second polymer field

$$\mathbf{j}_2(\mathbf{x}) = i\Psi_2^*(\mathbf{x})\boldsymbol{\nabla}\Psi_2(\mathbf{x}), \tag{16.200}$$

and a quadratic coefficient

$$\mathcal{A}_2 \equiv \frac{1}{4}\int d^3\mathbf{x} \; \mathbf{A}_2^2 |\Psi_2(\mathbf{x})|^2. \tag{16.201}$$

With these definitions we write with the help of (16.198):

$$P_{\vec{z}}\,(\vec{\mathbf{x}}_1, \vec{\mathbf{x}}_2; 0) = \int \mathcal{D}(\text{fields}) e^{-\mathcal{A}_0} \psi_1^{\alpha_1}(\mathbf{x}_1)\psi_1^{*\alpha_1}(\mathbf{x}_1')\psi_2^{\alpha_2}(\mathbf{x}_2)\psi_2^{\alpha_2}(\mathbf{x}'). \tag{16.202}$$

In the action (16.198), the fields Ψ_2, Ψ_2^* are obviously free, whereas the fields Ψ_1, Ψ_1^* are apparently not because of the couplings with the Chern-Simons fields in the covariant derivative $\mathbf{D}^1$. This coupling is, however, without physical consequences. Indeed, by integrating out A_2^i in (16.202), we find from $\mathcal{A}_{\rm CS12}$ the flatness condition:

$$\boldsymbol{\nabla} \times \mathbf{A}_1 = 0. \tag{16.203}$$

On a flat space with vanishing boundary conditions at infinity this implies $\mathbf{A}_1 = 0$. As a consequence, the functional integral (16.202) factorizes as follows [compare (15.370)]

$$P_{\vec{z}}\,(\vec{\mathbf{x}}_1, \vec{\mathbf{x}}_2; 0) = G_0(\mathbf{x}_1 - \mathbf{x}_1'; z_1) G_0(\mathbf{x}_2 - \mathbf{x}_2'; z_2), \tag{16.204}$$

where $G_0(\mathbf{x}_i - \mathbf{x}_i'; z_i)$ are the free correlation functions of the polymer fields:

$$G_0(\mathbf{x}_i - \mathbf{x}_i'; z_i) = \langle \psi_i^{\alpha_i}(\mathbf{x}_i)\psi_i^{*\alpha_i}(\mathbf{x}_i')\rangle. \tag{16.205}$$

In momentum space, the correlation functions are

$$\langle \tilde{\psi}_i^{\alpha_i}(\mathbf{k}_i)\tilde{\psi}_i^{*\alpha_i}(\mathbf{k}_i')\rangle = \delta^{(3)}(\mathbf{k}_i - \mathbf{k}_i')\frac{1}{\mathbf{k}_i^2 + m_i^2}, \tag{16.206}$$

such that

$$G_0(\mathbf{x}_i - \mathbf{x}_i'; z_i) = \int \frac{d^3k}{(2\pi)^3} e^{i\mathbf{k}\cdot\mathbf{x}} \frac{1}{\mathbf{k}_i^2 + m_i^2}, \tag{16.207}$$

and

$$\begin{aligned} G_0(\mathbf{x}_i - \mathbf{x}_i'; L_i) &= \int_{c-i\infty}^{c+i\infty} \frac{M dz_i}{2\pi i} e^{z_i L_i} G_0(\mathbf{x}_i - \mathbf{x}_i'; z_i) \\ &= \frac{1}{2}\left(\frac{M}{4\pi L_i}\right)^{3/2} e^{-M(\mathbf{x}_i - \mathbf{x}_i')/2L_i}. \end{aligned} \tag{16.208}$$

The partition function (16.196) is then given by the integral

$$Z = 2\pi \int d^3x_1 d^3x_2 \lim_{\substack{\mathbf{x}_1' \to \mathbf{x}_1 \\ \mathbf{x}_2' \to \mathbf{x}_2}} G_0(\mathbf{x}_1 - \mathbf{x}_1'; L_1) G_0(\mathbf{x}_2 - \mathbf{x}_2'; L_2). \tag{16.209}$$

The integrals at coinciding endpoints can easily be performed, yielding

$$Z = \frac{2\pi M^3 V^2}{(8\pi)^3} (L_1 L_2)^{-3/2}. \tag{16.210}$$

It is important to realize that in Eq. (16.195) the limits of coinciding endpoints $\mathbf{x}_i' \to \mathbf{x}_i$ and the inverse Laplace transformations do *not* commute unless a proper renormalization scheme is chosen to eliminate the divergences caused by the insertion of the composite operators $|\psi^\alpha(\mathbf{x})|^2$. This can be seen for a single polymer. If we were to commuting the limit of coinciding endpoints with the Laplace transform, we would obtain

$$\int_{c-i\infty}^{c+i\infty} \frac{dz}{2\pi} e^{zL} \lim_{\mathbf{x}' \to \mathbf{x}} G_0(\mathbf{x} - \mathbf{x}'; z) = \int_{c-i\infty}^{c+i\infty} \frac{dz}{2\pi i} e^{zL} G_0(\mathbf{0}, z), \tag{16.211}$$

where

$$G_0(\mathbf{0}; z) = \langle |\psi(\mathbf{x})|^2 \rangle. \tag{16.212}$$

This expectation value, however, is linearly divergent:

$$\langle |\psi(\mathbf{x})|^2 \rangle = \int \frac{d^3k}{k^2 + m^2} \to \infty. \tag{16.213}$$

16.8.3 Calculation of Numerator in Second Moment

Let us now turn to the numerator in Eq. (16.181):

$$N \equiv \int d^3x_1 d^3x_2 \int_{-\infty}^{\infty} dm\ m^2\, P_{L_1,L_2}(\mathbf{x}_1, \mathbf{x}_2; m). \tag{16.214}$$

We shall set up a functional integral for N in terms of the auxiliary probability $P_{\vec{z}}(\vec{\mathbf{x}}_1, \vec{\mathbf{x}}_2; 0)$ analogous to Eq. (16.195). First we observe that

$$\begin{aligned} N &= \int d^3x_1 d^3r_2 \int_{-\infty}^{\infty} dm\ m^2 \lim_{\substack{\mathbf{x}_1' \to \mathbf{x}_1 \\ \mathbf{x}_2' \to \mathbf{x}_2}} \int_{c-i\infty}^{c_\tau i\infty} \frac{M dz_i}{2\pi i} \frac{M dz_2}{2\pi i} \\ &\times e^{z_1 L_1 + z_2 L_2} \int_{-\infty}^{\infty} d\lambda e^{-im\lambda} P_{\vec{z}}(\vec{\mathbf{x}}_1, \vec{\mathbf{x}}_2; \lambda). \end{aligned} \tag{16.215}$$

The integration in m is easily performed after noting that

$$\int_{-\infty}^{\infty} dm\ m^2 e^{-im\lambda} P_{\vec{z}}(\vec{\mathbf{x}}_1, \vec{\mathbf{x}}_2; \lambda) = -\int_{-\infty}^{\infty} dm \left(\frac{\partial^2}{\partial \lambda^2} e^{-im\lambda} \right) P_{\vec{z}}(\vec{\mathbf{x}}_1, \vec{\mathbf{x}}_2; \lambda). \tag{16.216}$$

After two integrations by parts in λ, and an integration in m, we obtain

$$\begin{aligned} N &= \int d^3x_1 d^3x_2 \lim_{\substack{\mathbf{x}_1' \to \mathbf{x}_1 \\ \mathbf{x}_2' \to \mathbf{x}_2}} (-1) \int_{c-i\infty}^{c+i\infty} \frac{M dz_1}{2\pi i} \frac{M dz_2}{2\pi i} e^{z_1 L_1 + z_2 L_2} \\ &\times \int_{-\infty}^{\infty} d\lambda\ \delta(\lambda) \left[\frac{\partial^2}{\partial \lambda^2} P_{\vec{z}}(\vec{\mathbf{x}}_1, \vec{\mathbf{x}}_2; \lambda) \right]. \end{aligned} \tag{16.217}$$

Performing the now the trivial integration over λ yields

$$N = \int d^3x_1 d^3x_2 \lim_{\substack{\mathbf{x}_1' \to \mathbf{x}_1 \\ \mathbf{x}_2' \to \mathbf{x}_2}} (-1) \int_{c-i\infty}^{c+i\infty} \frac{Mdz_1}{2\pi i} \frac{Mdz_2}{2\pi i} e^{z_1 L_1 + z_2 L_2} \left[\frac{\partial^2}{\partial \lambda^2} P_{\vec{z}}(\vec{\mathbf{x}}_1, \vec{\mathbf{x}}_2; 0) \right]. \tag{16.218}$$

To compute the term in brackets, we use again (16.197) and Eqs. (16.198)–(16.223), to find

$$\begin{aligned} N &= \int d^3x_1 d^3x_2 \lim_{\substack{n_1 \to 0 \\ n_2 \to 0}} \int_{c-i\infty}^{c+i\infty} \frac{Mdz_1}{2\pi i} \frac{Mdz_2}{2\pi i} e^{z_1 L_1 + z_2 L_2} \\ &\times \int \mathcal{D}(\text{fields}) \ \exp(-\mathcal{A}_0) |\psi_1^{\alpha_1}(\mathbf{x}_1)|^2 |\psi_2^{\alpha_2}(\mathbf{x}_2)|^2 \\ &\times \left[\left(\int d^3x \, \mathbf{A}_2 \cdot \Psi_2^* \boldsymbol{\nabla} \Psi_2 \right)^2 + \frac{1}{2} \int d^3x \, \mathbf{A}_2^2 \, |\Psi_2|^2 \right]. \end{aligned} \tag{16.219}$$

In this equation we have taken the limits of coinciding endpoint inside the Laplace integral over z_1, z_2. This will be justified later on the grounds that the potentially dangerous Feynman diagrams containing the insertions of operations like $|\Psi_i|^2$ vanish in the limit $n_1, n_2 \to 0$.

In order to calculate (16.219), we decompose the action into a free part

$$\mathcal{A}_0^0 \equiv \mathcal{A}_{\text{CS}} + \int d^3x \left[|\mathbf{D}^1 \Psi_1|^2 + |\boldsymbol{\nabla} \Psi_2|^2 + \sum_{i=1}^{2} 2|\Psi_i|^2 \right], \tag{16.220}$$

and interacting parts

$$\mathcal{A}_1^0 \equiv \int d^3x \, \mathbf{j}_1(\mathbf{x}) \cdot \mathbf{A}_1(\mathbf{x}), \tag{16.221}$$

with a "current" of the first polymer field

$$\mathbf{j}_1(\mathbf{x}) \equiv i \Psi_1^*(\mathbf{x}) \boldsymbol{\nabla} \Psi_1(\mathbf{x}), \tag{16.222}$$

and

$$\mathcal{A}_0^2 \equiv \frac{1}{4} \int d^3\mathbf{x} \ \mathbf{A}_1^2 |\Psi_1(\mathbf{x})|^2. \tag{16.223}$$

Expanding the exponential

$$e^{\mathcal{A}_0} = e^{\mathcal{A}_0^0 + \mathcal{A}_0^1 + \mathcal{A}_0^2} = e^{\mathcal{A}_0} \left[1 - \mathcal{A}_0^1 + \frac{(\mathcal{A}_0^1)^2}{2} - \mathcal{A}_0^2 + \dots \right], \tag{16.224}$$

and keeping only the relevant terms, the functional integral (16.219) can be rewritten as a purely Gaussian expectation value

$$\begin{aligned} N &= \kappa^2 \int d^3x_1 d^3x_2 \lim_{\substack{n_1 \to 0 \\ n_2 \to 0}} \int_{c-i\infty}^{c+i\infty} \frac{Mdz_1}{2\pi i} \frac{Mdz_2}{2\pi i} e^{z_1 L_1 + z_2 L_2} \\ &\times \int \mathcal{D}(\text{fields}) \ \exp(-\mathcal{A}_0^0) |\psi_1^{\alpha_1}(\mathbf{x}_1)|^2 |\psi_2^{\alpha_2}(\mathbf{x}_2)|^2 \\ &\times \left[\left(\int d^3x \, \mathbf{A}_1 \cdot \Psi_1^* \boldsymbol{\nabla} \Psi_1 \right)^2 + \frac{1}{2} \int d^3x \, \mathbf{A}_1^2 \, |\Psi_1|^2 \right] \\ &\times \left[\left(\int d^3x \, \mathbf{A}_2 \cdot \Psi_2^* \boldsymbol{\nabla} \Psi_2 \right)^2 + \frac{1}{2} \int d^3x \, \mathbf{A}_2^2 \, |\Psi_2|^2 \right]. \end{aligned} \tag{16.225}$$

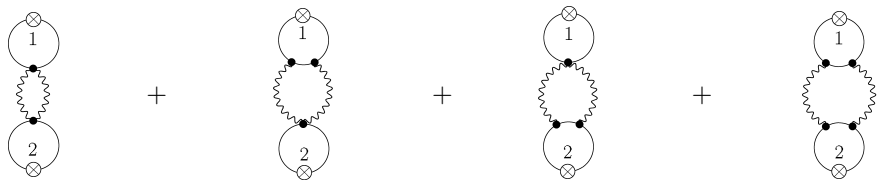

Figure 16.23 Four diagrams contributing in Eq. (16.225). The lines indicate correlation functions of Ψ_i-fields. The crossed circles with label i denote the insertion of $|\Psi_i(\mathbf{x}_i)|^2$.

Note that the initially asymmetric treatment of polymers C_1 and C_2 in the action (16.187) has led to a completely symmetric expression for the second moment.

Only four diagrams shown in Fig. 16.23 contribute in Eq. (16.225). The first diagram is divergent due to the divergence of the loop formed by two vector correlation functions. This infinity may be absorbed in the four-Ψ interaction accounting for the excluded volume effect which we do not consider at the moment. We now calculate the four diagrams separately.

16.8.4 First Diagram in Fig. 16.23

From Eq. (16.225) one has to evaluate the following integral

$$\begin{aligned} N_1 &= \frac{\kappa^2}{4} \lim_{\substack{n_1\to 0\\ n_2\to 0}} \int_{c-i\infty}^{c+i\infty} \frac{M dz_1}{2\pi i} \frac{M dz_2}{2\pi i} e^{z_1 L_1 + z_2 L_2} \int d^3x_1 d^3x_2 \int d^3x_1' d^3x_2' \\ &\times \left\langle |\psi_1^{\alpha_1}(\mathbf{x}_1)|^2 |\psi_2^{\alpha_2}(\mathbf{x}_2)|^2 \left(|\Psi_1|^2 \mathbf{A}_1^2\right)_{\mathbf{x}_1'} \left(|\Psi_2|^2 \mathbf{A}_2^2\right)_{\mathbf{x}_2'} \right\rangle. \end{aligned} \tag{16.226}$$

As mentioned before, there is an ultraviolet-divergent contribution which must be regularized. The system has, of course, a microscopic scale, which is the size of the monomers. This, however, is not the appropriate short-distance scale to be uses here. The model treats the polymers as random chains. However, the monomers of a polymer in the laboratory are usually not freely movable, so that polymers have a certain stiffness. This gives rise to a certain persistence length ξ_0 over which a polymer is stiff. This length scale is increased to $\xi > \xi_0$ by the excluded-volume effects. This is the length scale which should be used as a proper physical short-distance cutoff. We may impose this cutoff by imagining the model as being defined on a simple cubic lattice of spacing ξ. This would, of course, make analytical calculations quite difficult. Still, as we shall see, it is possible to estimate the dependence of the integral N_1 and the others in the physically relevant limit in which the lengths of the polymers are much larger than the persistence length ξ.

An alternative and simpler regularization is based on cutting off all ultraviolet-divergent continuum integrals at distances smaller than ξ.

After such a regularization, the calculation of N_1 is rather straightforward. Replacing the expectation values by the Wick contractions corresponding to the first diagram in Fig. 16.23, and performing the integrals as shown in Appendix 16A, we obtain

$$\begin{aligned} N_1 &= \frac{V}{4\pi} \frac{M^4}{(8\pi)^6} (L_1 L_2)^{-\frac{1}{2}} \int_0^1 ds \left[(1-s)s\right]^{-\frac{3}{2}} \int d^3x e^{-M\mathbf{x}^2/2s(1-s)} \\ &\times \int_0^1 dt \left[(1-t)t\right]^{-\frac{3}{2}} \int d^3y e^{-M\mathbf{y}^2/2t(1-t)} \int d^3x_1'' \frac{1}{|\mathbf{x}_1''|^4}. \end{aligned} \tag{16.227}$$

The variables $\mathbf{x}$ and $\mathbf{y}$ have been rescaled with respect to the original ones in order to extract the behavior of N_1 in L_1 and L_2. As a consequence, the lattices where $\mathbf{x}$ and $\mathbf{y}$ are defined have now spacings $\xi/\sqrt{L_1}$ and $\xi/\sqrt{L_2}$ respectively.

The $\mathbf{x}, \mathbf{y}$ integrals may be explicitly computed in the physical limit $L_1, L_2 \gg \xi$, in which the above spacings become small. Moreover, it is possible to approximate the integral in $\mathbf{x}_1''$ with an integral over a continuous variable l and a cutoff in the ultraviolet region:

$$\int d^3x_1'' \frac{1}{|\mathbf{x}_1''|^4} \sim 4\pi^2 \int_\xi^\infty \frac{dl}{l^2}. \tag{16.228}$$

After these approximations, we finally obtain

$$N_1 = V\pi^{1/2} \frac{M}{(4\pi)^3} (L_1 L_2)^{-1/2} \xi^{-1}. \tag{16.229}$$

16.8.5 Second and Third Diagrams in Fig. 16.23

Here we have to calculate

$$\begin{aligned} N_2 &= \kappa^2 \lim_{\substack{n_1\to 0 \\ n_2 \to 0}} \int_{c-i\infty}^{c+i\infty} \frac{M dz_1}{2\pi i} \frac{M dz_2}{2\pi i} e^{z_1 L_1 + z_2 L_2} \int d^3x_1 d^3x_2 \int d^3x_1' d^3x_1'' d^3x_2' \\ &\times \left\langle |\psi_1^{\alpha_1}(\mathbf{x}_1)|^2 |\psi_2^{\alpha_2}(\mathbf{x}_2)|^2 \left(\mathbf{A}_1 \cdot \Psi_1^* \boldsymbol{\nabla} \Psi_1\right)_{\mathbf{x}_1'} \left(\mathbf{A}_1 \cdot \Psi_1^* \boldsymbol{\nabla} \Psi_1\right)_{\mathbf{x}_1''} \left(\mathbf{A}_2^2 |\Psi_2|^2\right)_{\mathbf{x}_2'} \right\rangle. \end{aligned} \tag{16.230}$$

The above amplitude has no ultraviolet divergence, so that no regularization is required. The Wick contractions pictured in the second Feynman diagrams of Fig. 16.23 lead to the integral

$$N_2 = -4\sqrt{2} V L_2^{-1/2} L_1^{-1} \frac{M^3}{\pi^6} \int_0^1 dt \int_0^t dt' C(t,t'), \tag{16.231}$$

where $C(t,t')$ is a function independent of L_1 and L_2:

$$\begin{aligned} C(t,t') &= [(1-t)t'(t-t')]^{-3/2} \int d^3x d^3y d^3z e^{-M(\mathbf{y}-\mathbf{x})^2/2(1-t)} \\ &\times \left(\boldsymbol{\nabla}_{\mathbf{y}}^j e^{-M\mathbf{y}^2/2t'}\right) \left(\boldsymbol{\nabla}_{\mathbf{x}}^i e^{-M\mathbf{x}^2/2(t-t')}\right) \frac{[\delta_{ij}\mathbf{z}\cdot(\mathbf{z}+\mathbf{x}) - (z+x)_i z_j]}{|\mathbf{z}|^3 |\mathbf{z}+\mathbf{x}|^3}. \end{aligned} \tag{16.232}$$

As in the previous section, the variables $\mathbf{x}, \mathbf{y}, \mathbf{z}$ have been rescaled with respect to the original ones in order to extract the behavior in L_1.

If the polymer lengths are much larger than the persistence length one can ignore the fact that the monomers have a finite size and it is possible to compute $C(t,t')$ analytically, leading to

$$N_2 = -\frac{V L_2^{-1/2} L_1^{-1}}{(2\pi)^6} M^{3/2}\, 4K, \tag{16.233}$$

where K is the constant

$$K \equiv \frac{1}{6} B\left(\frac{3}{2}, \frac{1}{2}\right) + \frac{1}{2} B\left(\frac{5}{2}, \frac{1}{2}\right) - B\left(\frac{7}{2}, \frac{1}{2}\right) + \frac{1}{3} B\left(\frac{9}{2}, \frac{1}{2}\right) = \frac{19\pi}{384} \approx 0.154, \tag{16.234}$$

and $B(a,b) = \Gamma(a)\Gamma(b)/\Gamma(a+b)$ is the Beta function. For large $L_1 \to \infty$, this diagram gives a negligible contribution with respect to N_1.

The third diagram in Fig. 16.23 give the same as the second, except that L_1 and L_2 are interchanged.

$$N_3 = N_2|_{L_1 \leftrightarrow L_2}. \tag{16.235}$$

16.8.6 Fourth Diagram in Fig. 16.23

Here we have the integral

$$\begin{aligned} N_4 &= -4\kappa^2 \frac{1}{2} \lim_{\substack{n_1\to 0\\ n_2\to 0}} \int_{c-i\infty}^{c+i\infty} \frac{M dz_1}{2\pi i} \frac{M dz_2}{2\pi i} e^{z_1 L_1 + z_2 L_2} \int d^3x_1 d^3x_2 \int d^3x_1' d^3x_2' d^3x_1'' d^3x_2'' \\ &\times \Big\langle |\psi_1^{\alpha_1}(\mathbf{x}_1)|^2 |\psi_2(\mathbf{x}_2^{\alpha_2})|^2 (\mathbf{A}_1 \cdot \Psi_1^* \boldsymbol{\nabla} \Psi_1)_{\mathbf{x}_1'} (\mathbf{A}_1 \cdot \Psi_1^* \boldsymbol{\nabla} \Psi_1)_{\mathbf{x}_1''} \\ &\qquad \times (\mathbf{A}_2 \cdot \Psi_2^* \boldsymbol{\nabla} \Psi_2)_{\mathbf{x}_2'} (\mathbf{A}_2 \cdot \Psi_2^* \boldsymbol{\nabla} \Psi_2)_{\mathbf{x}_2''} \Big\rangle, \end{aligned} \tag{16.236}$$

which has no ultraviolet divergence. After some analytic effort we find

$$N_4 = -\frac{1}{16} \frac{M^5 V}{(2\pi)^{11}} (L_1 L_2)^{-1/2} \int_0^1 ds \int_0^s ds' \int_0^1 dt \int_0^t dt' C(s, s', t, t'), \tag{16.237}$$

where

$$\begin{aligned} C(s, s'; t, t') &= [(1-s)s'(s-s')]^{-3/2} [(1-t)t'(t-t')]^{-3/2} \\ &\times \int \frac{d^3p}{(2\pi)^3} \left[\epsilon_{ik\alpha} \frac{p^\alpha}{\mathbf{p}^2} \epsilon_{jl\beta} \frac{p^\beta}{\mathbf{p}^2} + \epsilon_{il\alpha} \frac{p^\alpha}{\mathbf{p}^2} \epsilon_{jk\beta} \frac{p^\beta}{\mathbf{p}^2} \right] \\ &\times \left[\int d^3x' d^3y' e^{-i\sqrt{L_1}\mathbf{p}(\mathbf{x}'-\mathbf{y}')} e^{-M\mathbf{x}'^2/2(1-s)} \left(\boldsymbol{\nabla}_{\mathbf{y}'}^j e^{-M\mathbf{y}'^2/2t'} \right) \left(\boldsymbol{\nabla}_{\mathbf{x}'}^i e^{-M(\mathbf{x}-\mathbf{y})^2/2(s-s')} \right) \right] \\ &\times \left[\int d^3u' d^3v' e^{-i\sqrt{L_2}\mathbf{p}(\mathbf{u}'-\mathbf{v}')} e^{-M\mathbf{v}'^2/2(1-t)} \left(\boldsymbol{\nabla}_{\mathbf{u}'}^l e^{-M\mathbf{u}'^2/2t'} \right) \left(\boldsymbol{\nabla}_{\mathbf{v}'}^k e^{-M(\mathbf{u}'-\mathbf{v}')^2/2(t-t')} \right) \right], \end{aligned} \tag{16.238}$$

and $\mathbf{x}', \mathbf{y}'$ are scaled variables. To take into account the finite persistence length, they should be defined on a lattice with spacing $\xi/\sqrt{L_1}$. Similarly, $\mathbf{u}', \mathbf{v}'$ should be considered on a lattice with spacing $\xi/\sqrt{L_2}$. Without performing the space integrations $d^3x' d^3\mathbf{y}' d^3\mathbf{u}' d^3\mathbf{v}'$, the behavior of N_4 as a function of the polymer lengths can be easily estimated in the following limits:

1. $L_1 \gg 1; L_1 \gg L_2$

$$N_4 \propto L_1^{-1} \tag{16.239}$$

2. $L_2 \gg 1; L_2 \gg L_1$

$$N_4 \propto L_2^{-1} \tag{16.240}$$

3. $L_1, L_2 \gg 1, \quad L_2/L_1 = \alpha = \text{finite}$

$$N_4 \propto L_1^{-3/2}. \tag{16.241}$$

Moreover, if the lengths of the polymers are considerably larger than the persistence length, the function $C(s, s', t, t')$ can be computed in a closed form:

$$\begin{aligned} N_4 &\approx -\frac{128V}{\pi^5} \frac{M}{\pi^{3/2}} (L_1 L_2)^{-1/2} \int_0^1 ds \int_0^1 dt (1-s)(1-t)(st)^{1/2} \\ &\times [L_1 t(1-s) + L_2(1-t)s]^{-1/2}. \end{aligned} \tag{16.242}$$

It is simple to check that this expression has exactly the above behaviors.

16.8.7 Second Topological Moment

Collecting all contributions we obtain the result for the second topological moment:

$$\langle m^2 \rangle = \frac{N_1 + N_2 + N_3 + N_4}{Z}, \tag{16.243}$$

with N_1, N_2, N_3, N_4, Z given by Eqs. (16.210), (16.229), (16.233), (16.235), and (16.231).

In all formulas, we have assumed that the volume V of the system is much larger than the size of the volume occupied by a single polymer, i.e., $V \gg L_1^3$

To discuss the physical content of the result (16.232), we assume C_2 to be a long effective polymer representing all polymers in a uniform solution. We introduce the polymer concentration l as the average mass density of the polymers per unit volume:

$$l = \frac{M}{V}, \tag{16.244}$$

where M is the total mass of the polymers

$$M = \sum_{i=1}^{N_p} m_a \frac{L_k}{a}. \tag{16.245}$$

Here m_a is the mass of a single monomer of length a, L_k is the length of polymer C_k, and N_p is the total number of polymers. Thus L_k/a is the number of monomers in the polymer C_k. The polymer C_1 is singled out as any of the polymers C_k, say $C_{\bar{k}}$, of length $L_1 = L_{\bar{k}}$. The remaining ones are replaced by a long effective polymer C_2 of length $L_2 = \sigma_{k \neq \bar{k}} L_k$. From the above relations we may also write

$$L_2 \approx \frac{aVl}{m_a}. \tag{16.246}$$

In this way, the length of the effective molecule C_2 is expressed in terms of physical parameters, the concentration of polymers, the monomer length, and the mass and volume of the system. Inserting (16.246) into (16.232), with N_1, N_2, N_3, N_4, Z given by Eqs. (16.210), (16.229), (16.233), (16.235), and (16.231). and keeping only the leading terms for $V \gg 1$, we find for the second topological moment $\langle m^2 \rangle$ the approximation

$$\langle m^2 \rangle \approx \frac{N_1 + N_2}{Z}, \tag{16.247}$$

and this has the approximate form

$$\langle m^2 \rangle = \frac{al}{m_a} \left[\frac{\xi^{-1} L_i}{2\pi^{1/2} M^2} - \frac{2K L_1^{1/2}}{\pi^4 M^{3/2}} \right], \tag{16.248}$$

with K of (16.234).

Thus we have succeeded in setting up a topological field theory to describe two fluctuating polymers C_1 and C_2, and calculated the second topological moment for the linking number m between C_1 and C_2. The result is used as an approximation for the second moment for a single polymer with respect to all others in a solution of many polymers.

An interesting remaining problem is to calculate the effect of the excluded volume.

16.9 Chern-Simons Theory of Statistical Interaction

The Chern-Simons theory (16.153) together with the coupling (16.152) generates the desired topological interaction corresponding to the Gaussian integral between

pairs of curves C and C'. We now demonstrate that this topological interaction is the same as the statistical interaction introduced in Eq. (7.279) and encountered again in (16.26), where it governed the physics of a charged particle running around a magnetic flux tube. This observation will make the Gaussian integral and thus the Chern-Simons action relevant for the description of the statistical properties of nonrelativistic particle orbits. In contrast to the electromagnetic generation of fractional statistics for particle orbits in Section 16.2 via the Aharonov-Bohm effect, the field theory involving the statisto-magnetic vector potential has the advantage of removing the asymmetry between the particles, of which one had to carry a charge, the other one a magnetic flux. An arbitrary number of identical particle orbits can now be endowed with a fractional statistics, the same that was produced by topological interaction (7.279).

To prove the equality between the two topological interactions in two space and one time dimension, consider an electron in a plane encircling an infinitely thin magnetic "flux tube" at the origin (the word flux tube stands between quotation marks since the "tube" is only a point in the two-dimensional space). In a Euclidean spacetime, the worldline of the electron C winds itself around the straight "flux tube" C' along the τ-axis. For this geometry, the integral over C' in (16.134) can easily be done using the formula $\int_{-\infty}^{\infty} dt/\sqrt{t^2+d^2}^3 = 2$. The result is

$$G(C,C') = \frac{1}{2\pi}\int d\tau\, \dot{\mathbf{x}}(\tau)\boldsymbol{\nabla}\varphi(\mathbf{x}(\tau)) = \frac{1}{2\pi}\int d\tau\, \dot{\varphi}(\mathbf{x}(\tau)), \tag{16.249}$$

where $\varphi(\mathbf{x}(\tau))$ denotes the azimuthal angle of the electron with respect to the "flux tube" at the time τ

Up to a factor 2π, the expression (16.249) agrees with the statistical interaction in (16.26) and (7.279). In two space and one time dimension, the behavior under particle exchange can be assigned to an amplitude at will by adding to the Euclidean action a Gaussian integral with a suitable prefactor. A phase factor $e^{i\theta}$ is produced by the exchange when choosing the following Euclidean action-at-a-distance:

$$\mathcal{A}_{\mathrm{e,int}} = i2\hbar\theta G(C,C'). \tag{16.250}$$

This topological interaction is generated by the Chern-Simons action

$$\mathcal{A}_{\mathrm{e,CS}} = \frac{1}{4\theta\hbar i}\int d^3x\, \mathbf{A}\cdot(\boldsymbol{\nabla}\times\mathbf{A}). \tag{16.251}$$

The phase angle θ is related to the former parameter μ_0 of the statistical interactions (16.26) and (7.279) by

$$\theta = \pi\mu_0. \tag{16.252}$$

For $\mu_0 = \pm1, \pm3, \pm5, \ldots$, the particle orbits have Fermi statistics; for $\mu_0 = 0, \pm2, \pm4, \ldots$, they have Bose statistics. Fractional values of μ_0 lead to fractional statistics. In contrast to the magnetic generation of fractional statistics, the Chern-Simons mechanism applies to any number of particle orbits. By one of the methods

discussed after Eq. (16.169) it must, however, be assured that the Gaussian "self-energy" does not render any undesirable nontopological contributions.

To maintain the analogy with the magnetic interactions as far as possible, we write the Chern-Simons action for a gas of electrons in the form

$$\mathcal{A}_{\mathrm{e,CS}} = \frac{1}{4\pi i}\frac{e^2}{c^2\hbar\mu_0}\int d^3x\, \mathbf{A}\times(\boldsymbol{\nabla}\times\mathbf{A}), \tag{16.253}$$

and the coupling of the statisto-magnetic vector potential to the particle orbits as

$$\mathcal{A}_{\mathrm{e,curr}} = -i\frac{e}{c}\oint_C d\mathbf{x}\,\mathbf{A}(\mathbf{x}) - i\frac{e}{c}\oint_{C'} d\mathbf{x}\,\mathbf{A}(\mathbf{x}). \tag{16.254}$$

This looks precisely like the Euclidean coupling of an ordinary vector potential to electrons. For an arbitrary number of orbits we define the Euclidean two-dimensional current density

$$\mathbf{j}(\mathbf{x}) \equiv ec\sum_\alpha \oint_{C_\alpha} d\mathbf{x}_\alpha\, \delta^{(3)}(\mathbf{x}-\mathbf{x}_\alpha) \tag{16.255}$$

and write the interaction (16.254) as

$$\mathcal{A}_{\mathrm{e,curr}} = -i\frac{1}{c^2}\int d^3x\, \mathbf{j}(\mathbf{x})\mathbf{A}(\mathbf{x}). \tag{16.256}$$

The curl of the vector potential

$$\mathbf{B} \equiv \boldsymbol{\nabla}\times\mathbf{A} \tag{16.257}$$

is referred to as a *statisto-magnetic field*. By varying (16.253) plus (16.256) with respect to $\mathbf{A}(\mathbf{x})$, we obtain the field equation

$$\mathbf{B}(\mathbf{x}) = \mu_0\frac{2\pi\hbar c}{e^2}\,\mathbf{j}(\mathbf{x}). \tag{16.258}$$

With the help of the elementary flux quantum Φ_0, this can also be written as

$$\mathbf{B}(\mathbf{x}) = \mu_0\Phi_0\frac{1}{e}\mathbf{j}(\mathbf{x}). \tag{16.259}$$

To apply the above formulas, we must transform them from the three-dimensional Euclidean spacetime to the Minkowski space, where the curves C_α become particle orbits in two space dimensions whose coordinates $\mathbf{x}_\perp = (x, y)$ are functions of the time t. Specifically, we substitute the three coordinates (x_1, x_2, x_3) as follows:

$$\begin{aligned}(x_1, x_2) &\rightarrow \mathbf{x}_\perp \equiv (x, y),\\ x_3 &\rightarrow ix_0 \equiv ict.\end{aligned}$$

The Euclidean field components $A_{1,2,3}$ go over into the Minkowskian *statisto-electric potential*ϕ and two spatial components $A_{x,y}$. The three fields $B_{1,2,3}$ turn into the Minkowskian *statisto-electric fields* E_y, E_x and a statisto-magnetic field B_z:

$$\begin{aligned} &A_3 = i\phi = iA_0, \quad A_1 = A_x, \quad A_2 = A_y, \\ &B_3 = iB_z, \quad B_1 = -iE_y, \quad B_2 = iE_x. \end{aligned} \tag{16.260}$$

The Euclidean currents become, up to a factor i, the two-dimensional charge and current densities:

$$\begin{aligned} j_3 &= ij_0 = ic\rho(\mathbf{x}_\perp), \qquad \rho(\mathbf{x}) \equiv e\sum_\alpha \delta^{(2)}(\mathbf{x}_\perp - \mathbf{x}_{\perp\alpha}), \\ j_1 &= ij_x(\mathbf{x}_\perp) = e\sum_\alpha \dot{x}_\alpha \delta^{(2)}(\mathbf{x}_\perp - \mathbf{x}_{\perp\alpha}), \\ j_2 &= ij_y(\mathbf{x}_\perp) = e\sum_\alpha \dot{y}_\alpha \delta^{(2)}(\mathbf{x}_\perp - \mathbf{x}_{\perp\alpha}), \end{aligned} \tag{16.261}$$

where ρ is the particle density per unit area. The motion of a particle in an external field ϕ, A_x, A_y is then governed by the interaction

$$\mathcal{A}_{\rm int} = \int dt d^2x \left[\rho\phi - \frac{1}{c}(j_x A_x + j_x A_y)\right]. \tag{16.262}$$

Conversely, particles with fractional statistics in a 2+1-dimensional spacetime generate Minkowskian *statisto-electromagnetic fields* following the equations

$$B_z = \mu_0\Phi_0\rho, \quad E_x = \mu_0\Phi_0\frac{1}{c}j_y, \quad E_y = \mu_0\Phi_0\frac{1}{c}j_x. \tag{16.263}$$

The electromagnetic normalization in Eq. (16.262) has the advantage that a charged particle cannot distinguish a statisto-magnetic field from a true magnetic field. This property forms the basis for a simple interpretation of the fractional quantum Hall effect as will be seen in Section 18.9.

16.10 Second-Quantized Anyon Fields

After the developments in Chapter 7, we should expect that the phase factor $e^{i\mu_0\pi}$, appearing in the path integral upon exchanging the endpoints of two anyonic orbits, can also be found in a second-quantized operator formulation. To verify this, we consider a free Bose field with the action (7.286) and couple it with a statisto-electromagnetic field subject to a Chern-Simons action. The resulting free anyon action reads

$$\mathcal{A}_{\rm anyon} = \mathcal{A}_{\rm CS} + \mathcal{A}_{\rm boson}, \tag{16.264}$$

where

$$\begin{aligned} \mathcal{A}_{\rm boson} = \int d^2x \int_{t_a}^{t_b} dt \Bigg\{ &\psi^*(\mathbf{x},t)\left[i\hbar\left(\partial_t + i\frac{e}{\hbar}\phi(\mathbf{x},t)\right) + \mu\right]\psi(\mathbf{x},t) \\ &- \frac{\hbar^2}{2M}\left|\left[\boldsymbol{\nabla} - i\frac{e}{\hbar c}\mathbf{A}(\mathbf{x},t)\right]\psi(\mathbf{x},t)\right|^2\Bigg\}. \end{aligned} \tag{16.265}$$

The latter corresponds to the action (7.286) in the continuum limit with the derivatives replaced by covariant derivatives according to the usual minimal substitution rule (2.644):

$$p_0 \to p_0 - \frac{e}{c}\phi, \quad \mathbf{p} \to \mathbf{p} - \frac{e}{c}\mathbf{A}. \tag{16.266}$$

The first field equation in (16.263) now reads

$$B_z(\mathbf{x},t) = \mu_0 \Phi_0 \psi^\dagger(\mathbf{x},t)\psi(\mathbf{x},t), \tag{16.267}$$

so that the vector potential satisfies the differential equation

$$\partial_x A_y(\mathbf{x},t) - \partial_y A_x(\mathbf{x},t) = \mu_0 \Phi_0 \psi^\dagger(\mathbf{x},t)\psi(\mathbf{x},t). \tag{16.268}$$

It determines (A_x, A_y) up to the gauge freedom $(\partial_x\Lambda, \partial_y\Lambda)$, where $\Lambda(\mathbf{x},t)$ is an arbitrary single-valued function satisfying Schwarz' integrability condition

$$(\partial_x\partial_y - \partial_y\partial_x)\Lambda(\mathbf{x},t) = 0. \tag{16.269}$$

In the present case, it is useful to allow for a violation of this condition by searching for a multivalued function $\alpha(\mathbf{x},t)$ whose gradient is equal to a given vector potential:

$$(A_x, A_y) = (\partial_x\alpha, \partial_y\alpha). \tag{16.270}$$

This function must obey the differential equation (recall the discussion in Appendix 10A)

$$(\partial_x\partial_y - \partial_y\partial_x)\alpha(\mathbf{x},t) = \mu_0 \frac{2\pi\hbar c}{e}\psi^\dagger(\mathbf{x},t)\psi(\mathbf{x},t). \tag{16.271}$$

The Green function of this differential equation, which is the elementary building block for the construction of all multivalued functions in two dimensions, is the function used before in Eq. (16.249) [see also (10A.30)]:

$$\varphi(\mathbf{x}-\mathbf{x}') \equiv \arctan[(y-y')/(x-x')]. \tag{16.272}$$

It gives the angle between the vectors $\mathbf{x}$ and $\mathbf{x}'$ and violates the Schwarz integrability condition at the points where the vectors coincide [recall (10A.33)]:

$$(\partial_x\partial_y - \partial_y\partial_x)\varphi(\mathbf{x}-\mathbf{x}') = 2\pi\delta^{(2)}(\mathbf{x}-\mathbf{x}'). \tag{16.273}$$

To satisfy this equation, the cut of the arctan in the complex plane must be avoided, which is always possible by deforming it appropriately. The function $\varphi(\mathbf{x}-\mathbf{x}')$ has the important property

$$\varphi(\mathbf{x}-\mathbf{x}') - \varphi(\mathbf{x}'-\mathbf{x}) = \pi. \tag{16.274}$$

In the two terms on the left-hand side, the point $\mathbf{x}'$ is moved around the point $\mathbf{x}$ in the anticlockwise sense.

With the help of the multivalued Green function (16.272) we find immediately the solution of Eq. (16.271):

$$\alpha(\mathbf{x},t)=\mu_0\frac{\hbar c}{e}\int d^2x\varphi(\mathbf{x}-\mathbf{x}')\psi^\dagger(\mathbf{x},t)\psi(\mathbf{x},t). \tag{16.275}$$

The relation (16.270) permits the elimination of the statisto-magnetic field from the action. Actually, this statement is true in general. One can always multiply the fields $\psi(\mathbf{x},t)$ by a phase factor

$$\exp\left[-i\frac{e}{\hbar c}\int^{\mathbf{x}}d\mathbf{x}'\mathbf{A}(\mathbf{x}',t)\right],$$

where the contour integral is taken to $\mathbf{x}$ from any fixed point along some fixed path. In front of the transformed field

$$\Psi(\mathbf{x},t)=e^{-i(e/\hbar c)\int^{\mathbf{x}}d\mathbf{x}'\mathbf{A}(\mathbf{x}',t)}\psi(\mathbf{x},t), \tag{16.276}$$

the covariant derivatives

$$D_i\psi(\mathbf{x},t)=(\partial_i-i\frac{e}{\hbar c}A_i)\psi(\mathbf{x},t) \tag{16.277}$$

become ordinary derivatives ∂_i. Unfortunately, the new field $\Psi(\mathbf{x},t)$ depends on the vector potential in a complicated nonlocal way so that this transformation is in general not worthwhile. In the present case, however, the equation of motion for the vector potential is so simple that the transformation *can* be done explicitly. In fact, the nonlocality has precisely the desired property of changing the statistics of the fields from Bose statistics to any statistics.

We show this by considering the field operators $\hat{\psi}(\mathbf{x},t)$ which are canonically quantized according to Eq. (7.294). In the continuum limit they satisfy the commutation rules

$$\begin{aligned}[\hat{\psi}(\mathbf{x},t),\hat{\psi}^\dagger(\mathbf{x}',t)] &= \delta^{(2)}(\mathbf{x}-\mathbf{x}'),\\ [\hat{\psi}^\dagger(\mathbf{x},t),\hat{\psi}^\dagger(\mathbf{x}',t)] &= 0,\\ [\hat{\psi}(\mathbf{x},t),\hat{\psi}(\mathbf{x}',t)] &= 0.\end{aligned} \tag{16.278}$$

The transformed field operators satisfy the corresponding commutation rules modified by a phase factor $e^{i\mu_0\pi}$:

$$\begin{aligned}\hat{\psi}(\mathbf{x},t)\hat{\psi}^\dagger(\mathbf{x}',t)-e^{i\pi\mu_0}\hat{\psi}^\dagger(\mathbf{x}',t)\hat{\psi}(\mathbf{x},t) &= \delta^{(2)}(\mathbf{x}-\mathbf{x}'),\\ \hat{\psi}^\dagger(\mathbf{x},t)\hat{\psi}^\dagger(\mathbf{x}',t)-e^{i\pi\mu_0}\hat{\psi}^\dagger(\mathbf{x}',t)\hat{\psi}^\dagger(\mathbf{x},t) &= 0,\\ \hat{\psi}(\mathbf{x},t)\hat{\psi}(\mathbf{x}',t)-e^{i\pi\mu_0}\hat{\psi}(\mathbf{x}',t)\hat{\psi}(\mathbf{x},t), &= 0.\end{aligned} \tag{16.279}$$

As in (16.274), the vector $\mathbf{x}'$ on the left-hand side has to be carried around $\mathbf{x}$ in the anticlockwise sense. Using the relation (16.270), the integral in the prefactor of

(16.276) can immediately be performed and the transformed fields are simply given by

$$\tilde{\psi}(\mathbf{x},t) = e^{-i\frac{e}{\hbar c}\alpha(\mathbf{x},t)}\psi(\mathbf{x},t), \qquad \tilde{\psi}^\dagger(\mathbf{x},t) = \psi(\mathbf{x},t)e^{i\frac{e}{\hbar c}\alpha(\mathbf{x},t)}. \tag{16.280}$$

The same relations hold for the second-quantized field operators. This makes it quite simple to prove the commutation rules (16.279). We do this here only for the second rule which controls the behavior of the many-body wave functions under the exchange of any two-particle coordinates:

$$\hat{\psi}^\dagger(\mathbf{x},t)\hat{\psi}^\dagger(\mathbf{x}',t) - e^{i\pi\mu_0}\hat{\psi}^\dagger(\mathbf{x}',t)\hat{\psi}^\dagger(\mathbf{x},t) = 0.$$

This amounts to the relation

$$\hat{\psi}^\dagger(\mathbf{x},t)e^{i\frac{e}{\hbar c}\hat{\alpha}(\mathbf{x},t)}\hat{\psi}^\dagger(\mathbf{x}',t)e^{i\frac{e}{\hbar c}\hat{\alpha}(\mathbf{x}',t)} = e^{i\pi\mu_0}\hat{\psi}^\dagger(\mathbf{x}',t)e^{i\frac{e}{\hbar c}\hat{\alpha}(\mathbf{x}',t)}\hat{\psi}^\dagger(\mathbf{x},t)e^{i\frac{e}{\hbar c}\hat{\alpha}(\mathbf{x},t)}. \tag{16.281}$$

The phase factors in the middle can be taken to the right-hand side by using the transformation formula

$$e^{i\int d^2x' f(\mathbf{x}',t)\hat{\psi}^\dagger(\mathbf{x},t)\hat{\psi}(\mathbf{x},t)}\hat{\psi}^\dagger(\mathbf{x},t)e^{-i\int d^2x' f(\mathbf{x}',t)\hat{\psi}^\dagger(\mathbf{x},t)\hat{\psi}(\mathbf{x},t)} = e^{if(\mathbf{x},t)}\hat{\psi}^\dagger(\mathbf{x},t), \tag{16.282}$$

which follows from the Lie expansion [recall (1.297)]

$$e^{i\hat{A}}\hat{B}e^{-i\hat{A}} = 1 + i[\hat{A},\hat{B}] + \frac{i^2}{2!}[\hat{A},[\hat{A},\hat{B}]] + \dots\ . \tag{16.283}$$

Setting $f(\mathbf{x})$ equal to $\mu_0\varphi(\mathbf{x}-\mathbf{x}')$, Eq. (16.281) goes over into

$$\begin{aligned}\hat{\psi}^\dagger(\mathbf{x},t)\hat{\psi}^\dagger(\mathbf{x}',t)&e^{i\mu_0\varphi(\mathbf{x}-\mathbf{x}')}e^{i\frac{e}{\hbar c}[\hat{\alpha}(\mathbf{x},t)+\hat{\alpha}(\mathbf{x}',t)]}\\ &= e^{i\pi\mu_0}\hat{\psi}^\dagger(\mathbf{x}',t)\hat{\psi}^\dagger(\mathbf{x},t)e^{i\mu_0\varphi(\mathbf{x}'-\mathbf{x})}e^{i\frac{e}{\hbar c}[\hat{\alpha}(\mathbf{x}',t)+\hat{\alpha}(\mathbf{x},t)]}\ .\end{aligned} \tag{16.284}$$

The correctness of this equation follows directly from the property (16.274) of the $\varphi(\mathbf{x})$ field and from the commutativity of the Bose fields $\psi^\dagger(\mathbf{x},t)$ with each other. This proves the second of the anyon commutation rules (16.279). The others are obtained similarly.

Note that we could just as well have constructed the anyon fields from Fermi fields by shifting the exchange phase by an angle π.

16.11 Fractional Quantum Hall Effect

If particles obeying fractional statistics move in an ordinary magnetic field, they are also subject to a *statisto-magnetic field*. As observed earlier, this acts upon each particle in the same way as an additional true magnetic field. This observation provides a key for the understanding of the *fractional quantum Hall effect*. The arguments will now be sketched.

To measure the effect experimentally, a thin slab of conducting material (the original experiment used the compound $\mathrm{Al_xGa_{1-x}As}$) is placed at low temperatures

(≈ 0.5 K) in the xy-plane traversed by a strong magnetic field B_z (between 10 and 200 kG) along the z-axis. An electric field E_x is applied in the x-direction and an electric *Hall current* j_y per length unit is measured in the y-direction. Such a current is expected in a dissipative electron gas with a number density (per unit area) ρ, where the fields satisfy the relation

$$E_x = -\frac{1}{\rho ec} j_y B_z \tag{16.285}$$

(see Appendix 16E). The transverse resistance defined by

$$R_{xy} \equiv \frac{B_z}{\rho ec} \tag{16.286}$$

rises linearly in B_z. Its dimension is sec/cm. In contrast with this naive expectation, the experimental data for R_{xy} rise stepwise with a number of plateaus whose resistance take the values $h/e^2\nu$, where ν is a rational number with odd denominators:

$$\nu = \tfrac{1}{5}, \tfrac{2}{7}, \tfrac{1}{3}, \tfrac{2}{5}, \tfrac{2}{3}, \dots \ . \tag{16.287}$$

We have omitted the observed number $\nu = \frac{5}{2}$ since its theoretical explanation requires additional physical considerations (see the references at the end of the chapter).

Similar plateaus had been observed at integer values of ν. Those are explained as follows.

In an ideal Fermi liquid at zero temperature, the electron orbits have energies $\mathbf{p}^2/2M$. Their momenta fill a Fermi sphere of radius p_F. The size of p_F is determined from the particle number per unit area ρ via the phase space integral

$$\rho L_x L_y = 2 \times \int \frac{dp_x dp_y L_x L_y}{(2\pi\hbar)^2}, \tag{16.288}$$

where L_x and L_y are the lengths of the rectangular layered material in the x- and y-directions. The factor 2 accounts for the two spin orientations. The rotationally invariant integration up to p_F yields

$$p_F = \sqrt{2\pi\rho}\hbar. \tag{16.289}$$

By switching on a magnetic field B_z, the rotational invariance is destroyed and the electrons circle with a velocity $v = \omega r$ on Landau orbits around the z-direction with the cyclotron frequency $\omega = eB/Mc$. In quantum mechanics, the system corresponds to an ensemble of harmonic oscillators which in the gauge $\mathbf{A} = (0, Bx, 0)$ [see Eq. (9.93)] move back and forth in the x-direction and have a spectrum $(n+1/2)\hbar\omega$ [see Eq. (9.100)]. The phase space integral in the x-direction $\int dp_x L_x/(2\pi\hbar)$ becomes therefore a sum over n. The center of oscillations is $x_0 = p_y/M\omega$ [see

Eq. (9.95)], so that the remaining phase space integral $\int dp_y L_y/(2\pi\hbar)$ can be integrated to $M\omega L_x/(2\pi\hbar)$. Thus (16.288) gives, for each spin orientation,

$$\rho = M\omega \frac{1}{2\pi\hbar} \sum_{n=0}^{n_F} . \tag{16.290}$$

The number of filled levels is $\nu = n_F + 1$. In the vacuum, the levels of one orientation are degenerate with those of the opposite orientation at a neighboring n (up to radiative corrections of the order $\alpha \approx 1/137$). This is due to the anomalous magnetic moment of the spin-1/2 electron being equal to one Bohr magneton $\mu_B = e\hbar/2Mc \approx 0.927 \times 10^{-20}$erg/gauss (i.e., twice as large as classically expected, the factor 2 being caused by the relativistic Thomas precession). Due to the factor 2, the energy levels for the two orientations are split by $\omega\hbar$, which is precisely equal to the energy difference between levels of neighboring n. In a solid material, however, the anomalous magnetic moment is strongly renormalized and the degeneracy is removed. There, every level has a definite spin orientation.

According to Eq. (16.290), the highest level is occupied completely if each level has taken up a particle number corresponding to its maximal filling density

$$\rho_{\max} = \frac{M\omega}{2\pi\hbar}. \tag{16.291}$$

At smaller magnetic fields, this density is small and the electrons are spread over many levels whose number ν is given by

$$\rho = \frac{M\omega}{2\pi\hbar}\nu. \tag{16.292}$$

Expressing ω in terms of B_z leads to

$$\frac{B_z}{\rho} = \frac{hc}{e}\frac{1}{\nu}. \tag{16.293}$$

Using the flux quantum $\Phi_0 = hc/e$, this equation states that the magnetic flux per electron

$$\Phi \equiv \frac{B_z}{\rho} \tag{16.294}$$

has the value

$$\frac{\Phi}{\Phi_0} = \frac{1}{\nu}. \tag{16.295}$$

If the magnetic field is increased, the Landau levels can accommodate more electrons which then reside in a decreasing number ν of levels. By inserting into Eq. (16.286) the values of B_z at which the highest level becomes depleted, one obtains precisely the experimentally observed quantized Hall resistances

$$R_{xy} = \frac{h}{e^2}\frac{1}{\nu} \tag{16.296}$$

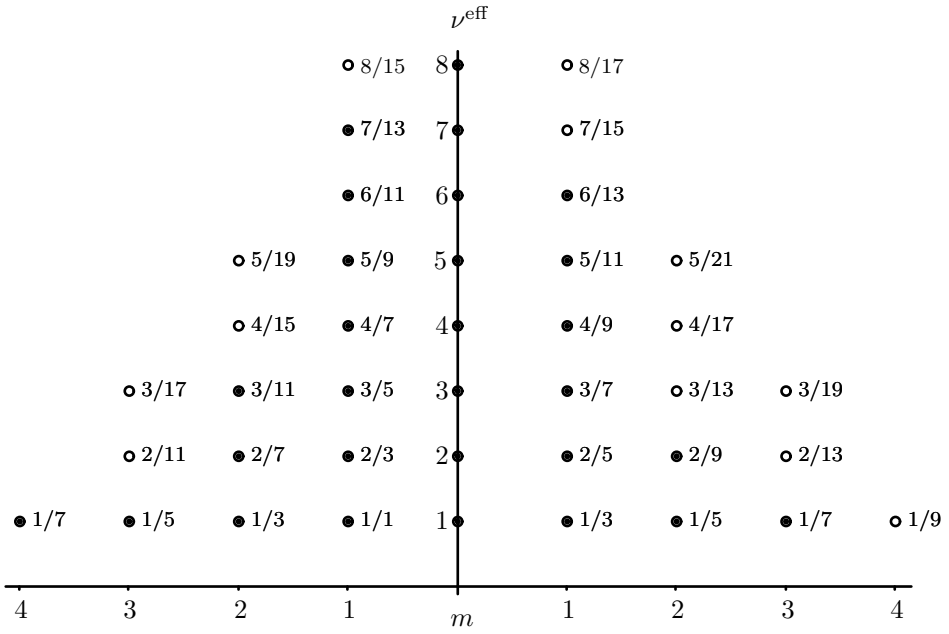

Figure 16.24 Values of parameter ν, at which plateaus in fractional quantum Hall resistance $h/e^2\nu$ are expected theoretically. The right-hand side shows the values $\nu^{\text{eff}}/(2m\nu^{\text{eff}}+1)$, the left-hand side $\nu^{\text{eff}}/(2m\nu^{\text{eff}}-1)$. The full circles indicate the values found experimentally.

with integer values of ν. The assumption of a statisto-magnetic interaction makes it possible to explain the fractional quantum Hall effect by reducing it to the ordinary quantum Hall effect.

In the fractional quantum Hall effect, the magnetic field is so strong that even the lowest Landau level is only partially filled. This is why one did not expect any plateaus at all. According to a simple idea due to Jain, however, it is possible to relate the fractional plateaus to the integer plateaus. For this one assumes that the electrons in the ground state of the fractional quantum Hall effect carry an even statisto-magnetic flux $-2m\Phi_0$ due to the presence of a Chern-Simons action. For the wave function, this amounts to a statistical phase factor $e^{i2\pi m}$ under the exchange of two particle coordinates; it leaves the Fermi statistics of the electrons unchanged. Now one takes advantage of the observation made in the last section that the electrons cannot distinguish a statisto-magnetic field from an external magnetic field. They move in Landau orbits enforced by the combined field

$$B_z^{\text{eff}} = B_z - B_z^{\text{stat}}, \qquad B_z^{\text{stat}} = 2m\Phi_0\rho. \tag{16.297}$$

The cyclotron frequency of the electrons in their Landau orbits is

$$\omega^{\text{eff}} = eB_z^{\text{eff}}/Mc. \tag{16.298}$$

Since the effective field is now much smaller than the external field, the Landau levels possess a greatly reduced capacity. Thus the electrons must be distributed

over several levels in spite of the large magnetic field. The number decreases as the field grows further. The steps appear at those places where the effective magnetic field has its integer quantum Hall plateaus, i.e., at the effective magnetic fields

$$B_z^{\text{eff}} = \pm\rho\Phi_0/\nu^{\text{eff}}, \qquad \nu^{\text{eff}} = 1,\, 2,\, 3, \dots \ . \tag{16.299}$$

The values of ν_{eff} are related to the ν-values of the external magnetic field as follows:

$$\pm\frac{1}{\nu^{\text{eff}}} = \frac{1}{\nu} - 2m. \tag{16.300}$$

From this one has

$$\nu = \frac{\nu^{\text{eff}}}{2m\nu^{\text{eff}} \pm 1}. \tag{16.301}$$

The resulting values of ν on the integer-valued plane spanned by the numbers m and ν^{eff} are shown in Fig. 16.24. Only odd denominators are allowed. The values of ν found by this simple hypothesis agree well with those of the lower experimental levels (16.287).

16.12 Anyonic Superconductivity

At the end of Section 16.3 we have mentioned that an ensemble of particles with fractional statistics in 2+1 spacetime dimensions exhibits Meissner screening. This has given rise to speculations that the presently poorly understood phenomenon of *high-temperature superconductivity* may be explained by anyons physics. The new kind of superconductivity is observed in materials which contain pronounced layer structures, and it is conceivable that the currents move in these two-dimensional subspaces without dissipation. With some effort it can indeed be shown that in 2+1 dimensions a Chern-Simons action may be generated in principle[10] by integrating out Fermi fields. Accepting this, we can easily derive that an addition of this action to the usual electromagnetic field action gives the magnetic field a finite range, i.e., a finite penetration depth. The usual electromagnetic action reads

$$\mathcal{A} = \frac{1}{8\pi}\int dt d^3x[\mathbf{E}^2 - (\boldsymbol{\nabla}\times\mathbf{A})^2], \tag{16.302}$$

where $\mathbf{E}$ is the electric field

$$\mathbf{E} = -\frac{1}{c}\frac{\partial\mathbf{A}}{\partial t} - \boldsymbol{\nabla}A_0. \tag{16.303}$$

In the Euclidean formulation with $x_4 = ict$, the action becomes

$$\mathcal{A}_{\text{e}} = \frac{1}{8\pi c}\int d^4x[\mathbf{E}^2 + (\boldsymbol{\nabla}\times\mathbf{A})^2]. \tag{16.304}$$

[10]See Notes and References at the end of the chapter.

To add the Chern-Simons action, we restrict the spacetime dimensionality to 3. The restriction is imposed by considering a system in 4 spacetime dimensions and assuming it to be translationally invariant along the fourth coordinate direction x_4. Then there are no electric fields, and the Euclidean action becomes

$$\mathcal{A}_{\rm e} = \frac{L}{8\pi c}\int d^3x(\boldsymbol{\nabla}\times\mathbf{A})^2, \tag{16.305}$$

where L denotes the length of the system in the x_4-direction. To this, we now add the Chern-Simons action (16.253) and the current coupling (16.256). By extremizing the total action, we obtain the field equation:

$$\frac{L}{4\pi c}\boldsymbol{\nabla}\times(\boldsymbol{\nabla}\times\mathbf{A}) + i\frac{e^2}{2\pi c^2\hbar\mu_0}\boldsymbol{\nabla}\times\mathbf{A} = i\,\frac{1}{c^2}\,\mathbf{j}. \tag{16.306}$$

For the magnetic field $\mathbf{B} = \boldsymbol{\nabla}\times\mathbf{A}$, the equation reads

$$\frac{L}{4\pi c}(\boldsymbol{\nabla}\times\mathbf{B} + i\lambda^{-1}\mathbf{B}) = i\,\frac{1}{c^2}\,\mathbf{j}, \tag{16.307}$$

where the parameter λ denotes the following length ($\alpha = e^2/\hbar c$ = fine-structure constant $\approx 1/137$):

$$\lambda \equiv \frac{c\hbar\mu_0}{2e^2}L = \frac{\mu_0}{2\alpha}L. \tag{16.308}$$

By multiplying (16.307) vectorially with $\boldsymbol{\nabla}$ and using the equation once more, we obtain

$$\frac{L}{4\pi c}(-\boldsymbol{\nabla}^2 + \lambda^{-2})\mathbf{B} = i\frac{1}{c^2}\boldsymbol{\nabla}\times\mathbf{j} + \frac{1}{c^2}\lambda^{-1}\mathbf{j}\ . \tag{16.309}$$

In the current-free case, the magnetic field is seen to have only a finite penetration depth λ into the material. In an ordinary superconductor, this phenomenon is known as the *Meissner effect*. There it can be understood as a consequence of the induction of supercurrents in an ideal (i.e., incompressible and frictionless) liquid of charged particles, which lowers the invading magnetic field according to Lenz' rule. In the absence of friction, there is a complete extinction.

Recall that a superconductor with time-dependent currents and fields is governed by the characteristic London equation (see Appendix 16D)

$$\boldsymbol{\nabla}\times\mathbf{j} \propto \mathbf{B}. \tag{16.310}$$

For a two-dimensional superconductor, this amounts to

$$(\boldsymbol{\nabla}\times\mathbf{j}_\perp)_z \propto B_z. \tag{16.311}$$

The above anyonic system shows a similar induction phenomenon. In the absence of currents, Eq. (16.309) determines the magnetic field B_z from the particle density by

$$B_z = \mu_0\Phi_0\rho. \tag{16.312}$$

If there are currents in the xy-plane $\mathbf{j}_\perp = (j_x, j_y)$, the magnetic field is increased by ΔB_z in accordance with the equation

$$\frac{L}{4\pi c}(-\boldsymbol{\nabla}^2 + \lambda^{-2})\Delta B_z = \frac{1}{c^2}(\boldsymbol{\nabla} \times \mathbf{j}_\perp)_z. \tag{16.313}$$

This is the desired relation between the magnetic field and the curl of the current which indicates the superconducting character of the system expressed before in the London equation (16.311). The contact with the London equation is established by a restriction to smooth field configurations in which the first term in (16.313) can be ignored.

Thus we conclude that the currents and magnetic fields in a two-dimensional system of anyons show Meissner screening. This is not sufficient to make the system superconductive since it does not automatically imply the absence of dissipation. In a usual superconductor, the existence of an energy gap makes the dissipative part of the current-current correlation function vanish for wave vectors smaller than some value k_c. This value determines the *critical current strength* above which superconductivity returns to normal. In the anyonic system, the absence of dissipation was proved in an approximation. Recent studies of higher corrections, however, have shown the presence of dissipation after all, destroying the hope for an anyonic superconductor.

16.13 Non-Abelian Chern-Simons Theory

The topological field interaction (16.153) can be generalized to nonabelian gauge groups. For the local symmetry group SU(N) it reads

$$\mathcal{A}_{\mathrm{e,CS}} = \frac{k}{4\pi i}\int d^3x \epsilon_{ijk} \mathrm{tr}_N \left(A_i \nabla_j A_k + \frac{2}{3} A_i A_j A_k\right), \tag{16.314}$$

where A_i are Hermitian traceless $N \times N$-matrices and tr_N denotes the associated trace. In the nonabelian theory, the gauge transformations are

$$A_i \leftrightarrow U A_i U^{-1} + i(\partial_i U)U^{-1}. \tag{16.315}$$

It can be shown that they transform $\mathcal{A}_{\mathrm{e,CS}}$ as follows [10]:

$$\mathcal{A}_{\mathrm{e,CS}} \to \mathcal{A}_{\mathrm{e,CS}} + 2\pi i n k \hbar, \qquad n = \text{integer}. \tag{16.316}$$

Thus, the action is not completely gauge-invariant. For integer values of k, however, the additional $2\pi i n k \hbar$ does not have any effect upon the phase factor $e^{-\mathcal{A}_{\mathrm{e,CS}}/\hbar}$ in the path integral associated with the orbital fluctuations. Thus there is gauge invariance for integer values of k (in contrast to the abelian case where k is arbitrary).

In the nonabelian theory, gauge fixing is a nontrivial issue. It is no longer possible to simply add a gauge fixing functional of the type (16.163). The reason is that the volume in the field space of gauge transformations depends on the gauge field. For

a consistent gauge fixing, this volume has to be divided out of the gauge-fixing functional as was first shown by Fadeev and Popov [11]. For an adequate discussion of this interesting topic which lies beyond the scope of this quantum-mechanical text the reader is referred to books on quantum field theory.

As in the abelian case, the functional derivative of the Chern-Simons action with respect to the vector potential gives the field strength

$$B_i \equiv \epsilon_{ijk} F_{jk}, \tag{16.317}$$

where F_{ij} is the nonabelian version of the curl:

$$F_{ij} \equiv \partial_i A_j - \partial_j A_i - i[A_i, A_j]. \tag{16.318}$$

In 1989, Witten found an important result: The expectation value of a gauge-invariant integral defined for any loop L,

$$W_L[\mathbf{A}] \equiv \mathrm{tr}_N \hat{W}[\mathbf{A}] \equiv \mathrm{tr}_N \hat{P} e^{i \oint_L d\mathbf{x}\mathbf{A}}, \tag{16.319}$$

the so-called *Wilson loop integral*, possesses a close relationship with the Jones polynomials of knot theory. The loop L can consist of several components linked in an arbitrary way, in which case the integral in $W_L[\mathbf{A}]$ runs successively over all components. The operator $\hat{P}$ in front of the exponential function denotes the *path-ordering operator*. It is defined in analogy with the time-ordering operator $\hat{T}$ in (1.241): If the exponential function in (16.319) is expanded into a Taylor series, it specifies the order in which the $N \times N$-matrices$A_i(\mathbf{x})$, which do not commute for different $\mathbf{x}$ and i, appear in the products. If the path is labeled by a "time parameter", the earlier matrices stand to the right of the later ones. The fluctuations of the vector potential are controlled by the Chern-Simons action (16.314). Expectation values of the loop integrals are defined by the functional integral

$$\langle W_L[\mathbf{A}] \rangle \equiv \frac{\int \mathcal{D}A_i e^{-\mathcal{A}_{\mathrm{e,CS}}/\hbar} W_L[\mathbf{A}]}{\int \mathcal{D}A_i e^{-\mathcal{A}_{\mathrm{e,CS}}/\hbar}}. \tag{16.320}$$

To calculate the self-interaction of a loop, we proceed as described in the abelian case after Eq. (16.169) by spreading the line out into an infinitely thin ribbon of parallel lines. The borders of the ribbon are positioned in such a way that their linking number L_{k} vanishes. If 0 denotes a circle, i.e., a trivial knot, one can show that

$$\langle W_0[\mathbf{A}] \rangle = \frac{q^{N/2} - q^{-N/2}}{q^{1/2} - q^{-1/2}}, \tag{16.321}$$

with

$$q \equiv e^{-2\pi i/(N+k)}. \tag{16.322}$$

For an arbitrary link L one finds the skein relation (see Appendix 16C)

$$q^{N/2} \langle W_{L_+}[\mathbf{A}] \rangle - q^{-N/2} \langle W_{L_-}[\mathbf{A}] \rangle = (q^{1/2} - q^{-1/2}) \langle W_{L_0}[\mathbf{A}] \rangle. \tag{16.323}$$

If $N = 2$, this agrees up to the sign of the right-hand side with the relation (16.114) for the Jones polynomials $J_L(t)$. For general values of $N \neq 2$, we obviously obtain with $t = q^{-N/2}$ and $\alpha = q^{1/2} - q^{-1/2} = -(t^{1/N} - t^{-1/N})$ the skein relations (16.122) of the HOMFLY polynomials. The important relation is

$$\frac{\langle W_L[\mathbf{A}]\rangle}{\langle W_0[\mathbf{A}]\rangle} = H_L(t, -(t^{1/N} - t^{-1/N})), \qquad t = e^{\pi i/k}. \tag{16.324}$$

Since the second variable in $H_L(t, \alpha)$ appears only in even or odd powers, $H_L(t, -(t^{1/2} - t^{-1/2}))$ is a Jones polynomial up to a sign $(-1)^{s+1}$, where s is the number of loops in L.

A favored choice of framing is one in which the self-linking number $L_{\rm k}$ of each component is equal to the twist number or writhe w introduced in Eq. (16.110). Then the ribbon lies flat on the projection plane of the knot. This framing can easily be drawn on the blackboard by splitting the line L into two parallel running lines; it is therefore called the *blackboard framing*. Incidentally, each choice of framing can be drawn as a blackboard framing if one adds to the loop L an appropriate number of windings via a Reidemeister move of type I. These are trivial for lines and nontrivial only for ribbons (see Fig. 16.6). In the blackboard framing, each such winding changes the values $L_{\rm k}$ and w simultaneously by one unit. Thus $L_{\rm k} = w$ can be brought to any desired value. Take, for example, the trefoil knot in Fig. 16.2. In the blackboard framing it has the self-linking number $L_{\rm k} = w = -3$. This can be brought to zero by adding three windings via a Reidemeister move of type I.[11]

In the framing $L_{\rm k} = w$, the right-hand side of (16.324) carries an extra phase factor c^w, where

$$c = e^{-i2\pi(N^2-1)/2Nk}. \tag{16.325}$$

For comparison: In the abelian Chern-Simons theory, the phase factor is $c = e^{-2\pi i/k}$, and the expectation $\langle W_L[\mathbf{A}]\rangle$ has the value $c^{\Sigma_{i\neq j} L_{{\rm k}ij}}$ for a link of several loops labeled by i with vanishing individual self-linking numbers $L_{{\rm k}i}$. In the framing $L_{{\rm k}i} = w_i$, the value is $c^{\Sigma_{i\neq j} L_{{\rm k}ij} + \Sigma_i w_i}$.

The investigation of the properties of loops with nonabelian topological interactions is an interesting task of present-day research.

Appendix 16A Calculation of Feynman Diagrams in Polymer Entanglement

For the calculation of the amplitudes $N_1, \ldots, N_4$ in Eqs. (16.226), (16.230), (16.235), and (16.236), we need the following simple tensor formulas involving two completely antisymmetric tensors ε^{ijl}:

$$\varepsilon_{ijk}\varepsilon^{imn} = \delta_j^m \delta_k^n - \delta_j^n \delta_k^m, \qquad \varepsilon_{ijk}\varepsilon^{ijl} = 2\delta_k^l. \tag{16A.1}$$

The Feynman diagrams shown in Fig. 16.23 corresponds to integrals over products of the polymer correlation functions G_0 defined in Eq. (16.213), which have to be integrated over space and

[11] Mathematicians usually prefer another framing in which the ribbons lie flat on the so-called *Seifert surfaces*.

Laplace transformed. For the latter we make use of the convolution property of the integral over two Laplace transforms $\tilde{f}(z)$ and $\tilde{g}(z)$ of the functions f, g:

$$\int_{c-i\infty}^{c+i\infty} \frac{Mdz}{2\pi i} e^{zL} \tilde{f}(z)\tilde{g}(z) = \int_0^L ds f(s) g(L-S). \tag{16A.2}$$

All spatial integrals are Gaussian of the form

$$\int d^3x e^{-a\mathbf{x}^2+2b\mathbf{x}\cdot\mathbf{y}} = (2\pi)^{3/2} a^{-3/2} e^{b^2\mathbf{y}^2/a}, \quad a>0. \tag{16A.3}$$

Contracting the fields in Eq. (16.226), and keeping only the contributions which do not vanish in the limit of zero replica indices, we find with the help of Eqs. (16A.1) and (16A.2):

$$\begin{aligned} N_1 &= \int d^3x_1, d^3x_2 \int_0^{L_1} ds \int_0^{L_2} dt \int d^3x_1' d^3x_2' \, G_0(\mathbf{x}_1 - \mathbf{x}_1'; s) G_0(\mathbf{x}_1' - \mathbf{x}_1; L_1 - s) \\ &\times \; G_0(\mathbf{x}_2 - \mathbf{x}_2'; t) G_0(\mathbf{x}_2' - \mathbf{x}_2; L_2 - t) \frac{l}{|\mathbf{x}_1' - \mathbf{x}_2'|^4}. \end{aligned} \tag{16A.4}$$

Performing the changes of variables

$$s' = \frac{s}{L_1}, \quad t' = \frac{t}{L_2}, \quad \mathbf{x} = \frac{\mathbf{x}_1 - \mathbf{x}_1'}{\sqrt{L_1}}, \quad \mathbf{y} = \frac{\mathbf{x}_2 - \mathbf{x}_2'}{\sqrt{L_2}}, \tag{16A.5}$$

and setting $\mathbf{x}_1'' \equiv \mathbf{x}_1' - \mathbf{x}_2'$, we easily derive (16.227).

For small $\xi/\sqrt{L_1}$ and $\xi/\sqrt{L_2}$, we use the approximation (16.228). The space integrals can be done using the formula (16A.3). After some work we obtain the result (16.240).

For the amplitude N_2 in Eq. (16.230) we obtain likewise the integral

$$\begin{aligned} N_2 = & \int d^3x_1 d^3x_2 \int d^3x_1' d^3x_1'' d^3x_2' \\ & \times \left[\int_0^{L_1} ds \int_0^S ds' G_0(\mathbf{x}_1' - \mathbf{x}_1; L_1 - s) \; \boldsymbol{\nabla}^j_{x_1''} G_0(\mathbf{x}_1 - \mathbf{x}_1''; s') \boldsymbol{\nabla}^i_{x_1'} G_0(\mathbf{x}_1'' - \mathbf{x}_1'; s - s') \right] \\ & \times D_{ik}(\mathbf{x}_1' - \mathbf{x}_2) D_{jk}(\mathbf{x}_1'' - \mathbf{x}_2') \left[\int_0^{L_2} dt \, G_0(\mathbf{x}_2 - \mathbf{x}_2'; L_2 - t) G_0(\mathbf{x}_2' - \mathbf{x}_2; t) \right], \end{aligned} \tag{16A.6}$$

where $D_{ij}(\mathbf{x}, \mathbf{x}')$ are the correlation functions (16.174) and (16.175) of the vector potentials. Setting $\mathbf{x}_2 \equiv \sqrt{L_2}\mathbf{u} + \mathbf{x}_2'$ and supposing that $\xi/\sqrt{L_2}$ is small, the integral over $\mathbf{u}$ can be easily evaluated with the help of the Gaussian integral (16A.3). After the substitutions $\mathbf{x}_1'' = \sqrt{L_1}\mathbf{y} + \mathbf{x}_1 \quad \mathbf{x}_1' = \sqrt{L_1}(\mathbf{y} - \mathbf{x}) + \mathbf{x}_1, \quad \mathbf{x}_2' = \sqrt{L_1}(\mathbf{y} - \mathbf{x} - \mathbf{z}) + \mathbf{x}_1$ and a rescaling of the variables s, s' by a factor L_1^{-1}, we derive Eq. (16.231) with (16.232).

For small $\xi/\sqrt{L_1}, \xi/\sqrt{L_2}$, the spatial integrals are easily evaluated leading to:

$$N_2 = \frac{-\sqrt{2} V L_2^{-1/2} L_1^{-1} M^{-1/2}}{(4n)^6} \int_0^1 dt \int_0^t dt' t' (1-t) \sqrt{\frac{t-t'}{1-t+t'}}. \tag{16A.7}$$

After the change of variable $t' \to t'' = t - t'$, the double integral is reduced to a sum of integrals the type

$$c(n,m) = \int_0^1 dt t^m \int_0^t dt' t'^n \sqrt{\frac{t'}{1-t'}}, \quad m, n = \text{integers}\,.$$

These can be simplified by replacing t^m by $dt^{m+1}/dt(m+1)$, and doing the integrals by parts. In this way, we end up with a linear combination of integrals of the form:

$$\int_0^1 dt \frac{t^{\kappa+\frac{1}{2}}}{\sqrt{1-t}} = B\left(\kappa + \frac{3}{2}, \frac{1}{2}\right). \tag{16A.8}$$

The calculations of N_3 and N_4 are very similar, and are therefore omitted.

Appendix 16B Kauffman and BLM/Ho Polynomials

The Kauffman polynomials are given by $F(a,x) = a^{-w}\Lambda(a,x)$, where w is the writhe and $\Lambda(a,x)$ satisfies the skein relation

$$\Lambda_{L_+}(a,x) + \Lambda_{L_-}(a,x) = x[\Lambda_{L_0}(a,x) + \Lambda_{L_\infty}(a,x)]. \tag{16B.1}$$

The subscripts refer to the same loop configurations as in Figs. 16.10 and 16.12. The trivial loop has

$$\Lambda(a,x) = \frac{a+a^{-1}}{z} - 1. \tag{16B.2}$$

While the Kauffman polynomial is a knot invariant, the Λ-polynomial is only a ribbon invariant.[12] If a winding L_{T+} or L_{T-} is removed from a loop with the help of a Reidemeister move of type I in Fig. 16.6 (which for infinitely thin lines would be trivial while changing the writhe of a ribbon by one unit) then $\Lambda(a,x)$ receives a factor a or a^{-1}, respectively (see Fig. 16.25).

Figure 16.25 Trivial windings L_{T+} and L_{T-}. Their removal by means of Reidemeister move of type I decreases or increases writhe w by one unit.

The Kauffman polynomials arise from Wilson loop integrals of a nonabelian Chern-Simons theory, if the action (16.314) is SO(N)- rather than SU(N)-symmetric. A list of these polynomials can be found in papers by Lickorish and Millet and by Doll and Hoste quoted at the end of the chapter.

The BLM/Ho polynomials are special cases of the Kauffman polynomials. The relation between them is $Q(x) \equiv F(1,x)$.

Appendix 16C Skein Relation between Wilson Loop Integrals

Here we sketch the derivation of the skein relation (16.323) for the expectation values of Wilson's loop integrals (16.319). Let us decompose A_i in terms of the N^2-1 generators T_a of the group SO(N):

$$A_i = \sum_a A_i^a T_a. \tag{16C.1}$$

They satisfy the commutation rules

$$[T_a, T_b] = i f_{abc} T_c. \tag{16C.2}$$

[12] More precisely, $F(a,x)$ is invariant under the three Reidemeister moves which, in the projected picture of the knot in Fig. 16.6, define the ambient isotopy, whereas Λ changes under the first Reidemeister move, associated only with regular isotopy. whereas

For simplicity, we assume k to be very large so that we can restrict the treatment to the lowest order in $1/k$. To avoid inessential factors of the constants $e, c, \hbar$, we set these equal to 1. Under a small variation of the fields one has

$$\frac{\delta \hat{W}_L[\mathbf{A}]}{\delta A_i^a(\mathbf{x})} = i\hat{P}\int_L dx_i' \delta^{(3)}(\mathbf{x}-\mathbf{x}')T_a(\mathbf{x}')\hat{W}_L[\mathbf{A}], \tag{16C.3}$$

where the path-ordering operator $\hat{P}$ arranges the expression to its right in such a way that T_a is situated in $\hat{W}_L$ at the correct path-ordered place. To emphasize this, we have recorded the position of T_a by means of an $\mathbf{x}$-argument. More precisely, if we discretize the loop integral and write

$$\hat{W}_L[\mathbf{A}] = e^{iA_i(\bar{\mathbf{x}}^1)\Delta x_i^1} e^{iA_i(\bar{\mathbf{x}}^2)\Delta x_i^2}\cdots e^{iA_i(\bar{\mathbf{x}}^n)\Delta x_i^n}\cdots, \tag{16C.4}$$

where $\bar{\mathbf{x}}^n$ are the midpoints of the intervals $\Delta\mathbf{x}^n$, a differentiation with respect to one of the $A_i(\bar{\mathbf{x}}^n)$-fields replaces the associated factor $e^{iA_i(\bar{\mathbf{x}}_n)\Delta x_i^n}$ by $iT_a e^{iA_i(\bar{\mathbf{x}}^n)\Delta x_i^n}$. With the δ-function on a line L defined in Eq. (10A.8), we write (16C.3) as

$$\frac{\delta \hat{W}_L[\mathbf{A}]}{\delta A_i^a(\mathbf{x})} = i\hat{P}\delta_i(\mathbf{x}, L)T_a(\mathbf{x})\hat{W}_L[\mathbf{A}]. \tag{16C.5}$$

For simplicity, we assume $\mathbf{x}$ to be only once traversed by the loop L.

If the shape of the loop is deformed infinitesimally by $dS_i = \epsilon_{ijk}dx_i d'x_j$, then $\hat{W}_L$ changes by

$$\delta\hat{W}_L = i dx_i d'x_j \hat{P}F_{ij}^a(\mathbf{x})T_a(\mathbf{x})\hat{W}_L, \tag{16C.6}$$

where F_{ij}^a are the N^2-1 components of the nonabelian field strengths

$$F_{ij} = \partial_i A_j - \partial_j A_i - i[A_i, A_j] \tag{16C.7}$$

and $\mathbf{x}$ the midpoints of the parallelograms spanned by $d\mathbf{x}$ and $d'\mathbf{x}$. The derivation of Eq. (16C.6) is based on the observation that a change of the path by a small parallelogram adds to the line integral $\hat{W}_L$ a factor $\hat{W}_\square$, which is a Wilson loop integral around the small parallelogram. The latter is evaluated as follows:

$$\begin{aligned}
\hat{W}_\square &= e^{iA_i(\mathbf{x}-d'\mathbf{x}/2)dx_i} e^{iA_j(\mathbf{x}+d\mathbf{x}/2)d'x_j} e^{-iA_i(\mathbf{x}+d'\mathbf{x}/2)dx_i} e^{-iA_j(\mathbf{x}-d\mathbf{x}/2)d'x_j} \\
&= e^{i[A_i(\mathbf{x})dx_i - \partial_j A_i(\mathbf{x})dx_i d'x_j + \ldots]} e^{i[A_j(\mathbf{x})d'x_j + \partial_i A_j(\mathbf{x})dx_i d'x_j + \ldots]} \\
&\times\ e^{-i[A_i(\mathbf{x})dx_i + \partial_j A_i(\mathbf{x})dx_i d'x_j + \ldots]} e^{-i[A_j(\mathbf{x})d'x_j - \partial_i A_j(\mathbf{x})dx_i d'x_j + \ldots]} \\
&= e^{iF_{ij}(\mathbf{x})dx_i d'x_j}.
\end{aligned} \tag{16C.8}$$

The last line is found with the help of the Baker-Hausdorff formula $e^A e^B = e^{A+B+[A,B]/2+\cdots}$ (recall Appendix 2A).

Let us denote the Chern-Simons functional integral over $\hat{W}_L[\mathbf{A}]$ by $\overline{\hat{W}}_L$. Their $N\times N$-traces are $W_L[A]$ and $\bar{W}_L$. The latter differs from the expectation $\langle W_L[\mathbf{A}]\rangle$ in (16.320) by not containing the normalizing denominator, i.e.,

$$\overline{W}_L \equiv \int \mathcal{D}\mathbf{A} e^{-\mathcal{A}_{\mathrm{e,CS}}} W_L[\mathbf{A}]. \tag{16C.9}$$

This changes under the loop deformation by

$$\begin{aligned}
\delta\overline{W}_L &= \int \mathcal{D}\mathbf{A}\delta W_L[\mathbf{A}] e^{-\mathcal{A}_{\mathrm{e,CS}}} \\
&= i dx_i d'x_j \int \mathcal{D}\mathbf{A} F_{ij}^a(\mathbf{x})T_a(\mathbf{x})W_L[\mathbf{A}] e^{-\mathcal{A}_{\mathrm{e,CS}}},
\end{aligned} \tag{16C.10}$$

with the tacit agreement that a generator $T_a(\mathbf{x})$ written in front of the trace has to be evaluated within the trace at the correct path-ordered position. Now we observe that F^a_{ij} can also be obtained by applying a functional derivative to the Chern-Simons action (16.314):

$$i\frac{4\pi}{k}\epsilon_{ijk}\frac{\delta\mathcal{A}_{\mathrm{e,CS}}}{\delta A^a_k(\mathbf{x})} = F^a_{ij}(\mathbf{x}). \tag{16C.11}$$

This allows us to rewrite (16C.10) as

$$-\frac{4\pi}{k}\int\mathcal{D}\mathbf{A}\int dS_i\frac{\delta\mathcal{A}_{\mathrm{e,CS}}}{\delta A^a_i(\mathbf{x})}T_a(\mathbf{x})W_L[\mathbf{A}]e^{-\mathcal{A}_{\mathrm{e,CS}}}$$

and further as

$$\frac{4\pi}{k}\int\mathcal{D}\mathbf{A}dS_iT_a(\mathbf{x})W_L\frac{\delta}{\delta A^a_i(\mathbf{x})}e^{-\mathcal{A}_{\mathrm{e,CS}}}.$$

A partial functional integration produces

$$-\frac{4\pi}{k}\int\mathcal{D}\mathbf{A}\int dS_iT_a(\mathbf{x})\frac{\delta W_L[\mathbf{A}]}{\delta A^a_i(\mathbf{x})}e^{-\mathcal{A}_{\mathrm{e,CS}}},$$

which brings the variation to the form

$$\delta\overline{W}_L = -\frac{4\pi i}{k}\int\mathcal{D}\mathbf{A}dS_i\delta_i(\mathbf{x},L)T_a(\mathbf{x})T_a(\mathbf{x})W_L[\mathbf{A}]e^{-\mathcal{A}_{\mathrm{e,CS}}}. \tag{16C.12}$$

The expectation of Wilson's loop integral $\overline{W}_L$ changes under a deformation only if the loop crosses another line element. This property makes $\overline{W}_L$ a ribbon invariant, i.e., an invariant of regular isotopy.

For a finite deformation, the right-hand side has to be integrated over the area S across which the line has swept. Using the integral formula

$$\int_S dS_i\delta_i(\mathbf{x},L) = \left\{\begin{array}{c}1\\0\end{array}\right\}\text{ if the line }L\left\{\begin{array}{ll}\text{pierces}&\text{S}\\\text{misses}&\text{S}\end{array}\right\}, \tag{16C.13}$$

we obtain for each crossing

$$\overline{W}_{L_+} - \overline{W}_{L_-} \equiv \Delta\overline{W}_L = -\frac{4\pi i}{k}\int\mathcal{D}\mathbf{A}T_a(\mathbf{x})T_a(\mathbf{x})W_L[\mathbf{A}]e^{-\mathcal{A}_{\mathrm{e,CS}}}. \tag{16C.14}$$

The two generators $T_a(\mathbf{x})$ lie path-ordered on the different line pieces of the crossing. To establish contact with the knot polynomials, the left-hand sides have been labeled by the loop subscripts L_+ and L_- appearing in the skein relations of Eq. 16.114.

The product of the generators on the right-hand side is the Casimir operator of the $N\times N$ -representation of SO(N):

$$(T_a)_{\alpha\beta}(T_a)_{\gamma\delta} = \frac{1}{2}\delta_{\alpha\delta}\delta_{\beta\gamma} - \frac{1}{2N}\delta_{\alpha\beta}\delta_{\gamma\delta}. \tag{16C.15}$$

When inserted into Eq. (16C.14), we obtain the graphical relation:

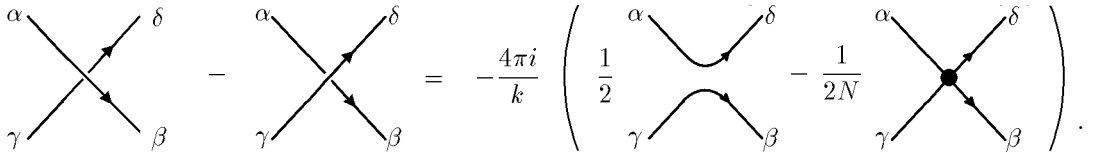

The second graph on the right-hand side can be decomposed into

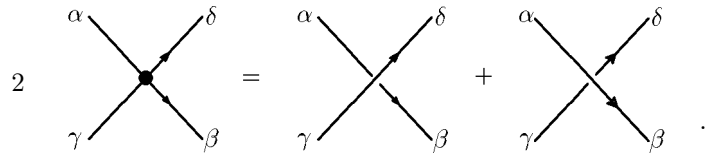

Taking these two terms to the left-hand side of (16C.14), we obtain the skein relation

$$\left(1-\frac{\pi i}{Nk}\right)\overline{W}_{L_+}-\left(1+\frac{\pi i}{Nk}\right)\overline{W}_{L_-}=-\frac{2\pi i}{k}\overline{W}_{L_0}. \tag{16C.16}$$

We now apply this relation to the windings displayed in Fig. 16.25. They decompose into a line and a circle. Due to the trace operation in $\overline{W}_{L_0}$, the circle contributes a factor N. Thus we obtain the relation

$$\left(1-\frac{\pi i}{Nk}\right)\overline{W}_{L_{T+}}-\left(1+\frac{\pi i}{Nk}\right)\overline{W}_{L_{T-}}=-\frac{2\pi i}{k}N\,\overline{W}_{L_{T0}}. \tag{16C.17}$$

Now we remove on the left-hand side the windings according to the graphical rules of Fig. 16.25. Under this operation, the Wilson loop integral is not invariant. Like BLM/Ho polynomials, it acquires a factor a or a^{-1}:

$$\overline{W}_{L_{T+}}=a\overline{W}_{L_{T0}},\quad \overline{W}_{L_{T-}}=a^{-1}\overline{W}_{L_{T0}}. \tag{16C.18}$$

To be compatible with (16C.17), the parameter a must satisfy

$$a=1-\frac{\pi i}{Nk}(N^2-1),\quad a^{-1}=1+\frac{\pi i}{Nk}(N^2-1). \tag{16C.19}$$

Due to (16C.18), the Wilson loop integral is only a ribbon invariant exhibiting regular isotopy. A proper knot invariant which distinguishes ambient isotopy classes arises when multiplying $\overline{W}_L$ by a^{-w}. The polynomials $H_L\equiv e^{-w}\overline{W}_L$ satisfy the skein relation

$$\left[\left(1-\frac{\pi i}{Nk}\right)a\right]H_{L_+}-\left[\left(1+\frac{\pi i}{Nk}\right)a^{-1}\right]H_{L_-}=-\frac{2\pi i}{k}H_{L_0}. \tag{16C.20}$$

The prefactors on the left-hand side can be written for large k as $1-2\pi iN/k\approx q^{N/2}$ and $1+2\pi iN/k\approx q^{-N/2}$ with $q=1-2\pi i\pi/k$. The prefactor on the right-hand side is equal to $q^{1/2}-q^{-1/2}$. To leading order in $1/k$, we have thus derived the skein relation (16.323) for the HOMFLY polynomials H_L.

Appendix 16D London Equations

Consider an ideal fluid of charged particles. By definition, it is non-viscous and incompressible, satisfying $\boldsymbol{\nabla}\cdot\mathbf{v}=0$. If the charge of the particles is e (which we take to be negative for electrons), the electric current density is

$$\mathbf{j}=\rho e\mathbf{v}, \tag{16D.1}$$

where ρ is the particle density. The current is obviously conserved.

The equation of motion of the particles in an electric and magnetic field is governed by the Lorentz force and reads

$$M\dot{\mathbf{v}}=e\left(\mathbf{E}+\frac{1}{c}\mathbf{v}\times\mathbf{B}\right). \tag{16D.2}$$

Using the kinematic identity

$$\frac{d\mathbf{v}}{dt} = \frac{\partial \mathbf{v}}{\partial t} + (\mathbf{v}\cdot\boldsymbol{\nabla})\mathbf{v} = \frac{\partial \mathbf{v}}{\partial t} + \boldsymbol{\nabla}\left(\frac{1}{2}\mathbf{v}^2\right) - \mathbf{v}\times(\boldsymbol{\nabla}\times\mathbf{v}), \tag{16D.3}$$

this leads to the partial differential equation for the velocity field $\mathbf{v}(\mathbf{x},t)$

$$M\frac{\partial \mathbf{v}}{\partial t} + \boldsymbol{\nabla}\left(\frac{M}{2}\mathbf{v}^2\right) = e\mathbf{E} + M\mathbf{v}\cdot\left(\boldsymbol{\nabla}\times\mathbf{v} + \frac{e}{Mc}\mathbf{B}\right). \tag{16D.4}$$

Consider the time dependence of the vector field on the right-hand side

$$\mathbf{X} = \boldsymbol{\nabla}\times\mathbf{v} + \frac{e}{Mc}\mathbf{B}. \tag{16D.5}$$

Using Maxwell's equation

$$\frac{\partial}{\partial t}\mathbf{B} = -c\boldsymbol{\nabla}\times\mathbf{E}, \tag{16D.6}$$

we derive

$$\frac{\partial}{\partial t}\mathbf{X} = \boldsymbol{\nabla}\times(\boldsymbol{\nabla}\times\mathbf{X}). \tag{16D.7}$$

Suppose now that there is initially no $\mathbf{B}$-field in the ideal fluid at rest which therefore has $\mathbf{X}\equiv 0$ everywhere. If a magnetic field is turned on, Eq. (16D.7) guarantees that $\mathbf{X}$ remains zero at all times. This implies that

$$\boldsymbol{\nabla}\times\mathbf{j} = -\frac{\rho e^2}{Mc}\mathbf{B}, \tag{16D.8}$$

which is the first London equation. By inserting the first London equation into Eq. (16D.4), we find the second London equation

$$\frac{\partial}{\partial t}\mathbf{v} + \boldsymbol{\nabla}\left(\frac{M}{2}\mathbf{v}^2\right) = e\mathbf{E}. \tag{16D.9}$$

If the vector potential is taken in the transverse gauge $\boldsymbol{\nabla}\cdot\mathbf{A} = 0$ (which in this context is also called *London gauge*), then the first London equation can be solved and yields

$$\mathbf{j} = -\frac{\rho e^2}{Mc}\mathbf{A}. \tag{16D.10}$$

By inserting this equation into the Maxwell equation with no electric field $\mathbf{E}$, we obtain

$$\boldsymbol{\nabla}\times\mathbf{B} = \frac{4\pi}{c}j = -\frac{\rho 4\pi e^2}{Mc^2}\mathbf{A}. \tag{16D.11}$$

When rewritten in the form

$$\boldsymbol{\nabla}\times(\boldsymbol{\nabla}\times\mathbf{A}) + \lambda^{-2}\mathbf{A} = 0, \tag{16D.12}$$

with

$$\lambda^{-2} = \frac{\rho 4\pi e^2}{Mc^2}, \tag{16D.13}$$

the equation exhibits directly the finite penetration depth λ of a magnetic field into the fluid, the celebrated Meissner effect. It is the ideal manifestation of the Lenz rule, according to which an incoming magnetic field induces currents reducing the magnetic field — in the present case to extinction.

Appendix 16E Hall Effect in Electron Gas

A gas of electrons with a density ρ carries an electric current

$$\mathbf{j} = \rho e \mathbf{v}. \tag{16E.1}$$

In a magnetic field, the particle velocities change due to the Lorentz force by

$$M\dot{\mathbf{v}} = e\left(\mathbf{E} + \frac{1}{c}\mathbf{v}\times\mathbf{B}\right). \tag{16E.2}$$

If σ_0 denotes the conductivity of the system without a magnetic field, the electric current is obviously given by

$$\begin{aligned}\mathbf{j} &= \sigma_0\left(\mathbf{E} + \frac{1}{c}\mathbf{v}\times\mathbf{B}\right)\\ &= \sigma_0\left(\mathbf{E} + \frac{1}{\rho e c}\mathbf{j}\times\mathbf{B}\right).\end{aligned} \tag{16E.3}$$

The second term shows the classical Hall resistance (16.286).

Notes and References

For the Aharonov-Bohm effect, see the original work by
Y. Aharonov and D. Bohm, Phys. Rev. **115**, 485 (1959).
For a review see
S. Ruijsenaars, Ann. Phys. (N.Y.) **146**, 1 (1983).
See also the papers
A. Inomata and V.A. Singh, J. Math. Phys. **19**, 2318 (1978);
E. Corinaldesi and F. Rafeli, Am. J. Phys. **46**, 1185 (1978);
M.V. Berry, Eur. J. Phys. **1**, 240 (1980);
S. Ruijsenaars, Ann. Phys. **146**, 1 (1983);
G. Morandi and E. Menossi, Eur. J. Phys. **5**, 49 (1984);
R. Jackiw, Ann. Phys. **201**, 83 (1990); and in "M. A. B. Bég Memorial Volume" (A. Ali and P. Hoodbhoy, Eds.), World Scientific, Singapore, 1991;
G. Amelino-Camelia, Phys. Lett. B **326**, 282 (1994); Phys. Rev. D **51**, 2000 (1995);
C. Manuel and R. Tarrach, Phys. Lett. B **328**, 113 (1994);
S. Ouvry, Phys. Rev. D **50**, 5296 (1994);
C.R. Hagen, Phys. Rev. D **31**, 848 (1985); D **52** 2466 (1995);
P. Giacconi, F. Maltoni, and R. Soldati, Phys. Rev. D **53**, 952 (1996);
R. Jackiw and S.-Y. Pi, Phys. Rev. D **42**, 3500 (1990);
O. Bergman and G. Lozano, Ann. Phys. (N.Y.) **229**, 416 (1994);
M. Boz, V. Fainberg, and N.K. Pak, Phys. Lett. A **207**,1 (1995); Ann. Phys (N.Y.) **246**, 347 (1996);
M. Gomes, J.M.C. Malbouisson, and A.J. da Silva, Phys. Lett. A **236**, 373 (1997); Int. J. Mod. Phys. A **13**, 3157 (1998); (hep-th/0007080).

Path integrals in multiply connected spaces and their history are discussed in the textbook
L.S. Schulman, *Techniques and Applications of Path Integration*, Wiley, New York, 1981.

Details on Lippmann-Schwinger equation is found in most standard textbooks, say
S.S. Schweber, *Relativistic Quantum Field Theory*, Harper and Row, New York, 1961, Section 11b.

In chemistry, the properties of self-entangled polymer rings, called *catenanes*, were first investigated by

H.L. Frisch and E. Wasserman, J. Am. Chem. Soc. **83**, 3789 (1961).
Their existence was proved mass-spectroscopically by
R. Wolovsky, J. Am. Chem. Soc. **92**, 2132 (1961);
D.A. Ben-Efraim, C. Batich, and E. Wasserman, J. Am. Chem. Soc. **92**, 2133 (1970).

In optics, the Kirchhoff diffraction formula can be rewritten as a path integral formula with linking terms:
J.H. Hannay, Proc. Roy. Soc. Lond. A **450**, 51 (1995),

In biophysics,
J.C. Wang, Accounts Chem. Res. D **10**, 2455 (1974)
showed that DNA molecules can get entangled and must be disentangled during replication.

The path integral approach to the entanglement problem in polymer systems was pioneered by
S.F. Edwards, Proc. Phys. Soc. **91**, 513 (1967);
S.F. Edwards, J. Phys. A **1**, 15 (1968).
See also
M.G. Brereton and S. Shaw, J. Phys. A **13**, 2751 (1980)
and later works of these authors.

Investigations via Monte Carlo simulations were made by
A.V. Vologodskii, A.V. Lukashin, M.D. Frank-Kamenetskii, and V.V. Anshelevin, Sov. Phys. JETP **39**, 1095 (1974);
A.V. Vologodskii, A.V. Lukashin, and M.D. Frank-Kamenetskii, Sov. Phys.-JETP **40**, 932 (1975).
See also the review article by
M.D. Frank-Kamenetskii and A.V. Vologodskii, Sov. Phys. Usp. **24**, 679 (1982).
This article also discussed ribbons.

For further computer work on knot distributions see
J.P.J. Michels and F.W. Wiegel, Phys. Lett. A **9**, 381 (1982); Proc. Roy. Soc. A **403**, 269 (1986), and references therein. The work is summarized in the textbook by
F.W. Wiegel, *Introduction to Path-Integral Methods in Physics and Polymer Science*, World Scientific, Singapore, 1986.
See also
S. Windwer, J. Chem. Phys. **93**, 765 (1990).
The parameter C at the end of Section 6.4 was found by
A. Kholodenko, Phys. Lett. A **159**, 437 (1991),
who mapped the problem onto a q-state Potts model with $q = 4$. This mapping gives $\alpha = 0$ and $C = 2e^{-\pi/6} \approx 1.18477$.

For the Gauss integral as a topological invariant of links see the original paper by
G.F. Gauss, Koenig. Ges. Wiss. Goettingen **5**, 602 (1877).
The *writhing number* W_{r} was introduced by
F.B. Fuller, Proc. Nat. Acad. Sci. USA **68**, 815 (1971),
who applied the mathematical relation to DNA. See also
F.H.C. Crick, Proc. Nat. Acad. Sci. USA **68**, 2639 (1976).
The relation $L_{\mathrm{k}} = T_{\mathrm{w}} + W_{\mathrm{r}}$ was first written down by
G. Calagareau, Rev. Math. Pur. et Appl. **4**, 58 (1959); Czech. Math. J. **4**, 588 (1961),
and extended by
J.H. White, Am. J. Math. **90**, 1321 (1968).

In particle physics, ribbons are used to construct path integrals over fluctuating fermion orbits:
A.M. Polyakov, Mod. Phys. Lett. A **3**, 325 (1988).
For more details see

C.H. Tze, Int. J. Mod. Phys. A **3**, 1959 (1988).

The construction of the Alexander polynomial of links is described in
A.V. Vologodskii, A.V. Lukashin, and M.D. Frank-Kamenetskii, JETP **40**, 932 (1974).
Their derivation from the skein relations is shown in
J.H. Conway, *An Enumeration of Knots and Links*, Pergamon, London, 1970, pp. 329–358;
L.H. Kauffman, Topology **20**, 101 (1981).
In the mathematical literature, the various knot polynomials are discussed by
L.H. Kauffman, Topology **26**, 395 (1987); Contemporary Mathematics AMS **78**, 283 (1988); Trans. Amer. Math. Soc. 318, 417 (1990); *On Knots*, Princeton University Press, Princeton, 1987; *Knots and Physics*, World Scientific, Singapore, 1991; J. Math. Phys. **36**, 2402 (1995).
V. Jones, Bull. Am. Math. Soc. **12**, 103 (1985); Ann. Math. **126**, 335 (1987);
P. Freyd, D. Yetter, J. Hoste, W. B. R. Lickorish, K.C. Millet, and A. Ocneanu, Bull. Am. Math. Soc. **12**, 239 (1985);
W. B. R. Lickorish and K.C. Millet, Math. Magazine **61**, 3 (1987).
The lower HOMFLY polynomials are tabulated in the text. For the higher ones see the microfilm accompanying the article
H. Doll and J. Hoste, Math. of Computation **57**, 747 (1991)
and the unpublished tables by
M.B. Thistlethwaite, University of Knoxville, Tennessee.
The author is grateful for a copy of them.
A collection of many relevant articles is found in
T. Kuhno (ed.), *New Developments in the Theory of Knots*, World Scientific, Singapore, 1990.
A short introduction to the classification problem of knots is given in the popular articles
W.F.R. Jones, Scientific American, November 1990, p. 52,
I. Stewart, Spektrum der Wissenschaft, August 1990, p. 12.

The Chern-Simons actions have in recent years received increasing attention due to their relevance for explaining the fractional quantum Hall effect and a possible presence in high-temperature superconductivity . Actions of this type were first observed in four-dimensional quantum field theories in the form of so-called anomalies by
J. Wess and B. Zumino, Phys. Lett. B **36**, 95 (1971).
The action (16.253) in three spacetime dimensions was first analyzed by
S. Deser, R. Jackiw, and S. Templeton, Ann. Phys. **140**, 372 (1982),
who pointed out the connection with the Chern classes of differential geometry described by
S. Chern, *Complex Manifolds without Potential Theory*, Springer, Berlin, 1979.
In particular they found the mass of the electromagnetic field which was conjectured to be the origin of the Meissner effect in high-temperature superconductors. See
A.L. Fetter, C. Hanna, and R.B. Laughlin, Phys. Rev. B **39**, 9679 (1989);
Y.-H. Chen and F. Wilczek, Int. J. Mod. Phys. B **3**, 117 (1989);
Y.-H. Chen, F. Wilczek, E. Witten, and B.I. Halperin, Int. J. Mod. Phys. B **3**, 1001 (1989);
A. Schakel, Phys. Rev. D **44**, 1198 (1992).
However, the recent finding of dissipation in anyonic systems by
D.V. Khveshchenko and I.I. Kogan, Int. J. Mod. Phys. B **5**, 2355 (1991) speaks against an anyon mechanism of this phenomenon.

A Chern-Simons type of action appeared when integrating out fermions in
H. Kleinert, Fortschr. Phys. **26**, 565 (1978) (`http://www.physik.fu-berlin.de/~kleinert/55`).

The relation with Chern classes was recognized by
M.V. Berry, Proc. Roy. Soc. A **392**, 45 (1984);
B. Simon, Phys. Rev. Lett. **51**, 2167 (1983).
The Chern-Simons action in the text was derived for a degenerate electron liquid in two dimensions by

T. Banks and J.D. Lykken, Nucl. Phys. B **336**, 500 (1990);
S. Randjbar-Daemi, A. Salam, and J. Strathdee, Nucl. Phys. B **340**, 403 (1990),
P.K. Panigrahi, R. Ray, and B. Sakita, Phys. Rev. B **42**, 4036 (1990).
There is related work by
M. Stone, Phys. Rev. D **33**, 1191 (1986);
I.J.R. Aitchison, Acta Physica Polonica B **18**, 207 (1987).
See also the reprints of many papers on this subject in
A. Shapere and F. Wilczek, *Geometric Phases in Physics*, World Scientific, Singapore, 1989.
F. Wilczek, *Fractional Statistics and Anyon Superconductivity*, World Scientific, Singapore, 1990, which itself provides a clear introduction to the subject and contains many important reprints. A good review is also contained in the lectures
J.J. Leinaas, *Topological Charges in Gauge Theories*, Nordita Preprint, 79/43, ISSN 0106-2646.

Textbooks on this subject are
A. Lerda, *Anyons-Quantum Mechanics of Particles with Fractional Statistics*, Lecture Notes in Physics, m14, Springer, Berlin 1992;
A. Khare, *Fractional Statistics and Quantum Theory*, World Scientific, Singapore, 1997.
The Lerda book contains many useful examples and explains the origin of difficulties in treating interacting anyons. The Khare book provides a well-motivated treatment and includes a brief introduction to the Braid group. Both include discussions of the Quantum Hall Effect and Anyon Superconductivity.

For the relation between the Chern-Simons theory and knot polynomials see
E. Witten, Comm. Math. Phys. **121**, 351 (1989), Nucl. Phys. B **330**, 225 (1990).
See also
P. Cotta-Ramusino, E. Guadagnini, M. Martellini, and M. Mintchev, Nucl. Phys. B **330**, 557 (1990);
G.V. Dunne, R. Jackiw, and C. Trugenburger, Ann. Phys. **194**, 197 (1989);
A. Polychronakos, Ann. Phys. **203**, 231 (1990);
E. Guadagnini, I. J. Mod. Phys. A **7**, 877 (1992).

The integer quantum Hall effect was found by
K. vonKlitzing, G. Dorda, and M. Pepper, Phys. Rev. Lett. **45**, 494 (1980);
the fractional one by
D.C. Tsui, H.L. Stormer, and A.C. Gossard, Phys. Rev. Lett. **48**, 1559 (1980).
Theoretical explanations are given in
R.B. Laughlin, Phys. Rev. Lett. **50**, 1395 (1983), Phys. Rev. B **23**, 3383 (1983);
F.D.M. Haldane, Phys. Rev. Lett. **51**, 605 (1983);
B.I. Halperin, Phys. Rev. Lett. **52**, 1583 (1984);
D.P. Arovas, J.R. Schrieffer, F. Wilczek, Phys. Rev. Lett. **53**, 722 (1984);
D.P. Arovas, J.R. Schrieffer, F. Wilczek, and A. Zee, Nucl. Phys. B **251**, 117 (1985);
J.K. Jain, Phys. Rev. Lett. **63**, 199 (1989).
The exceptional filling factor $\nu = \frac{5}{2}$ is discussed in
R. Willet et al., Phys. Rev. Lett. **59**, 17765 (1987);
S. Kivelson, C. Kallin, D.P. Arovas, and J.R. Schrieffer, Phys. Rev. Lett. **56**, 873 (1986).

The Chern-Simons path integral is treated semiclassically in
D.H. Adams, Phys. Lett. B **417**, 53 (1998) (hep-th/9709147).

For a simple discussion of the change from Bose to Fermi statistics at the level of creation and annihilation operators via a topological interaction see
E. Fradkin, Phys. Rev. Lett. **63**, 322 (1989); *Field Theories of Condensed Matter Physics*, Addison-Wesley, 1991.

The lattice form of the action $\sum_{\mathbf{x}} \epsilon_{\mu\nu\lambda} A^{\mu}(\mathbf{x}) \nabla_{\nu} A_{\lambda}(\mathbf{x})$ used by that author is not correct since it violates gauge invariance. This can, however, easily be restored without destroying the results by replacing the first $A_{\mu}(\mathbf{x})$-field by $A_{\mu}(\mathbf{x} - \mathbf{e}_{\mu})$, where $\mathbf{e}_{\mu}$ is the unit vector in the μ-direction. See the general discussion of lattice gauge transformations in
H. Kleinert, *Gauge Fields in Condensed Matter*, Vol. I, World Scientific, Singapore, 1989, Chapter 8 (`http://www.physik.fu-berlin.de/~kleinert/b1`).

See furthermore
D. Eliezer and G.W. Semenoff, *Anyonization of Lattice Chern-Simons Theory*, Ann. Phys. **217**, 66 (1992).

For the London equations see the original paper by
F. London and H. London, Proc. Roy. Soc. A **147**, 71 (1935)
and the extension thereof:
A.B. Pippard, *ibid.*, A **216**, 547 (1953).

The individual citations refer to

[1] P.A.M. Dirac, Proc. Roy. Soc. A **133**, 60 (1931); Phys. Rev. **74**, 817 (1948), Phys. Rev. **74**, 817 (1948).
See also
J. Schwinger, *Particles, Sources and Fields*, Vols. 1 and 2, Addison Wesley, Reading, Mass., 1970 and 1973.

[2] For a review, see
G. Giacomelli, in *Monopoles in Quantum Field Theory*, World Scientific, Singapore, 1982, edited by N.S. Craigie, P. Goddard, and W. Nahm, p. 377.

[3] B. Cabrera, Phys. Rev. Lett. **48**, 1378 (1982).

[4] For a detailed discussion of the physics of vortex lines in superconductors, see
H. Kleinert, *Gauge Fields in Condensed Matter*, World Scientific, Singapore, 1989, Vol. I, p. 331 (`http://www.physik.fu-berlin.de/~kleinert/b1`).

[5] See the reprint collection
A. Shapere and F. Wilczek, *Geometric Phases in Physics*, World Scientific, Singapore, 1989.
In particular the paper by
D.P. Arovas, *Topics in Fractional Statistics*, p.284.

[6] The Tait number or writhe must not be confused with the writhing number $W_{\rm r}$ introduced in Section 16.6 which is in general noninteger. See
P.G. Tait, *On Knots I, II, and III*, Scientific Papers, Vol. 1. Cambridge, England: University Press, pp. 273-347, 1898.

[7] See Ref. [7] of Chapter 19. There exists, unfortunately, no obvious extension to four space-time dimensions.

[8] The development in this Section follows
F. Ferrari, H. Kleinert, and I. Lazzizzera, Phys. Lett. A **276**, 1 (2000) (cond-mat/0002049); Eur. Phys. J. B **18**, 645 (2000) (cond-mat/0003355); nt. Jour. Mod. Phys. B **14**, 3881 (2000) (cond-mat/0005300); *Topological Polymers: An Application of Chern-Simons Field Theories*, in K. Lederer and N. Aust (eds.), *Chemical and Physical Aspects of Polymer Science and Engineering*, 5-th Oesterreichische Polymertage, Leoben 2001, Macromolecular Symposia, 1st Edition, ISBN 3-527-30471-1, Wiley-VCH, Weinheim, 2002.

[9] M.G. Brereton and S. Shah, J. Phys. A: Math. Gen. *15*, 989 (1982).

[10] R. Jackiw, in *Current Algebra and Anomalies*, ed. by S.B. Treiman, R. Jackiw, B. Zumino, and E. Witten, World Scientific, Singapore, 1986, p. 211.

[11] L.D. Faddeev and V.N. Popov, Phys. Lett. B *25*, 29 (1967).